Sediment Oxygen Demand Kinetics

Lindsay J. Olinde

Thesis submitted to the faculty of the Virginia Polytechnic Institute and State University in partial fulfillment of the requirements for the degree of

Master of Science
In
Environmental Engineering

Dr. John Little, Chair
Dr. Gregory Boardman
Dr. Peter Vikesland

April 24, 2007
Blacksburg, Virginia, USA

Keywords: diffusion, first-order, model, Monod, zero-order

Sediment Oxygen Demand Kinetics

Lindsay J. Olinde

Abstract

Hypolimnetic oxygen diffusers increase sediment oxygen demand (SOD) and, if not accounted for in design, can further exacerbate anoxic conditions. A study using extracted sediment cores, that included both field and laboratory experiments, was performed to investigate SOD kinetics in Carvin's Cove Reservoir, a eutrophic water supply reservoir for Roanoke, Virginia. A bubble-plume diffuser is used in Carvin's Cove to replenish oxygen consumed while the reservoir is thermally stratified. The applicability of zero-order, first-order, and Monod kinetics to describe transient and steady state SOD was modeled using analytical and numerical techniques. Field and laboratory experiments suggested that first-order kinetics characterize Carvin's Cove SOD. SOD calculated from field experiments reflected diffuser flow changes. Laboratory experiments using mini-diffusers to vary dissolved oxygen concentration and turbulence were conducted at 4°C and 20°C. Similar to field observations, the laboratory results followed changes in mini-diffuser flow. Kinetic-temperature relationships were also observed in the laboratory experiments. A definitive conclusion could not be made on the broad applicability of first-order kinetics to Carvin's Cove SOD due to variability within field experiments. However, *in situ* experiments are underway that should assist in the overall understanding of the reservoir's SOD kinetics.

Acknowledgements

I would like to thank Dr. John Little, my advisor, for his support and Dr. Gregory Boardman and Dr. Peter Vikesland for serving on my committee. I am grateful for the invaluable insight and field assistance provided by Lee Bryant and Paul Gantzer. Lee Bryant also provided the field data. Appreciation also goes to Julie Petruska for her technical laboratory expertise and innovative solutions, Ying Xu and Zhe Liu for their Matlab and numerical modeling assistance, Elizabeth Rumsey for her enthusiasm in the field, the employees at the Western Virginia Water Authority, and the Edna Bailey Sussman foundation.

I would also like to thank my family and friends for their unwavering humor, understanding, and encouragement.

I submit this in honor and in memory of my officemates, classmates, and professor: Brian Bluhm, Matt Gwaltney, Jeremy Herbstritt, Jarrett Lane, Dr. G.V. Loganathan, Partahi Mamora Halomoan Lumbantoruan, Dan O'Neil, Juan Ortiz-Ortiz, Julia Pryde, and Waleed Shaalan.

Table of Contents

List of Tables

List of Figures

Introduction

Anoxic conditions in lower hypolimnetic water can negatively affect water quality of hydropower reservoirs, water supply basins, and cold-water fisheries. State water quality regulations require minimum dissolved oxygen (DO) concentrations for hydropower reservoir releases. Anoxic conditions can cause benthic sediment to release hydrogen sulfide, ammonia, and orthophosphate and generate soluble reduced iron and manganese (Beutel et al. 2006; Bouldin 1968; Hem 2005; Singleton and Little 2006; Wetzel 2001). Internal orthophosphate loading can stimulate algal blooms and subsequently increase overall reservoir oxygen demand (Beutel et al. 2007; Singleton and Little 2006). Hydrogen sulfide and reduced iron and manganese in water supply reservoirs can cause color, taste, and odor problems and increased costs for drinking water authorities due to additional coagulant demand (Singleton and Little 2006; Viessman and Hammer 1998).

Hypolimnetic oxygen consumption is highly dependent on sediment oxygen demand (SOD). SOD represents oxygen consumption by living organisms and chemical reactions within benthic sediment (Higashino et al. 2004; House 2003; Nakamura and Stefan 1994). SOD can be calculated according to Fick's Law of diffusion, Equation 1 (Nakamura and Stefan 1994; Rasmussen and Jorgensen 1992; Revsbech et al. 1986). SOD monitoring provides more insight into true sediment/oxygen conditions than oxygen concentration monitoring alone (Wang 1981). Due to the strong relationship between oxygen depletion and SOD, water quality is often determined by SOD (Wetzel 2001).

$$SOD = J(y) = -D_m(y)\phi\frac{dC(y)}{dy} \quad (1)$$

where: J = diffusive flux of oxygen per unit area of sediment

D_m = molecular diffusion coefficient of oxygen in water

φ = sediment porewater porosity

C(y) = oxygen concentration

y = depth

SOD is influenced by DO concentration and the degree of turbulence within the overlying water (Arega and Lee 2005; Beutel et al. 2007; Edwards and Rolley 1965; Nakamura

and Stefan 1994; Rasmussen and Jorgensen 1992; Wiltshire et al. 1996). If turbulence exists, but does not stir up the sediments, the stagnant diffusive-boundary layer (DBL) immediately above the sediment becomes thinner allowing faster transport across the film and deeper oxygen penetration into the sediment (Revsbech et al. 1980). However, high turbulence that causes suspension of anoxic sediment can also increase SOD, promoting anoxic conditions (Jubb et al. 2001).

Water and hydropower authorities commonly install hypolimnetic oxygenation systems to reduce anoxia. While SOD is a principle parameter used in the design of oxygenation systems, SOD often increases after diffusers have been installed. The observed increase can exacerbate problems associated with anoxia. Increased SOD may be caused by the diffusers inducing higher oxygen concentrations as well as more rapid transport across the DBL due to increased turbulence. Diffusers are typically designed based on the oxygen depletion rate measured during summer stratification prior to installation of the oxygenation system. Diffusers that do not take into account diffuser-induced SOD are not able to supply the required amount of oxygen needed to meet the sediment demand (Beutel et al. 2006; House 2003; Moore et al. 1996). Research quantifying diffuser-induced SOD is lacking (Bryant and Little 2006).

In addition to DO concentrations and turbulence, organic matter (OM) within sediment also influences SOD. Higher OM increases SOD due to the additional oxygen consumption from mineralization of particulate OM (Arega and Lee 2005; Brewer et al. 1977; Wiltshire et al. 1996). In eutrophic lakes, significant amounts of OM from settling detritus accumulate in sediment and induce high oxygen demand (Moore et al. 1996). The effects of high OM were illustrated in a comparison of oxygen consumption within sediments composed of varying OM amounts (House 2003).

Temperature can affect SOD both directly and indirectly (Edberg and Hofsten 1973; Edwards and Rolley 1965). Oxygen consumption kinetics are a function of temperature. In addition, SOD depends on the supply of oxygen from the overlying water. Oxygen concentration is also affected by temperature to some extent because DO saturation decreases as temperature increases (Hem 2005; Rasmussen and Jorgensen 1992; Wetzel 2001) and DO saturation ultimately drives oxygen into the water. Seasonal temperature changes influence SOD due to changes in benthic organism composition. For example, growth of benthic algae in

warmer months induces more oxygen demand (Edwards and Rolley 1965). Similarly, certain benthic bacterial populations may be promoted during cooler months (Brewer et al. 1977).

The classic types of sediment/oxygen kinetics reported in the literature are zero-order, first-order, and Monod (also referred to as Michaelis-Menten in some studies), Equations 2–4 (Bouldin 1968; Higashino et al. 2004; House 2003). At steady state, concentration does not change with time, Equation 5. Interestingly, the Monod equation itself encompasses both zero- and first-order kinetics. When the oxygen concentration is much less than the half-saturation constant (K_{O_2}), Monod kinetics simplify to a pseudo first-order reaction. When the oxygen concentration is much greater than K_{O_2}, the Monod expression reduces to a pseudo zero-order reaction. Table 1 presents a summary of several sediment/oxygen kinetic studies (Beutel et al. 2007; Brewer et al. 1977; Hall et al. 1989; House 2003; Rasmussen and Jorgensen 1992; Wiltshire et al. 1996). Numerous studies have reported that Monod kinetics best described SOD and that zero-order kinetic reactions also adequately represented Monod kinetics (Higashino et al. 2004; House 2003; Wiltshire et al. 1996). Steady state models were applied in field data and experiments involving the incubation of cores for extended periods of time (House 2003; Rasmussen and Jorgensen 1992; Wiltshire et al. 1996). Transient models were used in laboratory experiments that manipulated factors within short time periods such as fluctuating aeration (Beutel et al. 2007). While many studies have investigated sediment/oxygen kinetics under steady-state sediment/oxygen conditions, few have examined transient SOD (Higashino et al. 2004).

$$\text{Zero-order: } \frac{\partial C}{\partial t} = D_s \frac{\partial^2 C}{\partial y^2} - A \tag{2}$$

$$\text{First-order: } \frac{\partial C}{\partial t} = D_s \frac{\partial^2 C}{\partial y^2} - k_1 C \tag{3}$$

$$\text{Monod: } \frac{\partial C}{\partial t} = D_s \frac{\partial^2 C}{\partial y^2} - \frac{\mu C}{K_{O_2} + C} \tag{4}$$

$$C << K_{O_2}, \frac{\mu}{K_{O_2}} \rightarrow k_1$$

$$C >> K_{O_2}, \mu \rightarrow A$$

Steady state: $\frac{\partial C}{\partial t} = 0$ (5)

where:

t = time

D_s = effective diffusion coefficient of DO in sediment = φD_m

A = zero-order rate constant

k_1 = first-order rate constant

μ = maximum oxidation rate constant

K_{O_2} = half-saturation constant

Reported SOD measurements presumed to express true sediment/oxygen conditions may be unrepresentative if the potential transient status of the water body is ignored (Bryant and Little 2006). SOD variation can arise with respect to location as observed from the effects of natural heterogeneity of biochemical processes and sediment composition within a water body (Beutel et al. 2007). SOD dissimilarities may also occur with respect to time such as recognized from the effects of seasonal temperatures, internal seiches, or eutrophic differences (Edwards and Rolley 1965; Lorke et al. 2003).

Table 1. Examples of sediment-oxygen kinetic results from previous studies (Beutel et al. 2007; Brewer et al. 1977; Hall et al. 1989; Rasmussen and Jorgensen 1992; Wiltshire et al. 1996).

Study	Base	Order of reaction	Sediment Type	Temperature	Value of kinetic parameters	Water Column Conditions	Time Span	Sediment Collection Method
Field experiments								
Brewer et al. 1977	SOD	1 when SOD reaches maximum	freshwater lake	18°C	*	circulating with in situ water	profiled immediately	extracted with dredge, placed in chamber
Rasmussen and Jorgensen 1992	SOD	0	marine	4°C	A=26 mg l^{-1} d^{-1}	stirred	profiled immediately	extracted sediment core
Hall et al. 1989	SOD	0**	marine	10°C	A=1860 mg l^{-1} d^{-1}	no mixing	profiled immediately	extracted sediment core
Laboratory experiments								
Wiltshire, Schroeder et al. 1996	SOD	0 when C>0.02 mg l^{-1} 1 when C<0.02 mg l^{-1}	marine	15-20°C	*	stirred	1-3 d	extracted cores
Beutel et al. 2007	SOD	1	freshwater reservoir	12°C	*	quiescent and mixed	oxic: 7 d oxic to anoxic: 10 d anoxic to oxic: 7 d	extracted cores
House 2003	DO profiles	0	fluvial sand, 0.9% OM***	18°C	$A_{high\ flow}$=160 mg l^{-1} d^{-1} $A_{low\ flow}$=95 mg l^{-1} d^{-1}	circulating water from river	high flow: 28 d low flow: 15 d	extracted, placed in fluviarium channel
			fluvial silt, 16.7% OM***	18°C	$A_{high\ flow}$=400 mg l^{-1} d^{-1} $A_{low\ flow}$=440 mg l^{-1} d^{-1}	circulating water from river	high flow: 28 d low flow: 15 d	extracted, placed in fluviarium channel
			fluvial silt/sand, 5% OM***	18°C	$A_{high\ flow}$=150 mg l^{-1} d^{-1} $A_{low\ flow}$=100 mg l^{-1} d^{-1}	circulating water from river	high flow: 28 d low flow: 15 d	extracted, placed in fluviarium channel

*Value of kinetic parameter not explicitly presented in study ** Hall et al. 1989 assumed 0-order ***OM= percent organic matter by mass

The strong impact of SOD on oxygen depletion highlights the importance of an understanding of SOD to the success of water quality enhancement. There is a lack of knowledge in quantifying diffuser influence on SOD (Bryant and Little 2006). This study investigated SOD kinetics using field and laboratory experiments. The main objectives of this research were:

1. To obtain steady-state, sediment/water DO profiles from field cores taken over a period of months that include changes in diffuser operation
2. To determine which kinetic model (zero-order, first-order, or Monod) best represents the steady-state oxygen micro-profiles collected in the field
3. To obtain transient, sediment/water DO profiles using an in-core, mini-diffuser in the laboratory cores taken over a period of days that mimic changes in diffuser operation
4. To determine which kinetic model (zero-order, first-order, or Monod) best represents the transient oxygen micro-profiles collected in the laboratory
5. To determine the dependence on temperature of parameter(s) for the model that best represents sediment oxygen demand kinetics
6. To calculate and compare sediment oxygen demand obtained from the field and laboratory cores as a function of diffuser operation
7. To compare the field and laboratory results to determine which kinetic model best represents sediment oxygen demand kinetics in Carvin's Cove reservoir

Materials and Methods

Study site

Carvin's Cove is a drinking water supply reservoir for Roanoke County, Virginia, Figures 1 and 2. The reservoir is monomictic and eutrophic. The local water authority installed an oxygenation system that replenishes the DO in the hypolimnetic water during seasonal thermal stratification. This system consists of two diffusers, diffusers B and C, each having a length of 625 m.

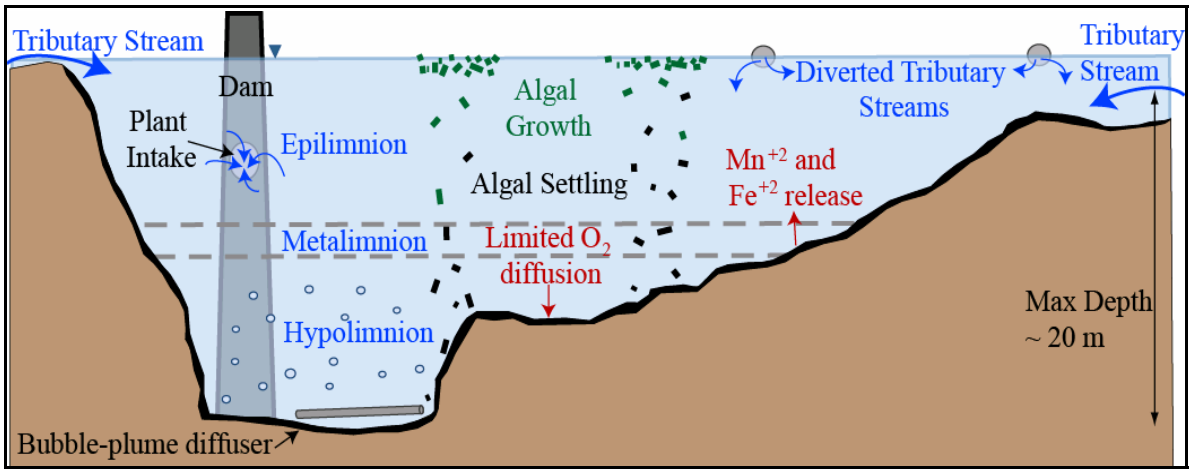

Figure 1. Schematic of Carvin's Cove.

Sediment samples

Sediment cores were used in both field and laboratory experiments. Cores from Carvin's Cove were taken from locations A, B, and C, Figure 3. Sediment cores, 90 mm in diameter, were collected from Carvin's Cove using a Uwitec ball corer, Figure 4. Only cores with undisturbed sediment surfaces were retained. Cores were covered to block light and stored on ice to prevent photosynthetic respiration and to reasonably maintain *in situ* reservoir temperatures. Sediment cores were sliced with a Uwitec core cutter. Cut cores had 10 cm of water column overlying the sediment.

Field cores were extracted periodically between October 2005 and April 2006. The reservoir was approximately 20 m deep at these sites. Cores profiled on the day of extraction monitored the seasonal variation of the sediment's oxygen microgradients and therefore SOD. *In situ* temperatures of the bottom water ranged from 8°C to 16°C during the sampling period. Diffuser flow fluctuated during this study, Table 2.

Cores used for the determination of DO microprofiles within the benthic sediment under controlled laboratory conditions were taken to Virginia Tech's Blacksburg campus. These cores were obtained from location B. Cores were taken in August and November 2006 for development of flow protocols for the laboratory constant temperature/DO variation experiments. Experiments altering DO concentration were conducted at 4°C and 20°C. The cores in the 20°C and 4°C experiments were extracted on December 8, 2006 and February 15, 2007, respectively.

Table 2. Carvin's Cove diffuser schedule during study.

Dates	Diffusers	Flow Rate, scfm
7/29/2005 - 11/18/2005	B & C on	10
11/18/2005 - 12/14/2005	B & C off	-
12/14/2005 - 01/13/2006	C on	10
01/13/2006 - end of study	B & C on	5

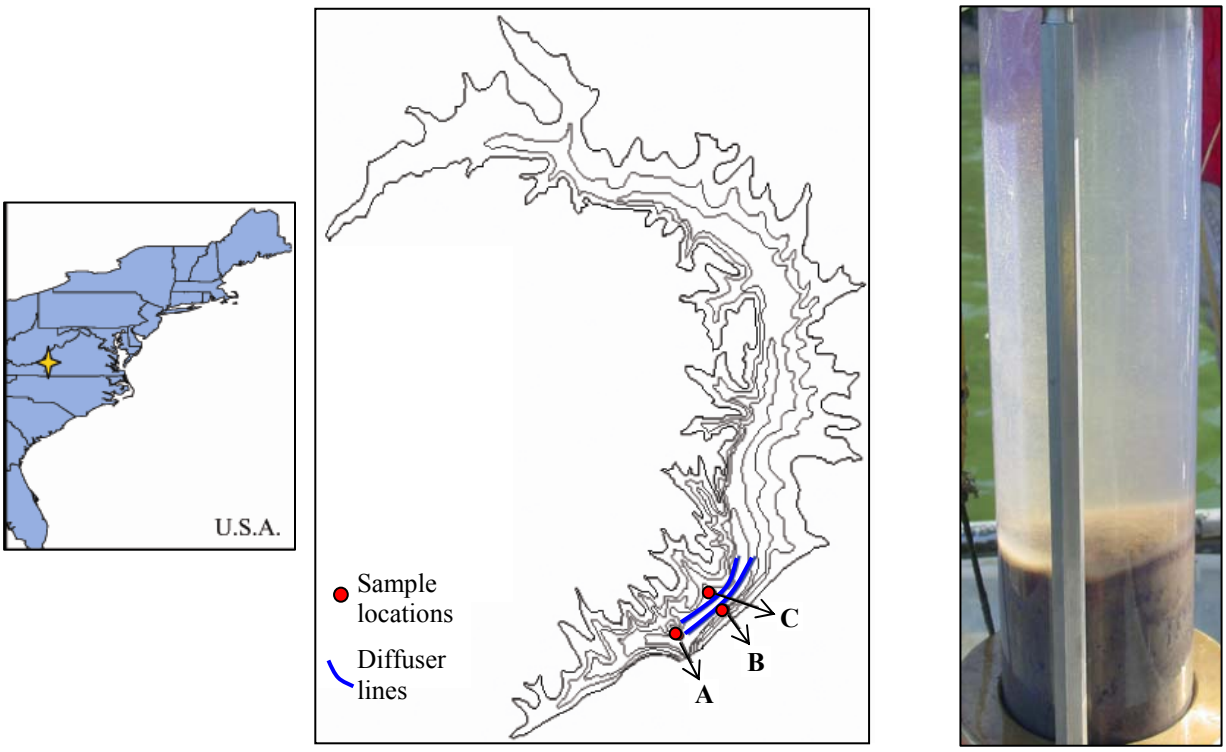

Figure 2. Aerial view of Carvin's Cove and locations of sediment core extraction, left.
Figure 3. Bathometric map of Carvin's Cove and sample locations, center.
Figure 4. Extracted sediment core from Carvin's Cove, right.

Laboratory experiments

In constant temperature rooms set to 4°C and 20°C, two cores were studied while varying oxygen in the sediment between oxic and anoxic conditions. Once transported to a constant temperature room, the cores were incubated at the appropriate temperature and brought to steady state by bubbling air through mini-diffusers for 5 to 6 days, similar to Beutel et al. (2007). A sandstone mini-diffuser (2 cm height, 1 cm diameter) was placed approximately 2 cm above the sediment for each core, Figure 5. Preliminary experiments were conducted in August and November 2006. The mini-diffuser was adjusted to a low flow rate because preliminary

experiments had excessive SOD due to high turbidity during high flow. At each temperature, one core was supplied with air using a low flow rotameter (Aalborg model P) set at 25 ml min^{-1}. A simple gang-valve controlled the airflow to the second core. This was adjusted to visually conform to the airflow rate of the first.

Figure 5. Laboratory sediment core microprofiling setup.

The laboratory cores were incubated in the dark except for the short periods while being profiled. During the transition period from saturation to anoxia, efforts were made to keep the cores as quiescent as possible to avoid transport of DO into the DBL due to the layer's role in supplying oxygen to benthic sediment. Water column temperature was monitored to insure that the desired temperatures were maintained.

Analysis of the cores' oxygen profiles determined when steady state conditions were achieved. Once the sediment reached steady state, the mini-diffusers were turned off until anoxic conditions persisted. Despite the water column being open to the atmosphere, the sediment was able to reach anoxia due to the complete depletion of DO in the DBL (Revsbech et al. 1980). After anoxia was established, the diffusers were again turned on at the original flow

rate, re-oxygenating the cores. Oxygen profiles measured during this cycle monitored the transient sediment response to the varying oxygen concentration.

Oxygen microelectrode measurements

The methods to obtain DO microprofiles for the field and laboratory experiments were similar to other studies that quantified DO distribution within extracted sediment using microelectrodes (House 2003; Rasmussen and Jorgensen 1992; Revsbech et al. 1986; Wiltshire et al. 1996). DO was measured with a 100 μm diameter tip glass oxygen microelectrode (Unisense OX-100) connected to a picoammeter (Unisense PA2000). The measurements were recorded using a microprofiling computer program (Unisense Profix) and calibrated using Winkler titrations. The sensor was manually lowered into the water column and sediment using the micromanipulator. DO profiles were collected 1 mm depth intervals.

Analytical and numerical modeling techniques

Analytical and numerical modeling techniques were applied to the DO profiles within the sediment using computer programs developed in Matlab. Profiles were simulated analytically and numerically according to zero-order, first-order, and Monod kinetics with appropriate boundary conditions, Equations 6–10 (Bouldin 1968; Clark 1996; Higashino et al. 2004; Rasmussen and Jorgensen 1992). For the non-linear Monod kinetics, numerical solutions were used for both steady and transient conditions because no steady state analytical solution exists (Lewandowski et al. 1991).

The numerical solution created DO curves by applying a finite shift to Equations 2 to 4 and iteratively solving for C_n^i, Figure 6.

$$\text{Numerical zero-order: } \frac{C_n^i - C_n^{i-1}}{\Delta t} = \frac{D_s}{\Delta y^2}\left(C_{n+1}^{i-1} - 2C_n^{i-1} + C_{n-1}^{i-1}\right) - A \tag{6}$$

$$\text{Analytical zero-order: } C(y) = \frac{A}{2D_s}y^2 - \left(\sqrt{\frac{2C_0 A}{D_s}}\right)y + C_0 \tag{7}$$

$$\text{Numerical first-order: } \frac{C_n^i - C_n^{i-1}}{\Delta t} = \frac{D_s}{\Delta y^2}\left(C_{n+1}^{i-1} - 2C_n^{i-1} + C_{n-1}^{i-1}\right) - k_1 C_n^{i-1} \tag{8}$$

$$\text{Analytical first-order: } C(y) = C_0 \exp\left(-\frac{y}{\sqrt{\frac{D_s}{k_1}}}\right) \tag{9}$$

$$\text{Numerical Monod: } \frac{C_n^i - C_n^{i-1}}{\Delta t} = \frac{D_s}{\Delta y^2}\left(C_{n+1}^{i-1} - 2C_n^{i-1} + C_{n-1}^{i-1}\right) - \frac{\mu C_n^{i-1}}{K_{O_2} + C_n^{i-1}} \tag{10}$$

where:

C_0 = DO concentration at the sediment-water interface

i = iteration number

n = depth along profile

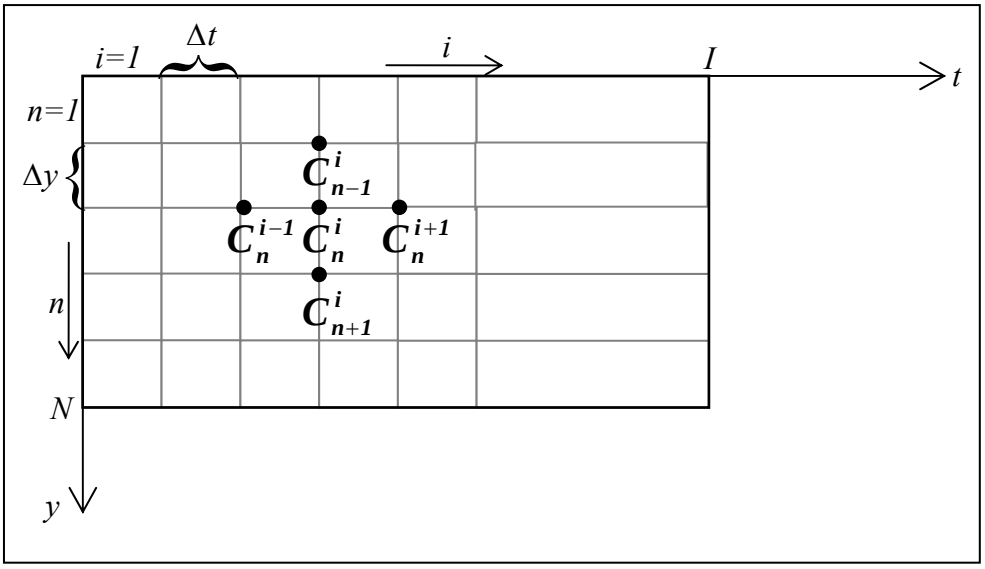

Figure 6. Visual representation of iterative numerical modeling applied to the reservoir and laboratory experiments.

Initial conditions and upper and lower boundary conditions must be specified for the diffusion/reaction models. The initial conditions were the observed initial profiles. For the field experiments, this was the actual profile measured. For the laboratory analyses, this was the profile measured at t=0 hr for each cycle. The depth resolution of 1 mm was too coarse for input to the numerical solution so smooth curves created from the profiles were used to obtain a finer discretization. To complete the analytical and numerical investigations, it was assumed that:

1. D_s is constant over the depth profiled
2. The field cores were at (or very close to) steady state when profiled

Because the field cores were assumed to be at steady state, the steady state zero- and first-order analytical solutions were applied directly to these profiles (Bouldin 1968; Clark 1996). Monod kinetics were solved numerically by allowing the system to run to steady state using short time steps over a long time period. The upper and lower boundary conditions for the Monod numerical solution for each profile was the observed DO concentrations at the sediment-water interface and deepest data point, respectively. Computer programs were created to analyze the field data, Appendix A.

The laboratory cores underwent two cycles: a transition from steady state oxic to steady state anoxic followed by a transition from steady state anoxic to steady state oxic. Due to the unsteady environment within the sediment during these periods, numerical solutions of the transient zero-order, first-order, and Monod kinetics were applied. The zero- and first-order numerical solutions were verified by comparing the numerical results at steady state to the steady-state analytical solution. The program for the numerical Monod solution was similar to the zero- and first-order procedures. Profiles created once the Monod numerical solution reached steady state appeared to be reliable with visual comparison despite not having a steady state analytical solution for comparison. Computer programs were created to analyze the laboratory data, Appendix B.

The field model was used to explore the applicability of kinetic rates for each profile due to its assumed steady state nature. This allowed simple boundary conditions to be applied. However, the upper boundary conditions for the laboratory profiles were more complex due to the transient nature of the experiment. The laboratory models were used to investigate the kinetic applicability within each cycle. Incorporating the numerous profiles within each period was essential. This was achieved by having the upper boundary conditions reflect the changing sediment-water interface DO conditions throughout each sequence. To do this, a transient upper boundary condition was created with a smooth curve through the interface concentrations as a function of time. The concentration at the upper boundary changed with time in the models. The upper boundary condition was allowed to be “permeable” to reflect the oxygen exchange with the overlying water. The lower boundary condition was set to anoxic and made impermeable because the cores reached anoxia at the deepest depths and no underlying oxygen supply existed.

Iterative fitting procedures were conducted to optimize the kinetic parameters for both field and laboratory experiments. For the field profiles, each profile for locations A, B, and C was evaluated according to the best relative least squares (RLS) fit (Saez and Rittman 1992). RLS were used due to the significant change in magnitude of DO with respect to depth. The normal least squares method was not applied because of the tendency for upper sediments to have larger DO concentrations than those at lower depths. In order to compare the results between profiles and locations, the RLS were normalized (RLS_n) by the total number of data points used for each profile, Equation 11 (Little et al. 1994; Saez and Rittman 1992).

$$RLS_n = \frac{\sum_{i=1}^{n} \frac{C_{i,observed} - C_{i,model}}{C_{i,observed}}}{n} \tag{11}$$

where:

$C_{i,observed}$ = measured DO

$C_{i,model}$ = model-predicted DO

n = number of points within the observed profile

The field models determined the appropriate kinetic parameters for the individual oxygen profiles obtained from the extracted cores. However, the laboratory models were required to produce suitable kinetic parameters within each deoxygenation/oxygenation cycle. Therefore, the chosen parameters reflected all the profiles and points within one sequence. Two features were recognized in the laboratory data:

1. Unless completely anoxic, the upper sediment was more oxic than the lower (similar to the field profiles)
2. The DO concentrations at upper depths naturally varied more over a cycle than at lower depths

To address these, weighted least squares (WLS) were applied to evaluate the agreement of the models (Press et al. 1990) with the data. The weights were the inverse of the DO variation at each depth over a particular cycle, Equation 12. WLS were also normalized (WLS_n) similar to the field models, Equation 13.

$$w_i = \frac{1}{\sigma^2} \tag{12}$$

where:

w_i = weights for corresponding depth at i

σ^2 = variation of DO with depth during a cycle

$$WLS_n = \frac{\sum_{i=1}^{n} w_i \left(C_{i,observed} - C_{i,model}\right)^2}{n} \tag{13}$$

Sediment oxygen demand

SOD can also be calculated by applying a finite shift to Equation 1, Equation 14 (Jorgensen and Revsbech 1985).

$$SOD = -D_m(y)\phi \frac{\Delta C(y)}{\Delta y} \tag{14}$$

SOD was calculated for each simulated profile. The model with the best agreement to the observed data was used for the SOD calculations. The difference between the concentration at the sediment-water interface and the concentration Δy below the interface was used to compute SOD.

Results and Discussion

Field kinetics

Location A was less stable than locations B and C due to its position near the dam and downstream from the diffusers, Figure 3. Locations B and C most likely responded more quickly to changes in diffuser flow than location A. This effect is supported by the SOD results and is discussed in the SOD section. Location A's close vicinity to the water withdrawal point at the dam may also have caused variability in the sediment-oxygen kinetics. Due to Location A's potential instability, the discussion of field kinetics will mainly focus on results from locations B and C.

Field RLS_n were calculated, Table 3 and Figures 7–9. For all locations, Monod had the lowest RLS_n and the Monod kinetics provided the best-fit to the observed data. This was expected because the Monod equation has two fitting parameters while only one can be adjusted with the zero- and first-order solutions. However, first-order simulations consistently fit almost as well as Monod across all locations. Overall, the zero-order model produced curves with relatively poor agreement to the observed profiles. According to the principle of Occam's razor, if two models have essentially the same degree of fit, the one with fewer parameters is preferred (Jaynes 2003). Due to the close agreement of the first-order results with those of Monod, the first-order model is preferred because it has only one fitting parameter.

Table 3. Normalized relative least squares results for the reservoir experiments. Calculations were made by comparing the observed dissolved oxygen profiles with the optimized model profiles.

Date	Location A		Location B		Location C	
	Kinetic Type	RLS_n	Kinetic Type	RLS_n	Kinetic Type	RLS_n
10/6/2005	Zero-order	0.021	Zero-order	0.090	Zero-order	0.145
	First-order	0.023	First-order	0.000	First-order	0.009
	Monod	0.003	Monod	0.001	Monod	0.010
11/10/2005	Zero-order	0.110	Zero-order	0.043	Zero-order	0.038
	First-order	0.048	First-order	0.028	First-order	0.057
	Monod	0.006	Monod	0.009	Monod	0.002
12/1/2005	Zero-order	0.099	Zero-order	0.044	Zero-order	0.140
	First-order	0.025	First-order	0.122	First-order	0.026
	Monod	0.013	Monod	0.034	Monod	0.002
1/13/2006	Zero-order	0.044	Zero-order	1.402	Zero-order	0.060
	First-order	0.013	First-order	0.034	First-order	0.014
	Monod	0.009	Monod	0.034	Monod	0.021
2/14/2006	Zero-order	0.228	Zero-order	1.649	Zero-order	0.176
	First-order	0.041	First-order	0.038	First-order	0.009
	Monod	0.040	Monod	0.038	Monod	0.005
3/23/2006	Zero-order	0.256	Zero-order	2.615	Zero-order	0.274
	First-order	0.007	First-order	0.008	First-order	0.007
	Monod	0.007	Monod	0.008	Monod	0.007
4/20/2006	Zero-order	0.500	Zero-order	1.440	Zero-order	0.140
	First-order	0.036	First-order	0.023	First-order	0.007
	Monod	0.037	Monod	0.022	Monod	0.003

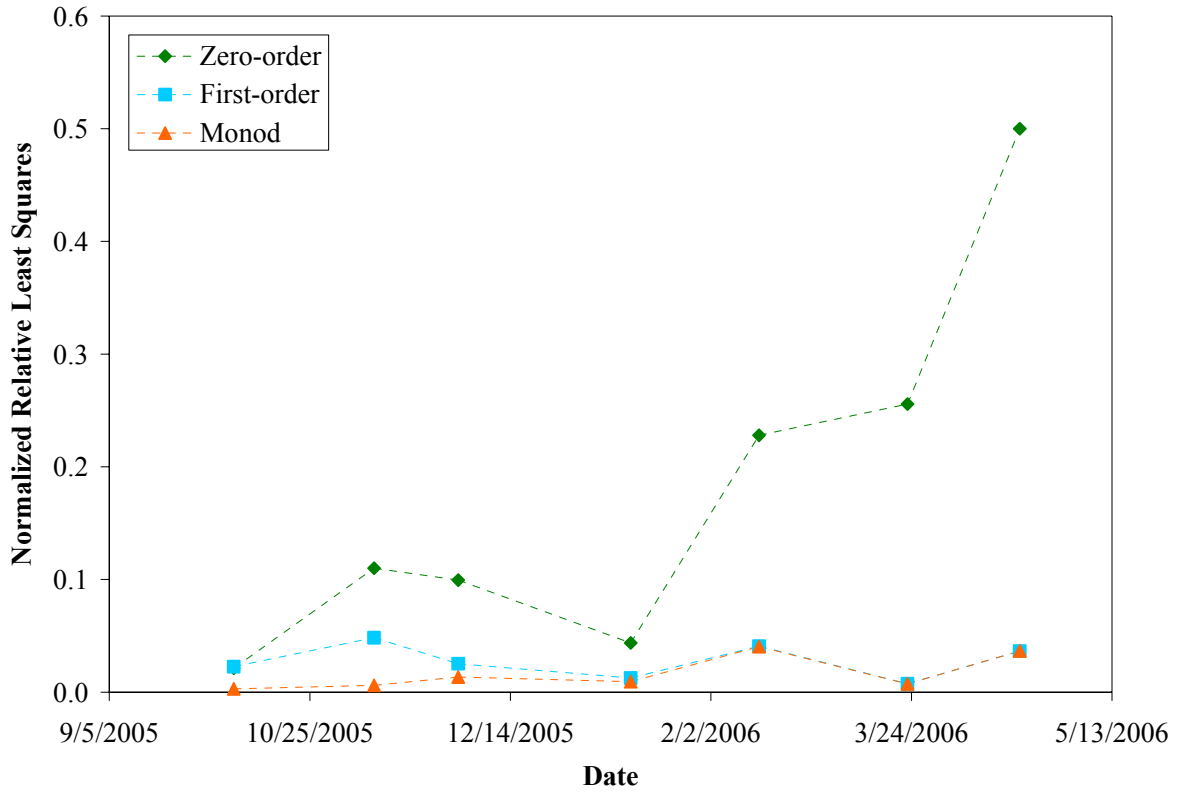

Figure 7. RLS_n results for Location A.

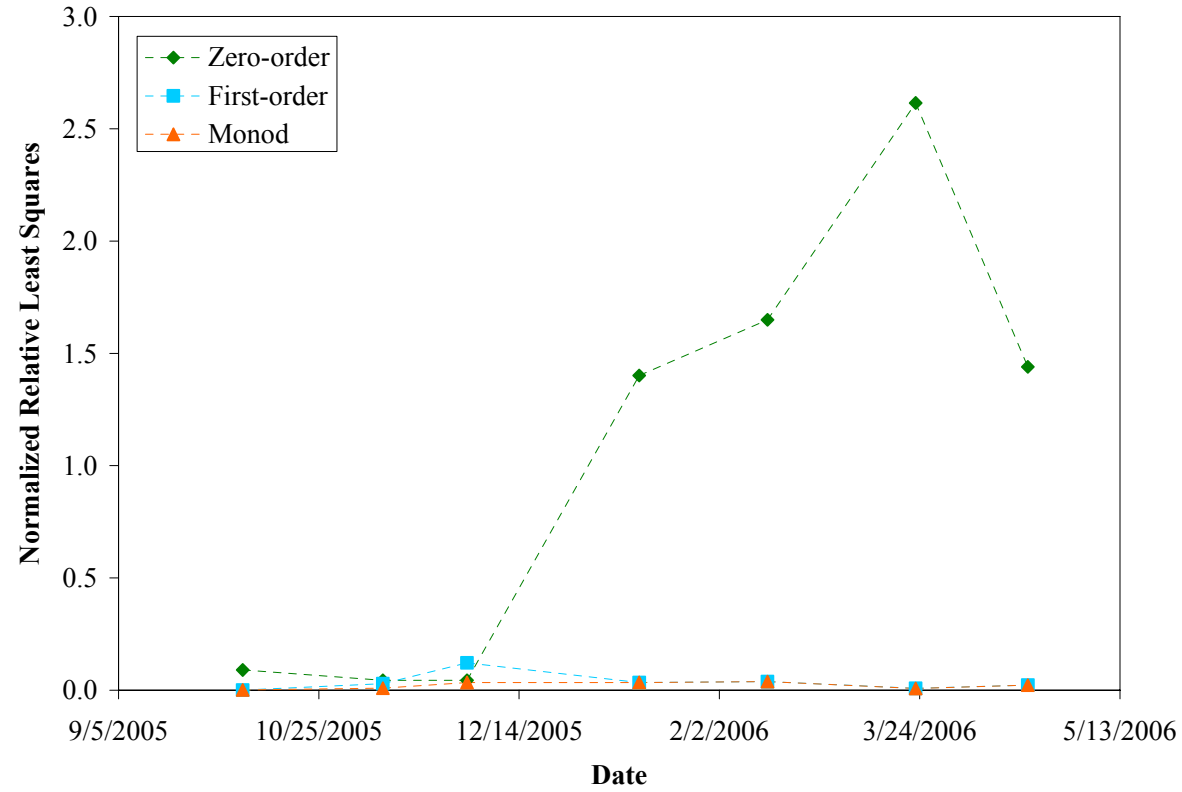

Figure 8. RLSn results for Location B.

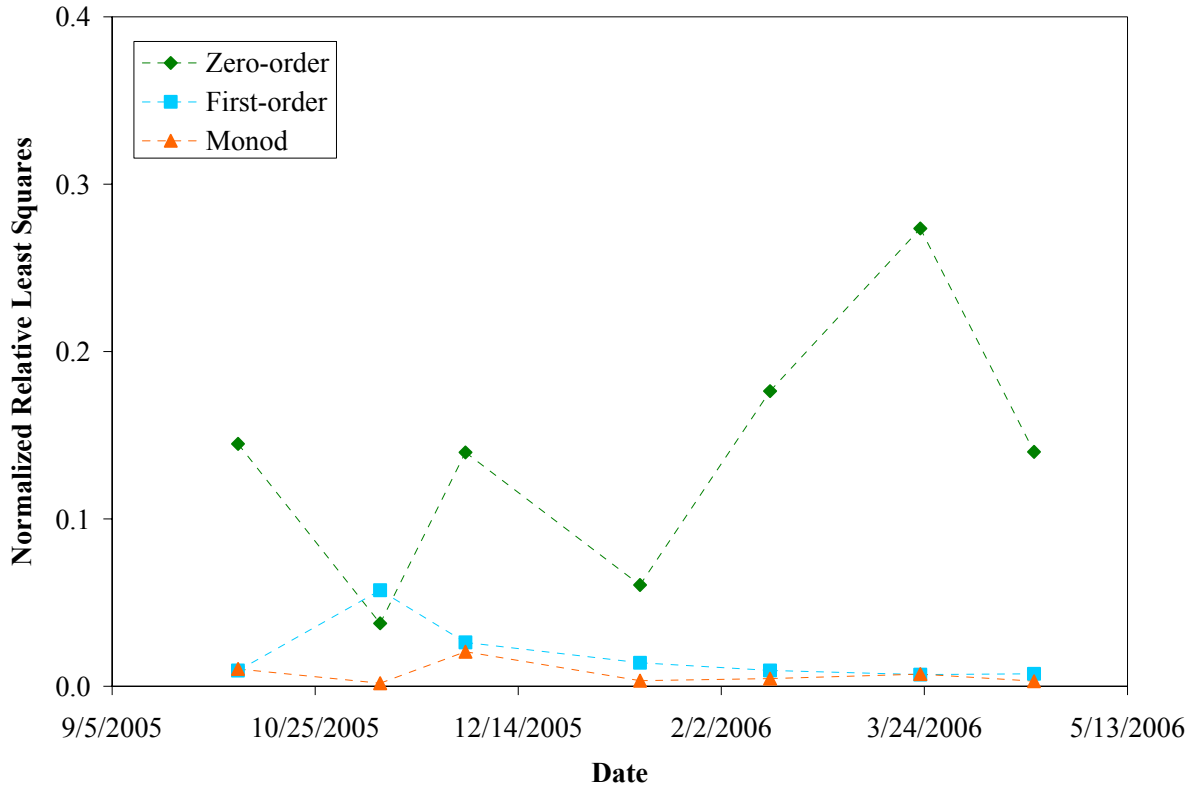

Figure 9. RLS_n results for Location C.

Zero-order, first-order, and Monod parameters were optimized, Table 4 and Figures 10–13. Scatter was observed for all kinetic parameters across the three locations. Although some scatter was recorded, the first-order k_1 values for locations B and C increased in a reasonably steady fashion. Individual Monod and zero-order constants did not exhibit such trends. Monod parameters displayed extremely high degrees of variations that were not observed in the zero- or first-order terms. All zero-order terms were lower than those reported by House with sediment of varying organics which ranged from 95 to 440 mg l^{-1} d^{-1}, Table 1 (House 2003). No k_1 values were found in literature for comparison. Despite individual Monod parameters not displaying trends, μ/K_{O2} and k_1 results were also compared to investigate if the Monod results collapse into first-order reactions, Table 4 and Figure 14. Monod did collapse into first-order reactions except for the November and December 2005 samples.

Theoretically, the kinetic parameters should be constant (Bouldin 1968; Higashino et al. 2004; House 2003). The parameter variations observed in the field results could be due to several factors such as hypolimnetic temperature changes and biochemical changes within the sediment. Edberg and Hofsten (1973) attributed *in situ* oxygen consumption variation within

sample sites to seasonal changes of benthic composition and activity, not to seasonal temperature changes. Edwards and Rolley (1965) found that significant changes of *in situ* oxygen consumption over time could be attributed to seasonal growth of benthic algae. These studies here specifically addressed the relationships between SOD and sediment biochemical transformations. However, correlations to oxygen and sediment-oxygen kinetics are intuitive and the concept can also translate to biochemical changes affecting sediment-oxygen kinetic parameters. House (2003) also reported this relationship based on a series of river sediment experiments.

Diffuser oxygenation varied over the course of the experiments. It was reasonable to expect that benthic microbial communities and chemical processes changed in response to the plentiful supply of oxygen. If biochemical changes did occur, the biochemical kinetics would change accordingly. The general trend seen in the first-order k_1 values for locations B and C may be due to aerobic microbial populations growing as DO was supplied over time and then stabilizing. The reflections of the probable microbial changes in the k_1 trends supported the preference of first-order reactions over zero-order in representing the system. The zero-order parameter values did not conform to any consistent trend.

Table 4. Summary of kinetic parameter results for field experiments.

Location A					
Date	**A, mg l^{-1} d^{-1}**	**k_1, d^{-1}**	**μ, mg l^{-1} d^{-1}**	**K_{O2}, mg l^{-1}**	**μ/K_{O2}, d^{-1}**
10/6/2005	0.07	0.7	57	17	3.4
11/10/2005	65	115	185	0.9	206
12/1/2005	39	91	422	4	106
1/13/2006	2	19	390	19	21
2/14/2006	15	76	2490	32	78
3/23/2006	64	93	2983	31	96
4/20/2006	32	47	2189	46	48
Location B					
Date	**A, mg l^{-1} d^{-1}**	**k_1, d^{-1}**	**μ, mg l^{-1} d^{-1}**	**K_{O2}, mg l^{-1}**	**μ/K_{O2}, d^{-1}**
10/6/2005	2	10	266	31	8.6
11/10/2005	46	32	59	0.1	590
12/1/2005	12	50	23	0.1	230
1/13/2006	15	96	6488	67	97
2/14/2006	35	94	5876	62	95
3/23/2006	71	106	4985	47	106
4/20/2006	35	122	6959	56	124
Location C					
Date	**A, mg l^{-1} d^{-1}**	**k_1, d^{-1}**	**μ, mg l^{-1} d^{-1}**	**K_{O2}, mg l^{-1}**	**μ/K_{O2}, d^{-1}**
10/6/2005	56	60	3367	55	61
11/10/2005	58	66	101	0.4	253
12/1/2005	13	85	95	0.9	106
1/13/2006	44	80	297	3	99
2/14/2006	50	91	626	6	104
3/23/2006	71	93	4172	44	95
4/20/2006	56	89	522	5	104

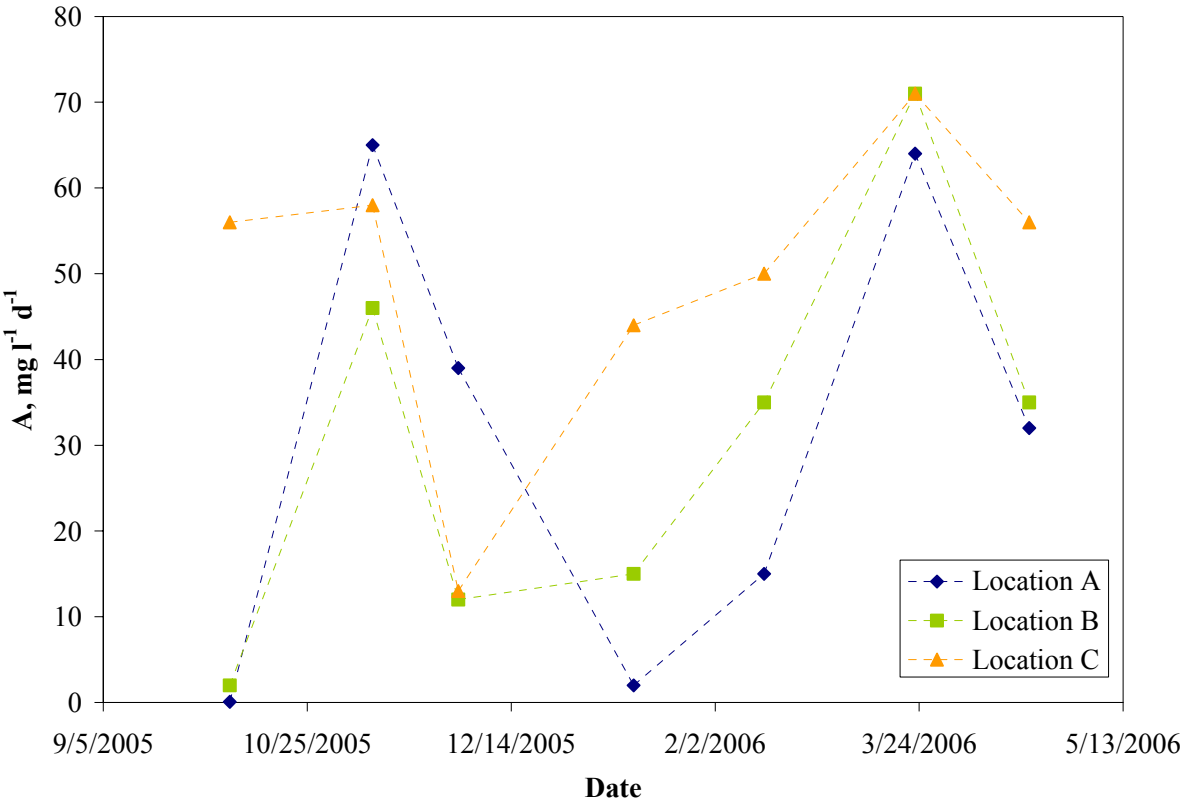

Figure 10. Zero-order parameter (A) results for reservoir experiments.

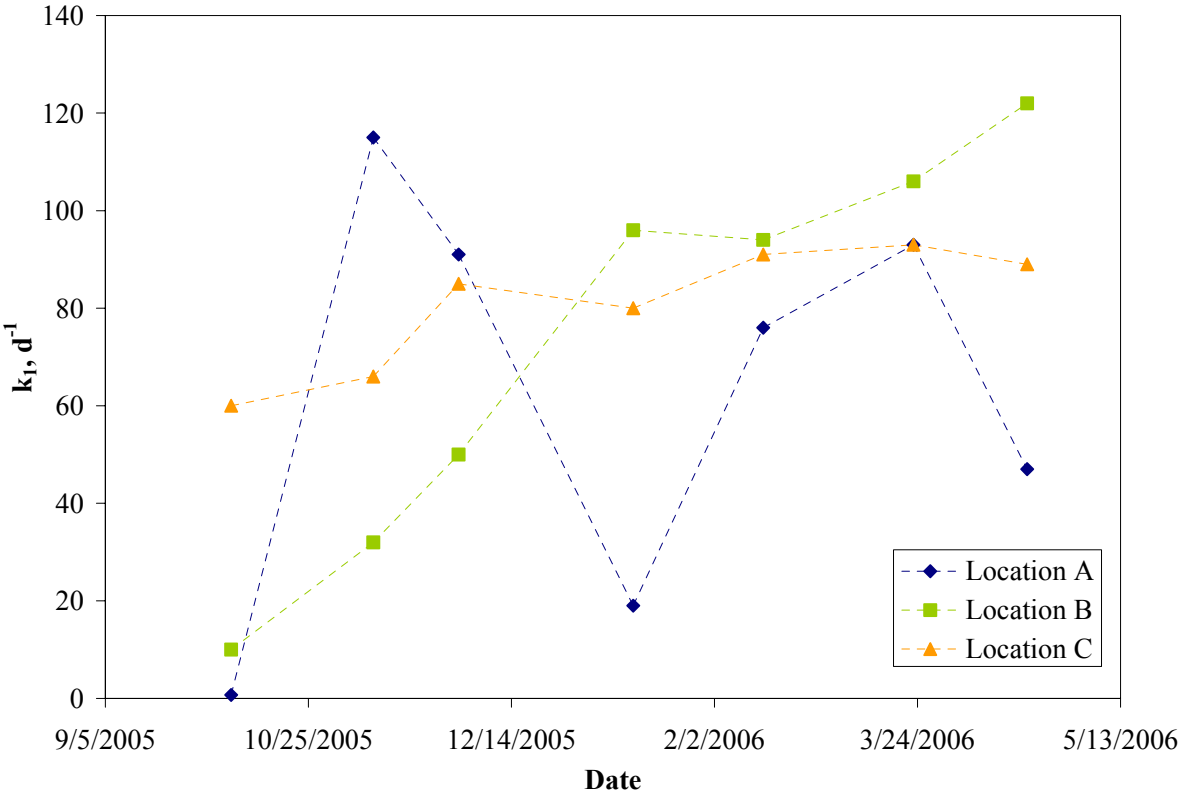

Figure 11. First-order parameter (k_1) results for reservoir experiments.

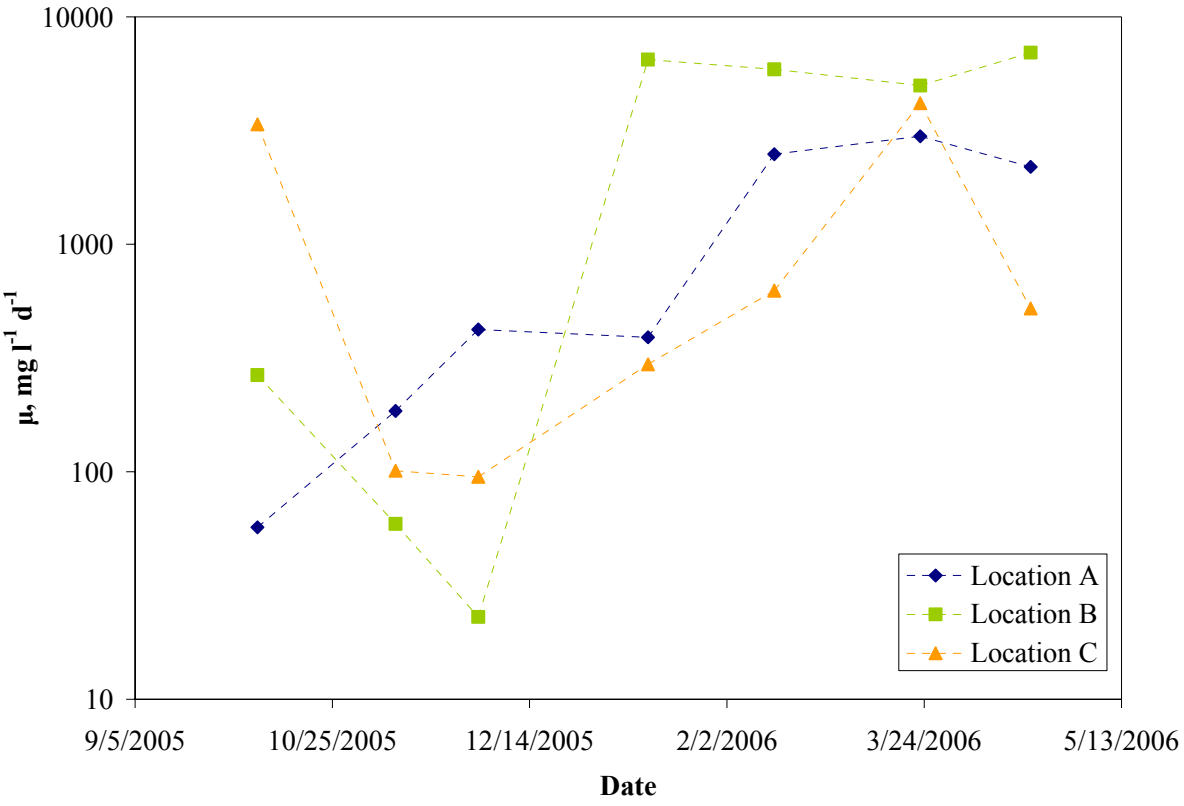

Figure 12. Monod parameter (μ) results for reservoir experiments.

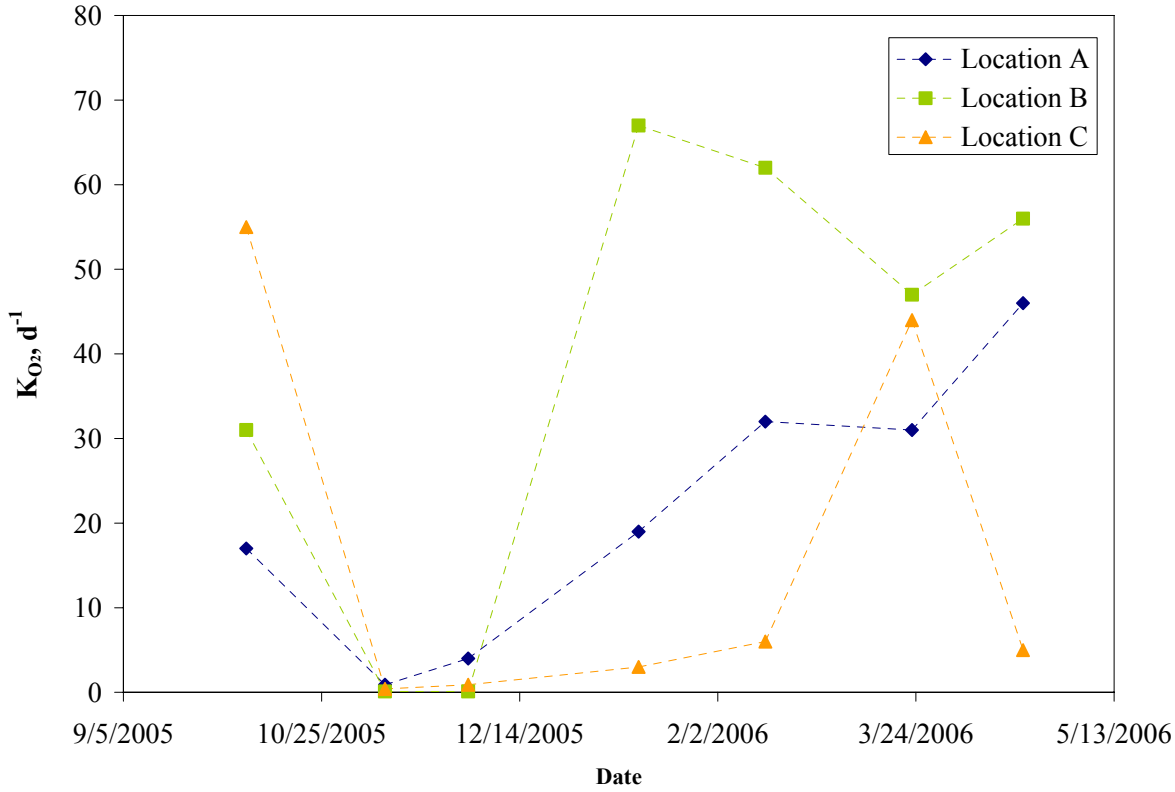

Figure 13. Monod parameter (K_{O2}) results for reservoir experiments.

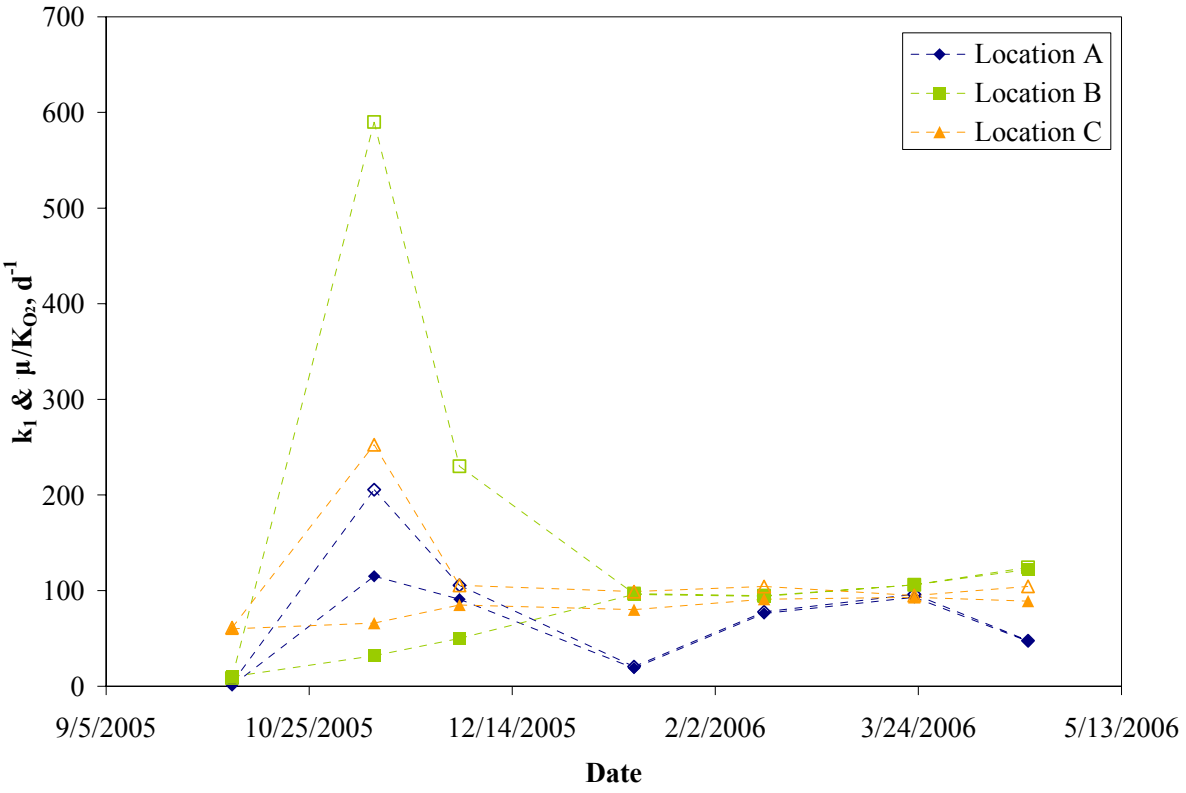

Figure 14. First-order parameter (k_1) and Monod parameters (μ/K_{O2}) plotted to inspect if Monod collapsed into first-order reactions for field experiments.

Laboratory DO profiles

The DO microgradients of 4°C Core A illustrate the observed profiles, Figures 15 and 16. Examples of both oxic to anoxic and anoxic to oxic cycles are shown. A DBL was observed for all profiles, as indicated by the linear gradient above the sediment surface (Arega and Lee 2005; Jorgensen and Revsbech 1985). As expected, during the quiescent oxic to anoxic phase, the thickness of the DBL increased and oxygen penetration depth into the sediment decreased. Accordingly, during the turbulent anoxic to oxic phase, the thickness of the diffusive-boundary layer decreased and oxygen penetration depth into the sediment increased (Arega and Lee 2005; Lorke et al. 2003; Rasmussen and Jorgensen 1992). DBL thickness changed much more rapidly during the anoxic to oxic cycle than the oxic to anoxic cycle. This occurred because the DBL was relatively thick at the end of the oxic to anoxic cycle as seen in the t=96 hour due to low turbulence. When turbulence was reintroduced by the mini-diffuser at the start of the anoxic-oxic cycle, DBL thickness immediately decreased, DO transport into the sediment increased as did DO penetration depth.

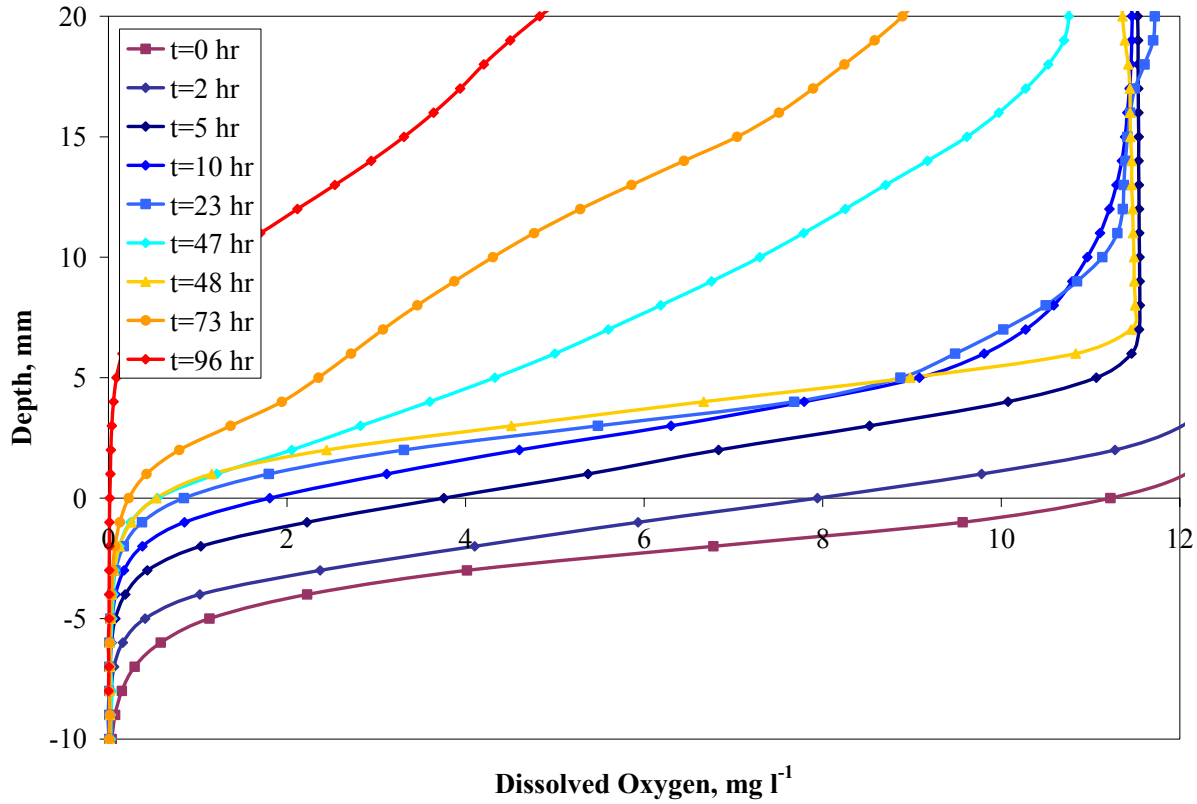

Figure 15. 4°C Core A, observed profiles during oxic to anoxic cycle.

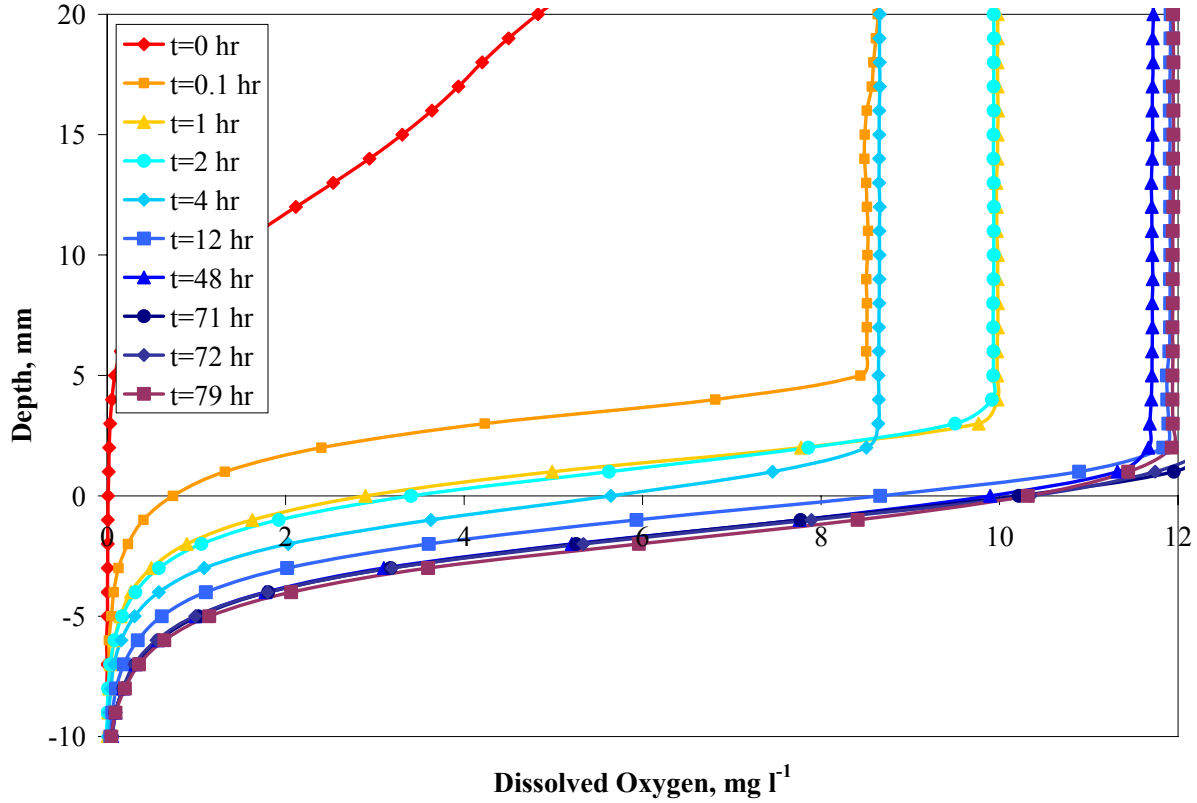

Figure 16. 4°C Core A, observed profiles during anoxic to oxic cycle.

Laboratory kinetics

The WLS_n for the laboratory models were calculated, Table 5 and Figure 17. All plots are shown in Appendix B. Similar to the field kinetic results, Monod simulations exhibited the best fit to the observed profiles with the lowest WLS_n and the first-order models fit almost as well as Monod. Overall, zero-order simulations fitted the oxygen profiles less well. As with the field experiments, first-order kinetics was preferred because there was only one fitting parameter. Another laboratory study utilizing fluctuating air flow over lake sediment also found that first-order reactions best represented the profiles obtained, although no values were provided for the rate constant (Beutel et al. 2007). Consistently, the WLS_n was higher during the anoxic-oxic cycle than the oxic-anoxic cycle. This may be due to the kinetic reactions occurring rapidly with the introduction of turbulence, causing a quick decrease in the DBL.

To better illustrate the model differences, the simulated curves for zero-order, first-order, and Monod are also displayed, Figures 17–19. Only the model results for the de-oxygenation cycle at 4°C in core B are presented in this section. The convergence of the transient numerical model to the steady state analytical solution is also shown for zero- and first-order models, Figures 17 and 18. The relatively poor fit of zero-order and good agreements of Monod and first-order were visually evident. All simulated model profiles were plotted, Appendix B.

Optimized kinetic parameters were calculated, Table 6 and Figures 21 and 22. To investigate if the first-order was preferred due to Monod to collapsing into first-order reactions, μ/K_{O_2} was also calculated, Table 6 and Figure 23. While the mean k_1 and μ/K_{O_2} values were not comparable, suggesting that first-order preference was independent of the Monod conditions, the standard deviations of the Monod and first-order parameters did intercept. Thus, it a definitive statement regarding the occurrence of Monod collapsing into first-order cannot be made. The 20°C zero-order, first-order, and Monod parameters were all higher than the 4°C constants. The average A value for the 20°C cores was 130 mg l^{-1} d^{-1} and was similar to those reported by House (2003) using fluvial sand and fluvial sand/silt mix sediment at 18°C, 100–150 mg l^{-1} d^{-1}. As with the field data, no k_1 values were found in the literature for comparison. The preferred fit of first-order kinetics over zero-order and Monod was supported by the relative consistency observed in k_1 between cycles and cores at 4°C. More variation was observed with the 20°C kinetic terms compared to the 4°C parameters.

Table 5. WLS_n results for laboratory experiments. Calculations were made by comparing the observed dissolved oxygen profiles with the optimized models.

Temperature	Core	Cyle	Kinetic Type	WLS_n
4°C	Core A	Oxic to Anoxic	Zero-order	0.018
			First-order	0.018
			Monod	0.001
		Anoxic to Oxic	Zero-order	0.737
			First-order	0.038
			Monod	0.005
	Core B	Oxic to Anoxic	Zero-order	0.124
			First-order	0.017
			Monod	0.004
		Anoxic to Oxic	Zero-order	0.424
			First-order	0.118
			Monod	0.029
20°C	Core C	Oxic to Anoxic	Zero-order	0.006
			First-order	0.013
			Monod	0.002
		Anoxic to Oxic	Zero-order	0.089
			First-order	0.017
			Monod	0.009
	Core D	Oxic to Anoxic	Zero-order	0.200
			First-order	0.006
			Monod	0.006
		Anoxic to Oxic	Zero-order	0.259
			First-order	0.028
			Monod	0.044

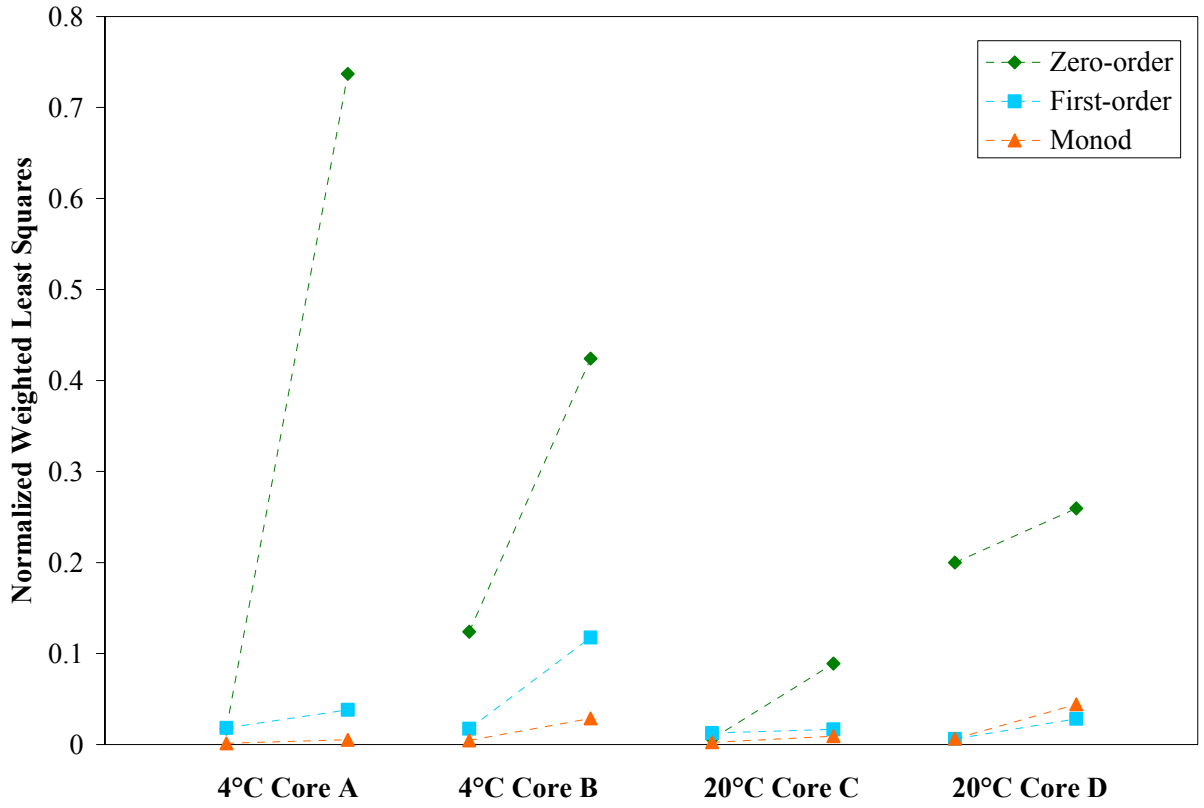

Figure 17. WLS_n results for laboratory experiments. First points within cores represent WLS_n for oxic to anoxic cycle and second points represent anoxic to oxic cycle.

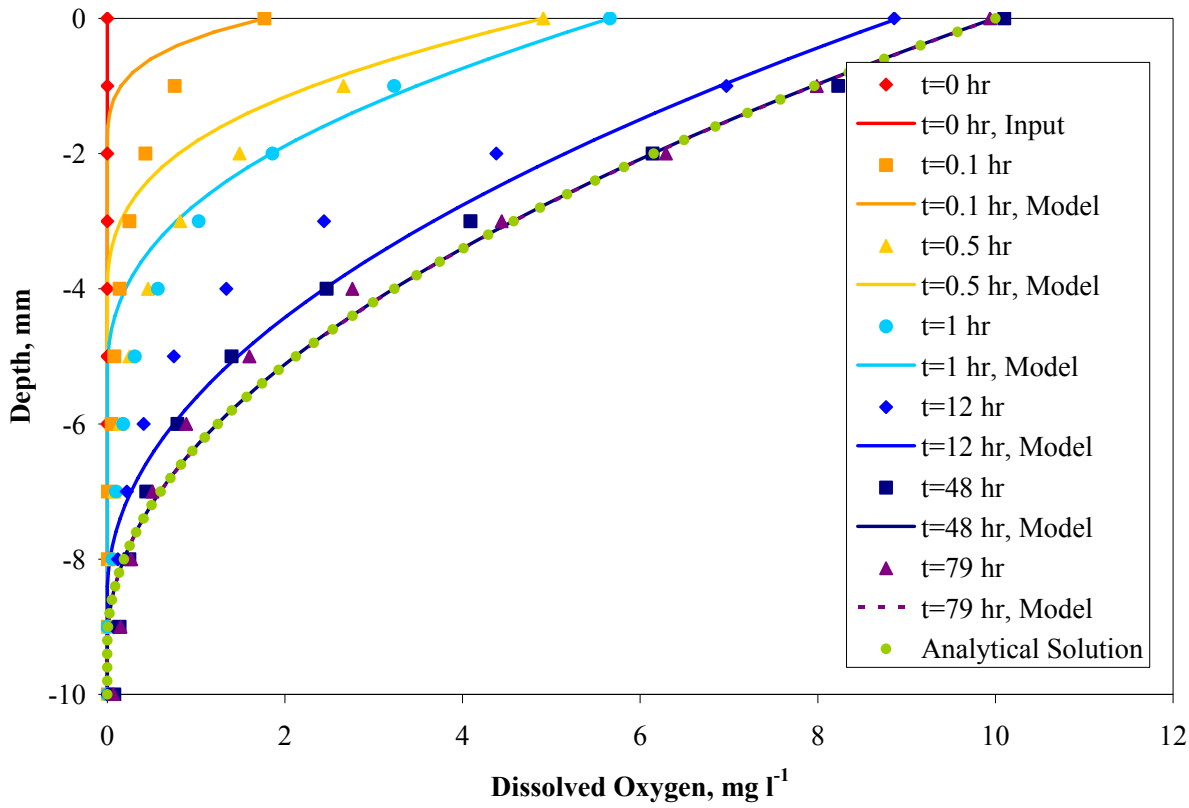

Figure 18. Zero-order model results during anoxic-oxic cycle plotted with observed profiles for 4°C Core B.

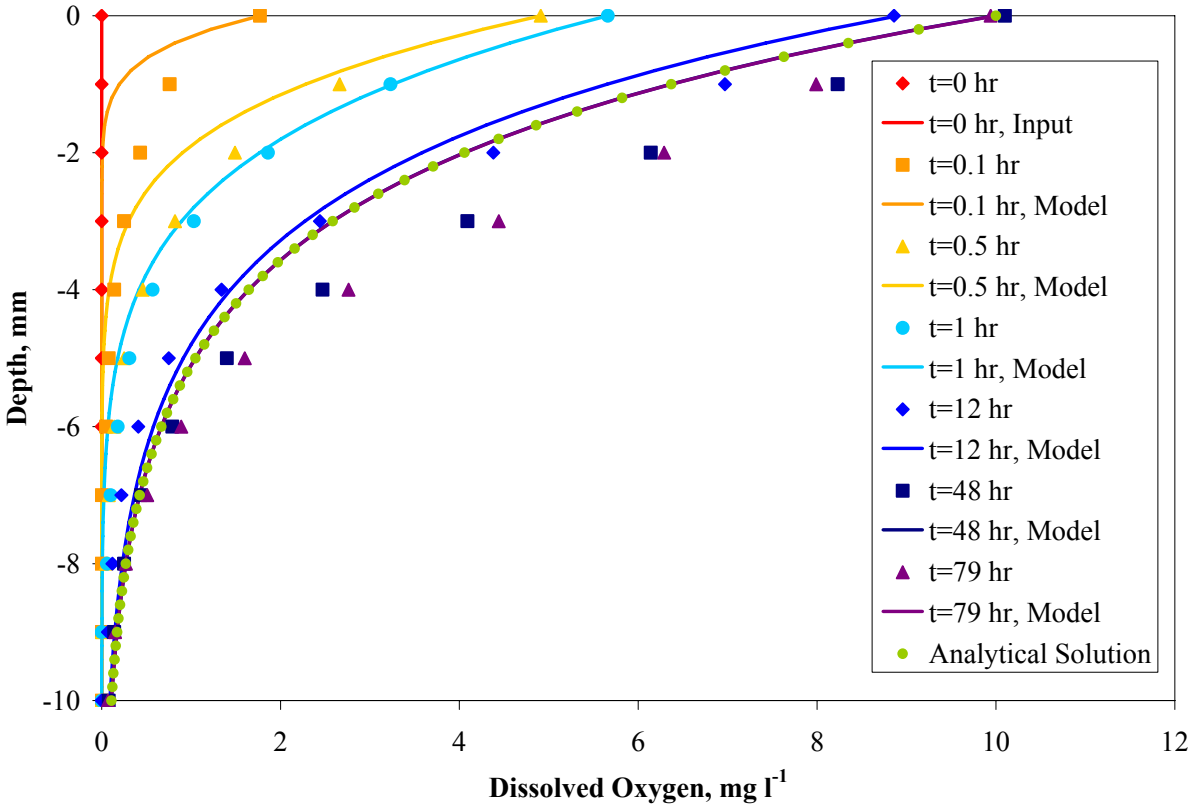

Figure 19. First-order model results during anoxic-oxic cycle plotted with observed profiles for 4°C Core B.

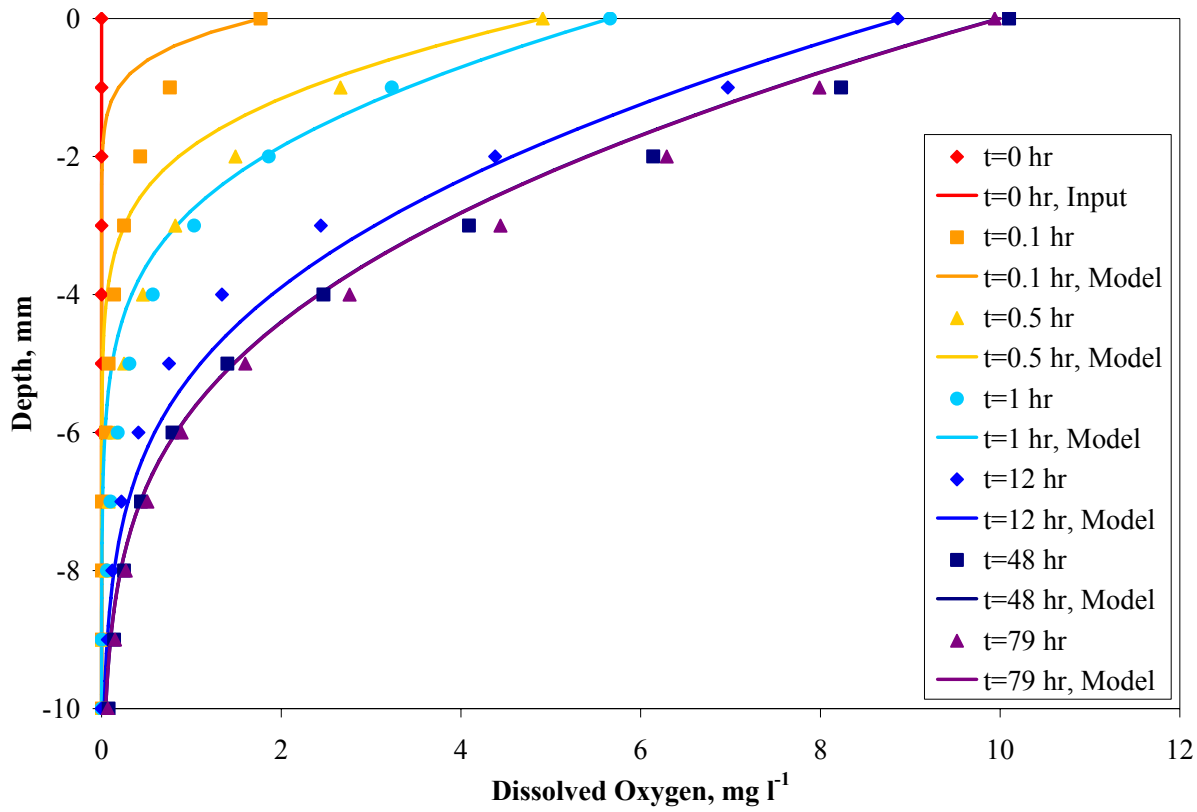

Figure 20. Monod model results during anoxic-oxic cycle plotted with observed profiles for 4°C Core B.

Table 6. Best-fit kinetic parameters for laboratory experiments with mean and standard deviation range for each temperature.

Temperature	Core	Cyle	A, mg l^{-1} d^{-1}	k_1, d^{-1}	μ, mg l^{-1} d^{-1}	K_{O2}, mg l^{-1}	μ/K_{O2}, d^{-1}
4°C	Core A	Oxic-Anoxic	47	45	62	0.13	480
		Anoxic-Oxic	33	24	64	0.82	78
	Core B	Oxic-Anoxic	38	41	130	1.4	93
		Anoxic-Oxic	24	21	47	0.70	67
		Mean+/-Stdev	36±9.6	34±12	75±35	0.77±0.53	180±200
20°C	Core C	Oxic-Anoxic	58	110	100	0.22	460
		Anoxic-Oxic	130	150	540	2.1	260
	Core D	Oxic-Anoxic	120	140	1600	10	160
		Anoxic-Oxic	220	260	1900	6	320
		Mean+Stdev	130±66	170±68	1000±850	4.6±4.3	300±125

The parameters from the 20°C experiment showed more variation than those at 4°C. This could be due to several factors. The 4°C experiment was the last experiment after a series of preliminary experiments and the 20°C experiment and the procedure may have been more refined. However, procedural differences alone probably cannot fully explain the variation in cores C and D. It was clear that steady state occurred considerably faster at 20°C than at 4°C. The slower kinetic response at 4°C allowed more information to be captured compared to 20°C. It is believed variation would be less had more data been successfully collected at 20°C.

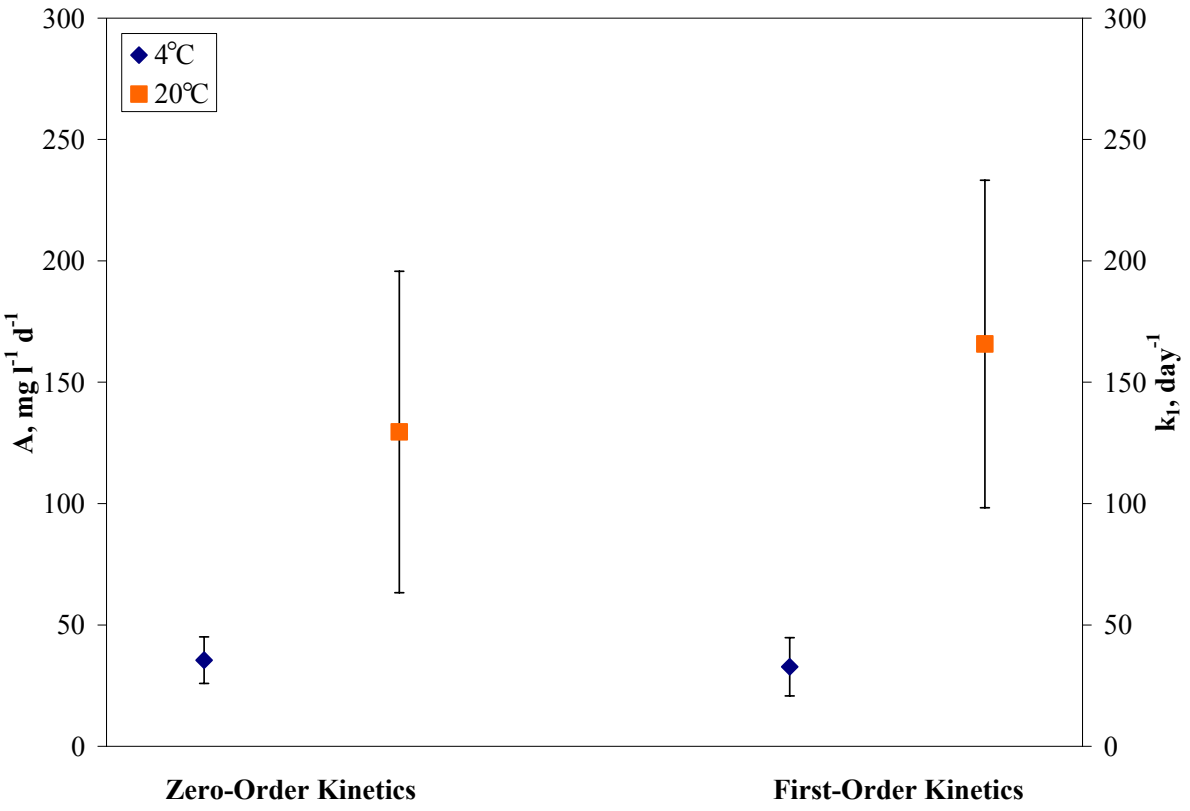

Figure 21. Mean zero-order (A) and first-order (k_1) parameters calculated from transient numerical modeling for oxic to anoxic and anoxic to oxic laboratory cycles. Error bars represent the standard deviation for each temperature.

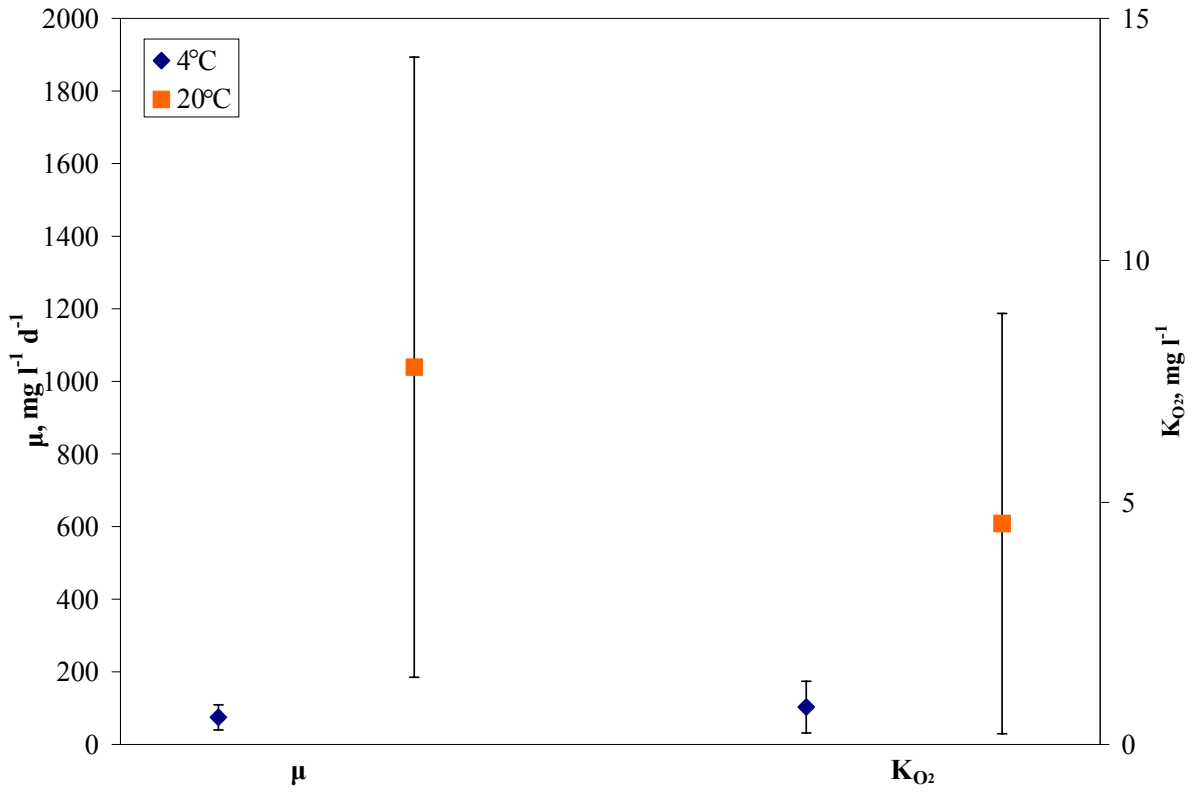

Figure 22. Results of the optimized Monod constants (μ) and (K_{O2}) from the laboratory experiments.

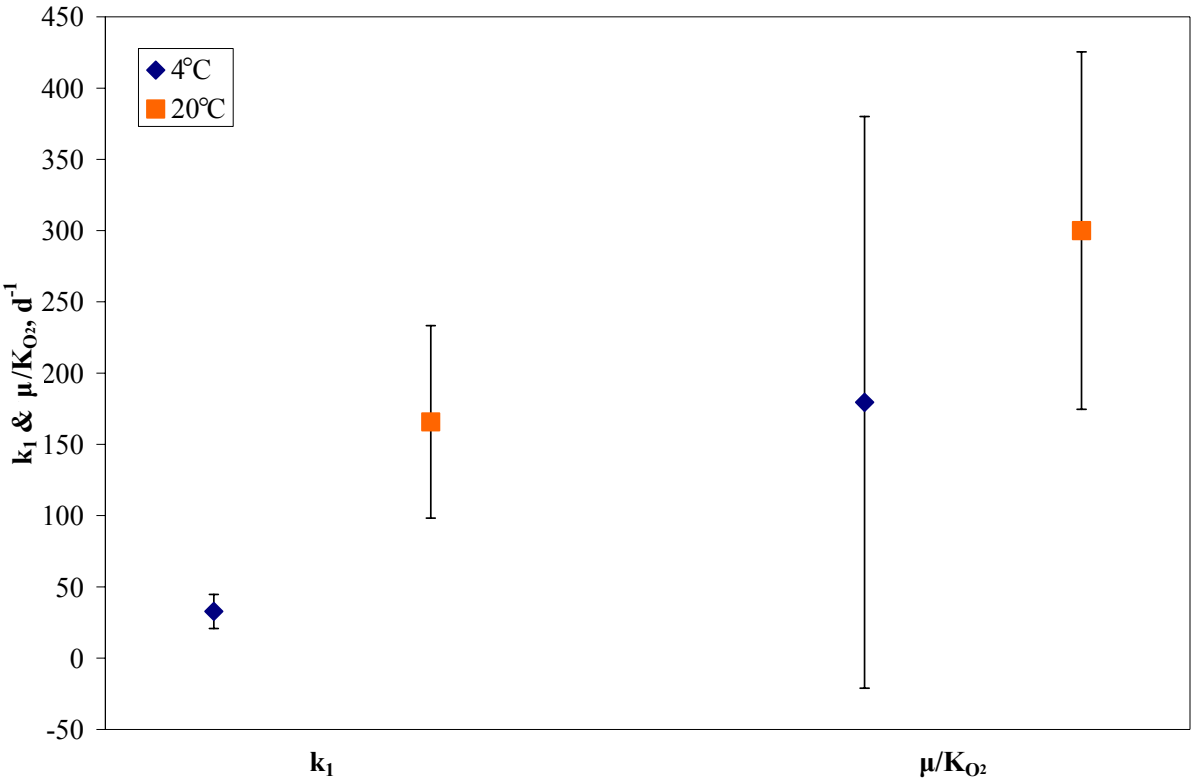

Figure 23. First-order parameter (k_1) and Monod parameters (μ/K_{O2}) plotted to inspect if Monod collapsed into first-order reactions for laboratory experiments.

Temperature effects

Zero- and first-order parameters were plotted with respect to temperature for both the field and laboratory experiments, Figures 24 and 25. To account for the fluctuating conditions in the laboratory experiments, only the mean values were plotted. Location A was excluded due to the associated instabilities. Expected trends were generally observed in the first-order results; with lower temperatures corresponding to lower kinetic parameter values (Hall et al. 1989). Numerous zero-order constants below 16°C from field experiments were less than those obtained at 4°C from the lab experiments. The general conformity of the first-order constants to the temperature relationship and the lack of conformity in the zero-order constants, adds further support to the preference of first-order over zero-order kinetics.

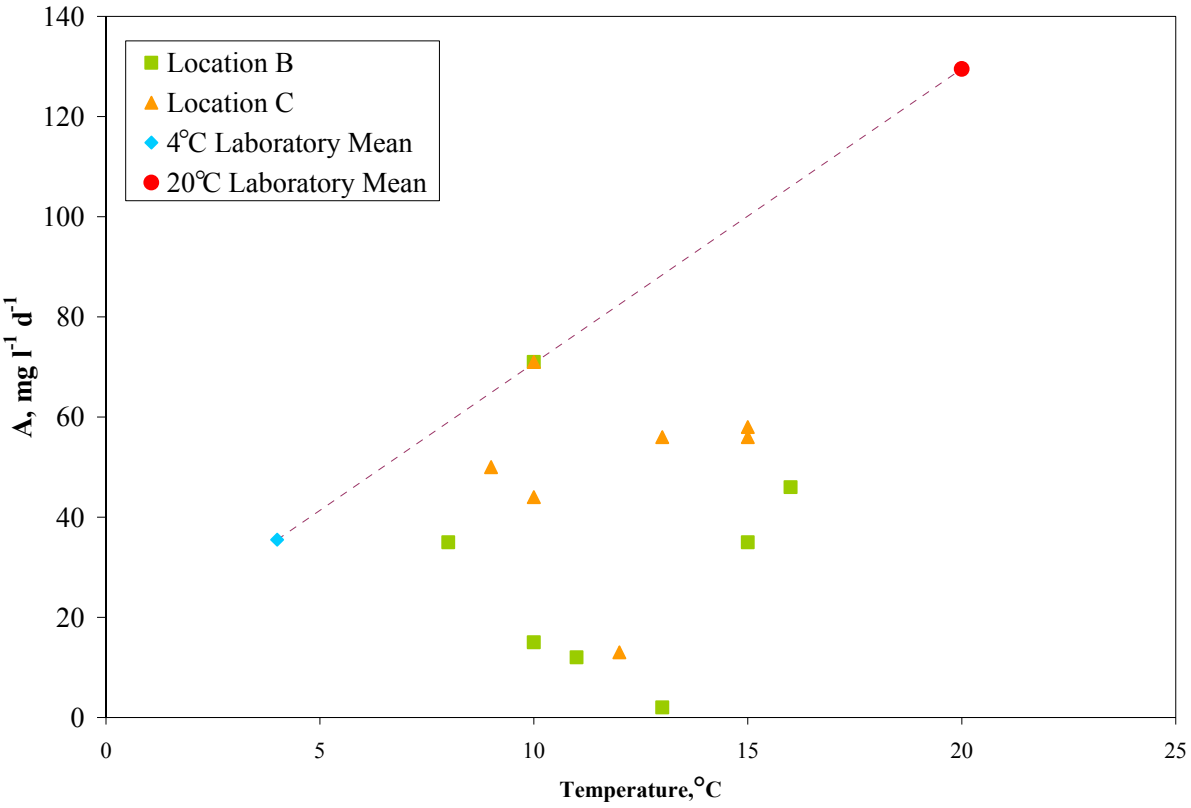

Figure 24. Zero-order parameter (A) with respect to temperature for field and mean laboratory results.

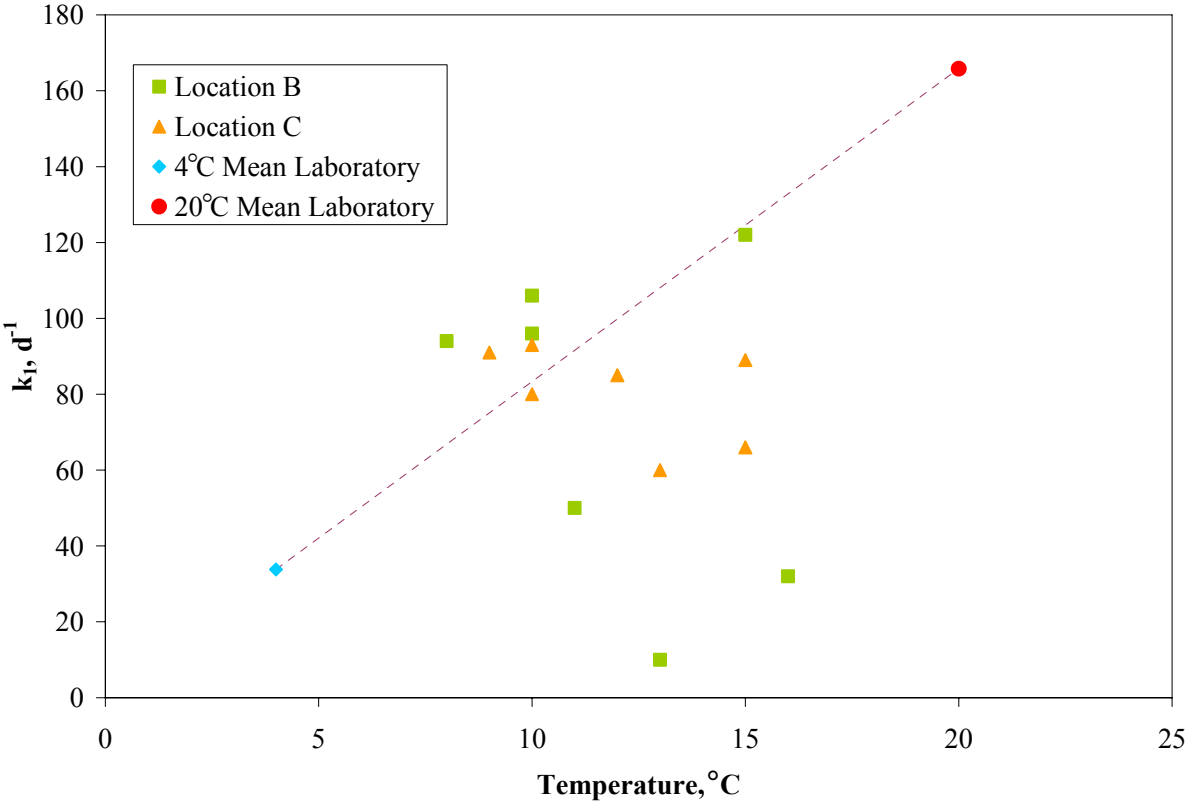

Figure 25. First-order parameter (k_1) with respect to temperature for field and mean laboratory results.

Sediment oxygen demand

The best-fit models were used to calculate field SOD values, Figure 26. The field results illustrated the influence of DO concentration and turbulence on SOD (Arega and Lee 2005 and others; Nakamura and Stefan 1994; Rasmussen and Jorgensen 1992). Field SOD appeared to reflect the fluctuating flow rates of the diffusers. The suggested lag time associated with location A was indicated by comparing the SOD responses at A to those at locations B and C. When diffusers B and C were turned off in October 2005, SOD decreased at all locations and faster at locations B and C than at location A. When diffuser C was turned on again in December 2005, SOD increased at location C but location A did not increase until January when diffusers B and C were back on. When both diffusers were on again, all locations exhibited increasing SOD. Within one month of the January diffuser flow change, locations B and C appeared to begin reaching steady state. These trends of SOD uniformity after an increase may have been due to microbial communities adapting to the changing reservoir conditions, multiplying, and reaching a new steady state as suggested by Edberg and Hofsten (1973).

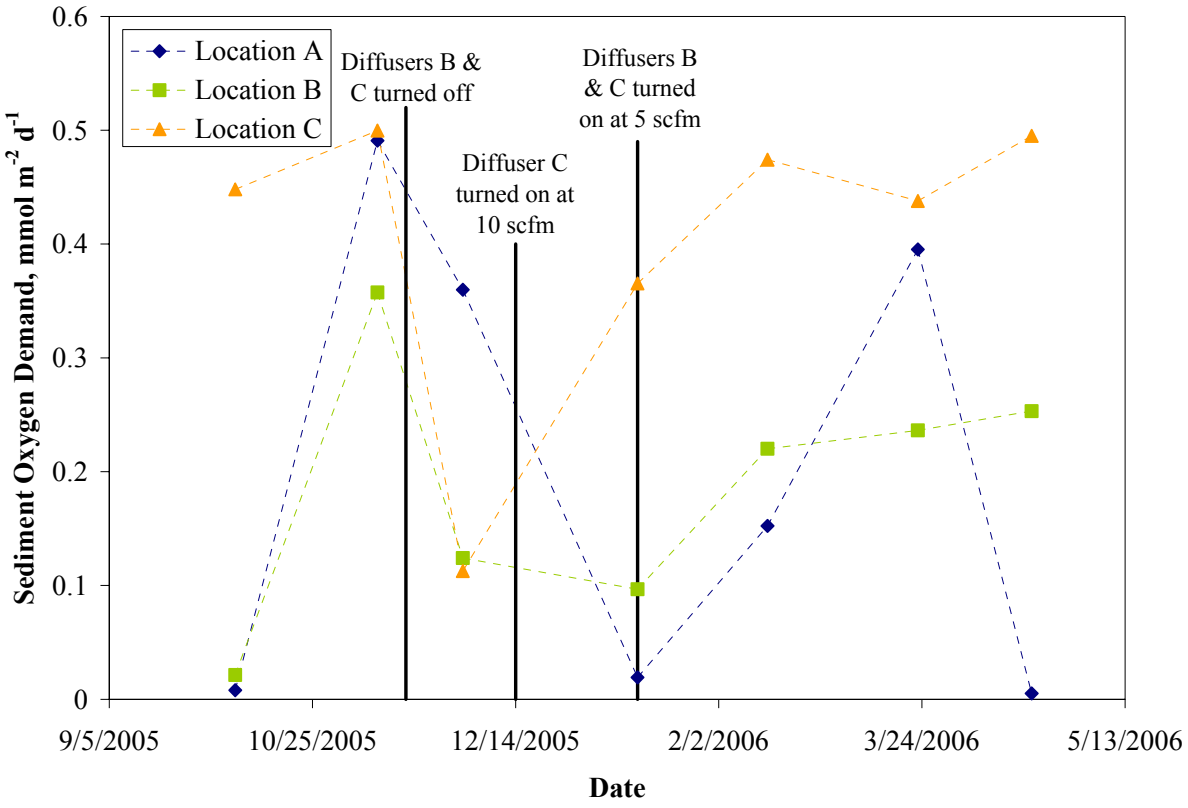

Figure 26. SOD results for field experiment with diffuser schedule.

Reservoir SOD changed over time. However, changes did not necessarily mean that the reservoir was at unsteady state at the time of sampling. Studies have shown that depending on sediment dynamics, steady state was usually achieved within minutes to hours (Beutel et al. 2007; Higashino et al. 2004; House 2003). Samples were taken at least ten days after diffuser flow changes took place. The reservoir sediment being at near steady state conditions during sampling remains a reasonable assumption.

The 4°C and 20°C SOD calculations for the oxic-anoxic and anoxic-oxic cycles were based on the simulated curves best representing the observed data, Figures 27 and 28. At both temperatures, SOD decreased during the oxic to anoxic cycles and increased during the anoxic to oxic cycle. Similar to the laboratory kinetic results, the two 4°C runs had comparable SOD values while the 20°C did not.

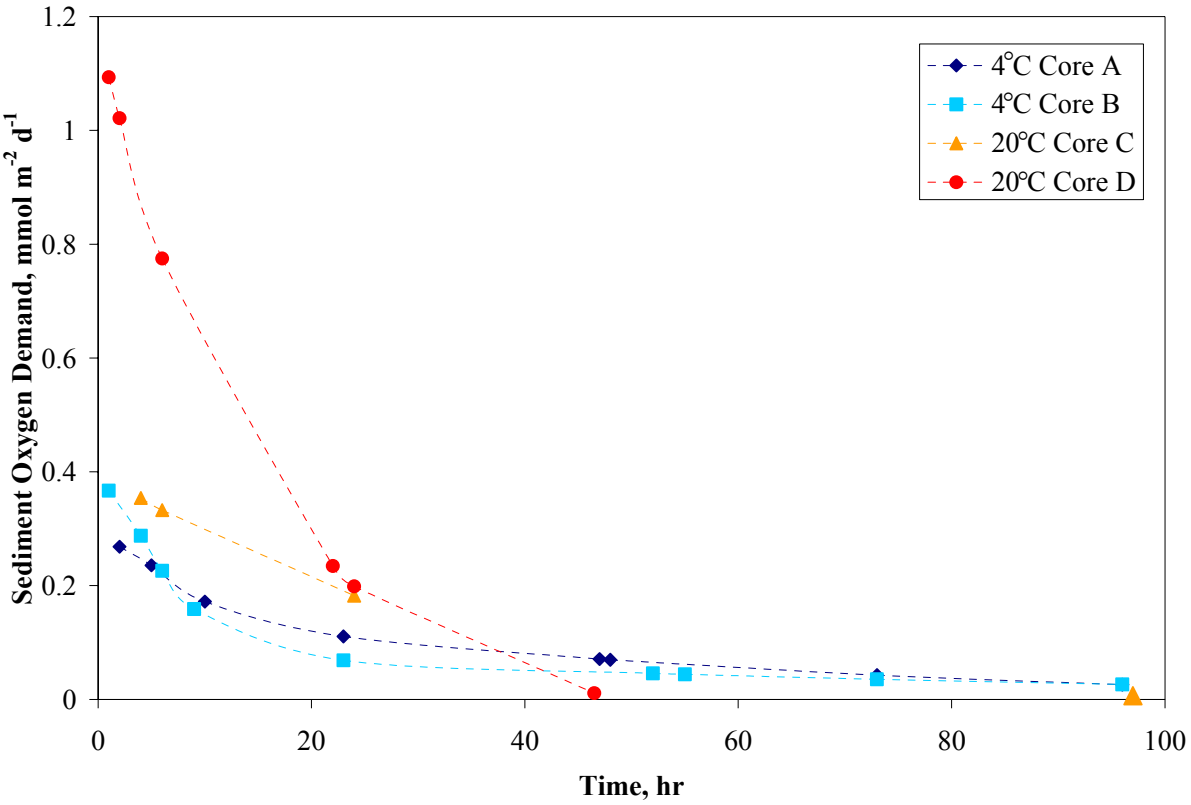

Figure 27. Sediment oxygen demand results for oxic to anoxic laboratory cycle.

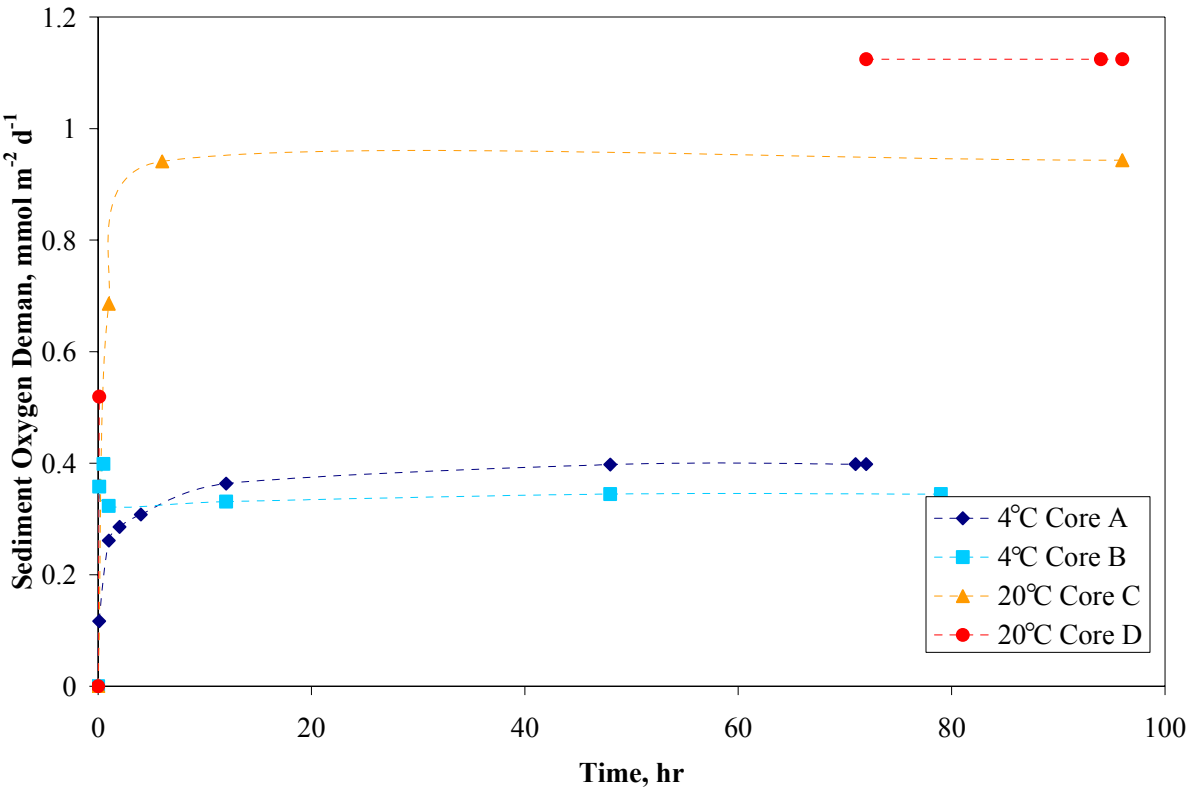

Figure 28. Sediment oxygen demand results for anoxic to oxic laboratory cycle.

Laboratory SOD values reproduced trends similar to the field results and previous studies (Arega and Lee 2005; Beutel et al. 2007; Nakamura and Stefan 1994; Revsbech et al. 1980). As discussed, SOD was strongly dependent on turbulence in the overlying water and the sediment-water interface DO concentration. During the oxic-anoxic cycle, SOD values were not influenced by turbulence due to quiescent conditions. However, during anoxic-oxic cycles, cores were affected by turbulence and DO concentration due to the mini-diffusers being on.

Similar to the zero- and first-order kinetic parameter observations, at steady state oxic conditions, 20°C sediment initially produced higher SOD values than 4°C sediment. As shown by core D, over time the 20°C oxic-anoxic SOD decreased below the 4°C values. The time to anoxia of Core D was supported by core C's sediment surface DO concentrations and 20°C preliminary experiments. During the oxic-anoxic cycle, core C profiles created between 24 and 97 hours could not be used due to microelectrode malfunction. It is believed that had more profiles been successful between 24 and 97 hours, core C SOD would have reached anoxia before the 4°C cores like core D due to faster kinetics at higher temperatures (Hall et al. 1989).

An intriguing pattern developed in the SOD values of 4°C core B when time was less than 1 hr. The SOD increased quickly during this time period then decreased after 1 hr. The observed SOD results were due to the steep oxygen gradient corresponding to this period of transition away from complete sediment anoxia. The slope was extremely steep because the DO concentration at the interface increased quickly due to the decreased DBL and the DO penetration depth remained small due to the recent anoxic status. It is speculated that all cores would have displayed a similar pattern had profiles been successfully captured during the very initial stages of the anoxic to oxic cycles. On the other hand, it is not believed that this pattern occurred in the initial phases of the oxic-anoxic cycle. At that time, the DBL in contact with the sediment was still oxic and supplied oxygen to the sediment for quite some time during this phase as suggested by 4°C and 20°C SOD times to steady state. Steady state was attained significantly slower over the oxic to anoxic cycles and much more rapidly during the anoxic to oxic cycles.

If SOD changed over time while the sample was at a constant temperature, the changes may have been due to a decrease in porosity (from sediment settling after extraction in the field) or shifting biochemical processes (Bouldin 1968). While some settling may have taken place, it was considered negligible compared to the influence of DO concentration at the sediment-water interface and water column turbulence.

Conclusions

A study of benthic sediment oxygen microprofiles was made and the DO profiles of reservoir field conditions and manipulated laboratory conditions reported. It was demonstrated that simulations based on zero-order, first-order, and Monod kinetics could be compared to the study's observed field and laboratory profiles. In field and laboratory experiments using Carvin's Cove sediment, Monod and first-order kinetics models agreed well with observed data but zero-order did not. According to the principle of Occam's razor, first-order kinetics was preferred to Monod (Jaynes 2003). Field and laboratory first-order rate constants were found to increase with temperature. Also, as anticipated, field and laboratory SOD values increased with increased DO and turbulence.

Field and laboratory experiments suggested that diffuser influenced SOD in Carvin's Cove followed first-order kinetics. However, it was difficult to make a definitive conclusion

about the best kinetics for Carvin's Cove SOD without having *in situ* measurements due to the inherent sediment disturbances associated with sediment extraction. This study is currently being expanded to *in situ* experiments within Carvin's Cove that will be conducted with an automated, microprofiling lander. The variability of *in situ* first order constants values may be significantly less than values determined from extracted cores because the sediment structure will remain intact. This would provide greater support for the suggestion that first-order reactions characterize Carvin's Cove SOD.

References

Arega, F., and Lee, J. (2005). "Diffusional Mass Transfer at Sediment-Water Interface of Cylindrical Sediment Oxygen Demand Chamber." *Journal of Environmental Engineering*, 131(5), 755-766.

Beutel, M., Burley, N., and Culmer, K. (2006). "Quantifying the effects of water velocity and oxygen concentration on sediment oxygen demand." *Hydrologic Sciences and Technology Journal*, 24(4), 1-13.

Beutel, M., Hannoun, I., Pasek, J., and Kavanagh, K. (2007). "Evaluation of hypolimnetic oxygen demand in a large eutrophic raw water reservoir, San Vicente Reservoir, California." *Journal of Environmental Engineering*, 133(2), 130-138.

Bouldin, D. (1968). "Models for describing the diffusion of oxygen and other mobile constituents across the mud-water interface." *Journal of Ecology*, 56(1), 77-87.

Brewer, W., Abernathy, A., and Paynter, M. (1977). "Oxygen consumption by freshwater sediments." *Water Research*, 11, 471-473.

Bryant, L., and Little, J. "Transient variation in sediment oxygen demand as a function of diffuser-induced turbulence." *10th European workshop on physical processes in natural waters*, Granada, Spain, 117-126.

Clark, M. (1996). *Transport modeling for environmental engineers and scientists*, John Wiley & Sons, Inc., New York.

Edberg, N., and Hofsten, B. (1973). "Oxygen uptake of bottom sediments studied in situ and in the laboratory." *Water Research*, 7, 1285-1294.

Edwards, R., and Rolley, H. (1965). "Oxygen consumption of river muds." *The Journal of Ecology*, 53(1), 1-19.

Hall, H., Anderson, L., Loeff, M. R. v. d., Sundby, B., and Westerlund, S. (1989). "Oxygen uptake kinetics in the benthic boundary layer." *Limnology and Oceanography*, 34(4), 734-746.

Hem, J. (2005). *Study and interpretation of the chemical characteristics of natural water*, University Press of the Pacific, Honolulu, HI.

Higashino, M., Gantzer, C., and Stefan, H. (2004). "Unsteady diffusional mass transfer at the sediment/water interface: Theory and significance for SOD measurement." *Water Research*, 38, 1-12.

House, W. (2003). "Factors influencing the extent and development of the oxic zone in sediment." *Biogeochemistry*, 63, 317-333.

Jaynes, E. (2003). *Probability Theory: The Logic of Science* Cambridge University Press, New York, NY.

Jorgensen, B., and Revsbech, N. (1985). "Diffusive boundary layers and the oxygen uptake of sediments and detritus." *Limnology and Oceanography*, 30(1), 111-122.

Jubb, S., Guymer, I., Licht, G., and Prochnow, J. (2001). "Relating oxygen demand to flow: development of an in situ sediment oxygen demand measurement device." *Water Science and Technology*, 43(5), 203-210.

Lewandowski, Z., Walser, G., and Characklis, W. (1991). "Reaction kinetics in biofilms." *Biotechnology and Bioengineering*, 38, 877-882.

Little, J., Hodgson, A., and Gadgil, A. (1994). "Modeling emissions of volatile organic compounds from new carpets." *Atmospheric Environment*, 28(2), 227-234.

Lorke, A., Muller, B., Maerki, M., and Wuest, A. (2003). "Breathing sediment: The control of diffusive transport across the sediment-interface by periodic boundary-layer turbulence." *Limnology and Oceanography*, 48(6), 2077-2085.

Moore, B., Chen, P., Funk, W., and Yonge, D. (1996). "A model for predicting lake sediment oxygen demand following hypolimnetic aeration." *Water Resources Bulletin*, 32(4), 723-731.

Nakamura, Y., and Stefan, H. (1994). "Effect of flow velocity on sediment oxygen demand: theory." *Journal of Environmental Engineering*, 120(5), 996-1016.

Press, W., Flannery, B., Teukolsky, S., and Vetterling, W. (1990). *Numerical Recipes: The Art of Scientific Computing (FORTRAN version)*, Cambridge University Press, Cambridge, MA.

Rasmussen, H., and Jorgensen, B. (1992). "Microelectrode studies of seasonal oxygen uptake in a coastal sediment: role of molecular diffusion." *Marine Ecology Progress Series*, 81, 289-303.

Revsbech, N., Madsen, B., and Jorgensen, B. (1986). "Oxygen production and consumption in sediments determined at high spatial resolution by computer simulation of oxygen microelectrode data." *Limnology and Oceanography*, 31(2), 293-304.

Revsbech, N., Sorensen, J., Blackburn, T., and Lomholt, J. (1980). "Distribution of oxygen in marine sediments measured with microelectrodes." *Limnology and Oceanography*, 25(3), 403-411.

Saez, P., and Rittman, B. (1992). "Model-parameter estimation using least squares." *Water Research*, 26(6), 789-796.

Singleton, V., and Little, J. (2006). "Designing hypolimnetic aeration and oxygenation systems-a review." *Environmental Science and Technology*, 40, 7512-7520.

Viessman, W., and Hammer, M. (1998). *Water Supply and Pollution Control*, Addison-Wesley, Menlo Park, CA.

Wang, W. (1981). "Kinetics of sediment oxygen demand." *Water Research*, 15, 475-482.

Wetzel, R. (2001). *Limnology: Lake and river ecosystems*, Academic Press, San Diego.

Wiltshire, K., Schroeder, F., H. Knauth, and Kausch, H. (1996). "Oxygen consumption and production rates and associated fluxes in sediment-water systems: A combination of microelectrode, incubation and modeling techniques." *Archiv für Hydrobiologie* 137(4), 457-486.

Appendix A

Examples of iterative solutions for location A October 10, 2005 sampling are shown below.

```
%Example of October, 2005 models
SED;
RSS_depth;
dy;

depth_mm=(0:-dy:SED);
depth_model_mm=(0:-dy:SED)

Ds_10_06_05=0.0000150790095741924; %Sediment diffusion coefficients
RawData_10_06_05=[.224
0.262
0.224
0.207
0.178
0.132
0.112
0.106
0.078
0.080
0.075];

%Zero-order, analytical solution
RSS_check=10*10^20;
for A_mgPERliterday=0.01:.01:0.1
    A=A_mgPERliterday/(24*60^2);
    Model_0Order_10_06_05=zeros(SED/dy+1,1);
    Cmax=RawData_10_06_05(1,1);
    for i=1:SED/dy+1
      Model_0Order_10_06_05(i,1)=(A/(2*Ds_10_06_05))*((-depth_mm(i,1))^2)-
(2*Cmax*A/(Ds_10_06_05))^0.5*(-depth_mm(i,1))+Cmax;
      if i>1
        if Model_0Order_10_06_05(i-1,1)<Model_0Order_10_06_05(i,1)
        Model_0Order_10_06_05(i,1)=0;
        else Model_0Order_10_06_05(i,1)=Model_0Order_10_06_05(i,1)
        end
      end
    end;
    for r=1:(RSS_depth+1)
      if (RawData_10_06_05(r,1)-Model_0Order_10_06_05(r,1))>=-0.01 & (RawData_10_06_05(r,1)-
Model_0Order_10_06_05(r,1))<=0.01
        RSS_10_06_05(r,1)=0;
      elseif r==1;
        RSS_10_06_05(r,1)=0;
      else RSS_10_06_05(r,1)=((RawData_10_06_05(r,1)-
Model_0Order_10_06_05(r,1))/RawData_10_06_05(r,1))^2;
      end;
    end;
    RSS_10_06_05_sum=sum(RSS_10_06_05);
        if RSS_10_06_05_sum<RSS_check
          RSS_check=RSS_10_06_05_sum
          RSS_FINAL_10_06_05=RSS_10_06_05_sum;
          A_mgPERliterday_10_06_05=A_mgPERliterday
```

```
                Profiles_10_06_05=Model_0Order_10_06_05;
                RSS_MATRIX_FINAL_10_06_05=RSS_10_06_05;
              end;
end;
for i=1:1:31
Profiles_10_06_05_plot(i,1)=(A/(2*Ds_10_06_05))*((-depth_model_mm(i,1))^2)-
(2*Cmax*A/(Ds_10_06_05))^0.5*(-depth_model_mm(i,1))+Cmax;
      if i>1
         if Profiles_10_06_05_plot(i-1,1)<Profiles_10_06_05_plot(i,1);
         Profiles_10_06_05_plot(i,1)=0;
         else Profiles_10_06_05_plot(i,1)=Profiles_10_06_05_plot(i,1);
         end
      end
end;

%First-order, analytical solution
for k1_PERday=.55:.05:2
    k1=k1_PERday/(24*60^2);
    Model_1Order_10_06_05=zeros(SED/dy+1,1);
    Cmax=RawData_10_06_05(1,1);
    for i=1:SED/dy+1
       Model_1Order_10_06_05(i,1)=Cmax*exp(-(-depth_cm(i,1)/((Ds_10_06_05/k1)^0.5)));
       if Model_1Order_10_06_05(i,1)<0
          Model_1Order_10_06_05(i,1)=0;
       end;
    end;
    for r=1:(RSS_depth+1)
       if (RawData_10_06_05(r,1)-Model_1Order_10_06_05(r,1))>-0.0001 & (RawData_10_06_05(r,1)-
Model_1Order_10_06_05(r,1))<0.0001
          RSS_10_06_05(r,1)=0;
       elseif r==1
          RSS_10_06_05(r,1)=0;
       else RSS_10_06_05(r,1)=((RawData_10_06_05(r,1)-
Model_1Order_10_06_05(r,1))/RawData_10_06_05(r,1))^2;
       end;
    end;
    RSS_10_06_05_sum=sum(RSS_10_06_05);
            if RSS_10_06_05_sum<RSS_check
               RSS_check=RSS_10_06_05_sum
               RSS_FINAL_10_06_05=RSS_10_06_05_sum;
               k1_10_06_05=k1_PERday
               Profiles_10_06_05=Model_1Order_10_06_05;
               RSS_MATRIX_FINAL_10_06_05=RSS_10_06_05;
            end;
end; %end main loop

%Monod, numerical solution
RSS_check=10*10^20;
mu_mgPERliterday_start=56;
mu_mgPERliterday_end=59;
d_mu_mgPERliterday=1;
k_start=16;
k_end=18;
d_k=1;
t_hrs=20;  %RUN TIME
dt_hrs=0.001; %dt
```

```
dt=dt_hrs*60^2;
for k=k_start:d_k:k_end
   for mu_mgPERliterday=mu_mgPERliterday_start:d_mu_mgPERliterday:mu_mgPERliterday_end
      k
      mu_mgPERliterday
      core10_06=1
      mu=mu_mgPERliterday/(24*60^2);
           t=t_hrs*60^2;
      t_loop=dt;
      Model_Monod_10_06_05=zeros(t_hrs/dt_hrs+1,SED/dy+1);

      for j=1:SED/dy+1
         Model_Monod_10_06_05(1, j)=RawData_10_06_05_model(1, j);
      end;
      for m=2:t_hrs/dt_hrs+1
            Model_Monod_10_06_05(m,1)=Model_Monod_10_06_05(1,1);
            Model_Monod_10_06_05(m,SED/dy+1)=Model_Monod_10_06_05(1,SED/dy+1); %explicitly setting
bottom boundary condition
      t_loop=t_loop+dt;
      end;
         for i=2:(t_hrs/dt_hrs+1)
            for j=2:SED/dy
              Model_Monod_10_06_05(i,j)=dt*Ds_10_06_05*(1000^2)/(dy^2)*(Model_Monod_10_06_05(i-1,j-1)-
2*Model_Monod_10_06_05(i-1,j)+Model_Monod_10_06_05(i-1,j+1))+Model_Monod_10_06_05(i-1,j)-
dt*mu*Model_Monod_10_06_05(i-1,j)/(k+Model_Monod_10_06_05(i-1,j));
            end;
                  if Model_Monod_10_06_05(i,j)<0
                     Model_Monod_10_06_05(i,j)=0;
                  elseif Model_Monod_10_06_05(i,j)>Model_Monod_10_06_05(i,j-1)
                     Model_Monod_10_06_05(i,j)=0;
                  end;
         end;
         Model_Monod_10_06_05_last=Model_Monod_10_06_05(t_hrs/dt_hrs+1, 1:SED/dy+1);
         Model_Monod_10_06_05_last_1mm=Model_Monod_10_06_05_last(1,1:5:SED/dy+1);
         for r=1:(RSS_depth*dy+1)
            if (RawData_10_06_05(1,r)- Model_Monod_10_06_05_last_1mm(1,r))>-0.001 &
(RawData_10_06_05(1,r)- Model_Monod_10_06_05_last_1mm(1,r))<0.001
               RSS_10_06_05(1,r)=0;
            else RSS_10_06_05(1,r)=((RawData_10_06_05(1,r)-
Model_Monod_10_06_05_last_1mm(1,r))/RawData_10_06_05(1,r))^2;
            end;
         end;
        RSS_10_06_05_sum=sum(RSS_10_06_05);
              if RSS_10_06_05_sum<RSS_check
                 RSS_check=RSS_10_06_05_sum
                 RSS_FINAL_10_06_05=RSS_10_06_05_sum;
                 mu_FINAL_10_06_05=mu_mgPERliterday
                 k_FINAL_10_06_05=k
                 Profiles_10_06_05=Model_Monod_10_06_05_last;
                 Profiles_10_06_05_checksteadystate=Model_Monod_10_06_05;
                 RSS_MATRIX_FINAL_10_06_05=RSS_10_06_05;
              end;

    end; end;
```

Appendix B

Examples of iterative numerical solutions for Core A are shown below.

```
%4C Core A
Dm_m2perS=1.1943*10^-9;
Dm=Dm_m2perS*1000^2;

Ds_m2perS=Dm_m2perS;
Ds=Ds_m2perS*1000^2;
SED;
dy;
dt_hrs=0.001;
dt=0.001*60^2;
WSS_check=1000000000;
depth_plot=[0:-dy:SED]
depth=[0:-1:SED];
   RawData2
   RawData5
   RawData10
   RawData23
   RawData47
   RawData48
   RawData73
   RawData96
  original_profile=[];

%Zero-order numerical solution
for A_mgPERliterday=20:1:100
   A=A_mgPERliterday/(24*60^2);
   ANOXICt_hrs=100;
   ANOXICt_loop=dt;
   C_ANOXIC=zeros(ANOXICt_hrs/dt_hrs+1,SED/dy+1);
   ANOXICt=ANOXICt_hrs*60^2;
   for j=1:SED/dy+1
      C_ANOXIC(1, j)=original_profile(1, j);
   end;
   for m=2:ANOXICt_hrs/dt_hrs+1
         C_ANOXIC(m,1)=9.28211*exp(-(ANOXICt_loop/(60^2))/3.9555)+1.73589*exp(-
(ANOXICt_loop/(60^2))/38.03609);
         if  C_ANOXIC(m,1)<0
             C_ANOXIC(m,1)=0;
         end;
   ANOXICt_loop=ANOXICt_loop+dt;
   end;
   for i=2:(ANOXICt_hrs/dt_hrs-1)
      for j=2:SED/dy+1
            if j==SED/dy+1
               C_ANOXIC(i,j)=0; %explicitly setting bottom boundary condition
            else  C_ANOXIC(i,j)=dt*Ds/(dy^2)*(C_ANOXIC(i-1,j-1)-2*C_ANOXIC(i-1,j)+C_ANOXIC(i-
1,j+1))+C_ANOXIC(i-1,j)-dt*A;
            end;
               if C_ANOXIC(i,j)<0
                  C_ANOXIC(i,j)=0;
               elseif C_ANOXIC(i,j)>C_ANOXIC(i,j-1)
                  C_ANOXIC(i,j)=0;
```

```
            end;
    end;
end;
C_ANOXIC2_plot=C_ANOXIC(2/dt_hrs+1,(1:SED/dy+1));
C_ANOXIC5_plot=C_ANOXIC(5/dt_hrs+1,(1:SED/dy+1));
C_ANOXIC10_plot=C_ANOXIC(10/dt_hrs+1,(1:SED/dy+1));
C_ANOXIC23_plot=C_ANOXIC(23/dt_hrs+1,(1:SED/dy+1));
C_ANOXIC47_plot=C_ANOXIC(47/dt_hrs+1,(1:SED/dy+1));
C_ANOXIC48_plot=C_ANOXIC(48/dt_hrs+1,(1:SED/dy+1));
C_ANOXIC73_plot=C_ANOXIC(73/dt_hrs+1,(1:SED/dy+1));
C_ANOXIC96_plot=C_ANOXIC(96/dt_hrs+1,(1:SED/dy+1));
for r=0:SED
    C_ANOXIC2(1,r+1)=C_ANOXIC2_plot(1,r*1/dy+1);
    C_ANOXIC5(1,r+1)=C_ANOXIC5_plot(1, r*1/dy+1);
    C_ANOXIC10(1,r+1)=C_ANOXIC10_plot(1, r*1/dy+1);
    C_ANOXIC23(1,r+1)=C_ANOXIC23_plot(1,r*1/dy+1);
    C_ANOXIC47(1,r+1)=C_ANOXIC47_plot(1, r*1/dy+1);
    C_ANOXIC48(1,r+1)=C_ANOXIC48_plot(1, r*1/dy+1);
    C_ANOXIC73(1,r+1)=C_ANOXIC73_plot(1, r*1/dy+1);
    C_ANOXIC96(1,r+1)=C_ANOXIC96_plot(1, r*1/dy+1);
end;
for r=1:(SED+1)
    SS_ANOXIC2(1,r)=(RawData2(1,r)-C_ANOXIC2(1,r))^2;
        if abs(RawData2(1,r)-C_ANOXIC2(1,r))<0.1
            SS_ANOXIC2(1,r)=0; end;
    SS_ANOXIC5(1,r)=(RawData5(1,r)-C_ANOXIC5(1,r))^2;
            if abs(RawData5(1,r)-C_ANOXIC5(1,r))<0.1
            SS_ANOXIC5(1,r)=0; end;
    SS_ANOXIC10(1,r)=(RawData10(1,r)-C_ANOXIC10(1,r))^2;
            if abs(RawData10(1,r)-C_ANOXIC10(1,r))<0.1
            SS_ANOXIC10(1,r)=0; end;
    SS_ANOXIC23(1,r)=(RawData23(1,r)-C_ANOXIC23(1,r))^2;
            if abs(RawData23(1,r)-C_ANOXIC23(1,r))<0.1
            SS_ANOXIC23(1,r)=0; end;
    SS_ANOXIC47(1,r)=(RawData47(1,r)-C_ANOXIC47(1,r))^2;
            if abs(RawData47(1,r)-C_ANOXIC47(1,r))<0.1
            SS_ANOXIC47(1,r)=0; end;
    SS_ANOXIC48(1,r)=(RawData48(1,r)-C_ANOXIC48(1,r))^2;
            if abs(RawData48(1,r)-C_ANOXIC48(1,r))<0.1
            SS_ANOXIC48(1,r)=0; end;
    SS_ANOXIC73(1,r)=(RawData73(1,r)-C_ANOXIC73(1,r))^2;
            if abs(RawData73(1,r)-C_ANOXIC73(1,r))<0.1
            SS_ANOXIC73(1,r)=0; end;
    SS_ANOXIC96(1,r)=(RawData96(1,r)-C_ANOXIC96(1,r))^2;
            if abs(RawData96(1,r)-C_ANOXIC96(1,r))<0.1
            SS_ANOXIC96(1,r)=0; end;
end
SS_ANOXIC_MATRIX=[SS_ANOXIC2
    SS_ANOXIC5
    SS_ANOXIC10
    SS_ANOXIC23
    SS_ANOXIC47
    SS_ANOXIC48
    SS_ANOXIC73
    SS_ANOXIC96];
SS_ANOXIC_depth=sum(SS_ANOXIC_MATRIX);
```

```
   Weighted_ANOXIC=[0.0685, 0.0888, 0.1742, 0.4927, 1.7233, 6.8977, 25.7069, 107.9784, 400.0000, 1836.7347,
0.0000, 0.0000, 0.0000, 0.0000, 0.0000, 0.0000];
      for r=1:SED+1
         WSS(1,r)=SS_ANOXIC_depth(1,r)*Weighted_ANOXIC(1,r);
      end;
      WSS_ANOXIC=sum(WSS);
ANOXIC_PROFILES=[C_ANOXIC2_plot
   C_ANOXIC5_plot
   C_ANOXIC10_plot
   C_ANOXIC23_plot
   C_ANOXIC47_plot
   C_ANOXIC48_plot
   C_ANOXIC73_plot
   C_ANOXIC96_plot];
               if WSS_ANOXIC<WSS_check
                  WSS_check=WSS_ANOXIC
                  WSS_ANOXIC_FINAL=WSS_ANOXIC;
                  A_FINAL=A_mgPERliterday
                  ANOXIC_PROFILES_FINAL=ANOXIC_PROFILES;
                  SS_ANOXIC_MATRIX_FINAL=SS_ANOXIC_MATRIX;
               end;
end;

%First Order numerical solution
for k1_PERday=35:1:60
   k1=k1_PERday/(24*60^2);
   ANOXICt_hrs=100;
   ANOXICt_loop=dt;
   C_ANOXIC=zeros(ANOXICt_hrs/dt_hrs+1,SED/dy+1);

   ANOXICt=ANOXICt_hrs*60^2;
   for j=1:SED/dy+1
      C_ANOXIC(1, j)=original_profile(1, j);
   end;
   for m=2:ANOXICt_hrs/dt_hrs+1
         C_ANOXIC(m,1)=9.28211*exp(-(ANOXICt_loop/(60^2))/3.9555)+1.73589*exp(-
(ANOXICt_loop/(60^2))/38.03609);
         if  C_ANOXIC(m,1)<0
             C_ANOXIC(m,1)=0;
         end;
   ANOXICt_loop=ANOXICt_loop+dt;
   end;
   for i=2:(ANOXICt_hrs/dt_hrs-1)
      for j=2:SED/dy+1
            if j==SED/dy+1
               C_ANOXIC(i,j)=0;
            else  C_ANOXIC(i,j)=dt*Ds/(dy^2)*(C_ANOXIC(i-1,j-1)-2*C_ANOXIC(i-1,j)+C_ANOXIC(i-
1,j+1))+C_ANOXIC(i-1,j)-dt*k1*C_ANOXIC(i-1,j); %j-l refers to the last profile
            end;
               if C_ANOXIC(i,j)<0
                  C_ANOXIC(i,j)=0;
               elseif C_ANOXIC(i,j)>C_ANOXIC(i,j-1)
                  C_ANOXIC(i,j)=0;
               end;

      end;
```

```
end;
C_ANOXIC2_plot=C_ANOXIC(2/dt_hrs+1,(1:SED/dy+1));
C_ANOXIC5_plot=C_ANOXIC(5/dt_hrs+1,(1:SED/dy+1));
C_ANOXIC10_plot=C_ANOXIC(10/dt_hrs+1,(1:SED/dy+1));
C_ANOXIC23_plot=C_ANOXIC(23/dt_hrs+1,(1:SED/dy+1));
C_ANOXIC47_plot=C_ANOXIC(47/dt_hrs+1,(1:SED/dy+1));
C_ANOXIC48_plot=C_ANOXIC(48/dt_hrs+1,(1:SED/dy+1));
C_ANOXIC73_plot=C_ANOXIC(73/dt_hrs+1,(1:SED/dy+1));
C_ANOXIC96_plot=C_ANOXIC(96/dt_hrs+1,(1:SED/dy+1));

for r=0:SED
   C_ANOXIC2(1,r+1)=C_ANOXIC2_plot(1,r*1/dy+1);
   C_ANOXIC5(1,r+1)=C_ANOXIC5_plot(1, r*1/dy+1);
   C_ANOXIC10(1,r+1)=C_ANOXIC10_plot(1, r*1/dy+1);
   C_ANOXIC23(1,r+1)=C_ANOXIC23_plot(1,r*1/dy+1);
   C_ANOXIC47(1,r+1)=C_ANOXIC47_plot(1, r*1/dy+1);
   C_ANOXIC48(1,r+1)=C_ANOXIC48_plot(1, r*1/dy+1);
   C_ANOXIC73(1,r+1)=C_ANOXIC73_plot(1, r*1/dy+1);
   C_ANOXIC96(1,r+1)=C_ANOXIC96_plot(1, r*1/dy+1);
end;
for r=1:(SED+1)
   SS_ANOXIC2(1,r)=(RawData2(1,r)-C_ANOXIC2(1,r))^2;
      if abs(RawData2(1,r)-C_ANOXIC2(1,r))<0.1
         SS_ANOXIC2(1,r)=0; end;
   SS_ANOXIC5(1,r)=(RawData5(1,r)-C_ANOXIC5(1,r))^2;
         if abs(RawData5(1,r)-C_ANOXIC5(1,r))<0.1
         SS_ANOXIC5(1,r)=0; end;
   SS_ANOXIC10(1,r)=(RawData10(1,r)-C_ANOXIC10(1,r))^2;
         if abs(RawData10(1,r)-C_ANOXIC10(1,r))<0.1
         SS_ANOXIC10(1,r)=0; end;
   SS_ANOXIC23(1,r)=(RawData23(1,r)-C_ANOXIC23(1,r))^2;
         if abs(RawData23(1,r)-C_ANOXIC23(1,r))<0.1
         SS_ANOXIC23(1,r)=0; end;
   SS_ANOXIC47(1,r)=(RawData47(1,r)-C_ANOXIC47(1,r))^2;
         if abs(RawData47(1,r)-C_ANOXIC47(1,r))<0.1
         SS_ANOXIC47(1,r)=0; end;
   SS_ANOXIC48(1,r)=(RawData48(1,r)-C_ANOXIC48(1,r))^2;
         if abs(RawData48(1,r)-C_ANOXIC48(1,r))<0.1
         SS_ANOXIC48(1,r)=0; end;
   SS_ANOXIC73(1,r)=(RawData73(1,r)-C_ANOXIC73(1,r))^2;
         if abs(RawData73(1,r)-C_ANOXIC73(1,r))<0.1
         SS_ANOXIC73(1,r)=0; end;
   SS_ANOXIC96(1,r)=(RawData96(1,r)-C_ANOXIC96(1,r))^2;
         if abs(RawData96(1,r)-C_ANOXIC96(1,r))<0.1
         SS_ANOXIC96(1,r)=0; end;
end
SS_ANOXIC_MATRIX=[SS_ANOXIC2
   SS_ANOXIC5
   SS_ANOXIC10
   SS_ANOXIC23
   SS_ANOXIC47
   SS_ANOXIC48
   SS_ANOXIC73
   SS_ANOXIC96];
SS_ANOXIC_depth=sum(SS_ANOXIC_MATRIX);
```

```
   Weighted_ANOXIC=[0.0685, 0.0888, 0.1742, 0.4927, 1.7233, 6.8977, 25.7069, 107.9784, 400.0000, 1836.7347,
0.0000, 0.0000, 0.0000, 0.0000, 0.0000, 0.0000];
      for r=1:SED+1
         WSS(1,r)=SS_ANOXIC_depth(1,r)*Weighted_ANOXIC(1,r);
      end;
      WSS_ANOXIC=sum(WSS);
ANOXIC_PROFILES=[C_ANOXIC2_plot
   C_ANOXIC5_plot
   C_ANOXIC10_plot
   C_ANOXIC23_plot
   C_ANOXIC47_plot
   C_ANOXIC48_plot
   C_ANOXIC73_plot
   C_ANOXIC96_plot];
               if WSS_ANOXIC<WSS_check
                  WSS_check=WSS_ANOXIC
                  WSS_ANOXIC_FINAL=WSS_ANOXIC;
                  k1_FINAL=k1_PERday
                  ANOXIC_PROFILES_FINAL=ANOXIC_PROFILES;
                  SS_ANOXIC_MATRIX_FINAL=SS_ANOXIC_MATRIX;
               end;
end;

%Monod numerical solutions
for k=k_start:d_k:k_end
   for mu_mgPERliterday=mu_mgPERliterday_start:d_mu_mgPERliterday:mu_mgPERliterday_end
      mu=mu_mgPERliterday/(24*60^2);
      ANOXICt_hrs=100;
      ANOXICt_loop=dt;
      C_ANOXIC=zeros(ANOXICt_hrs/dt_hrs+1,SED/dy+1);
      ANOXICt=ANOXICt_hrs*60^2;
      for j=1:SED/dy+1
         C_ANOXIC(1, j)=original_profile(1, j);
      end;
      for m=2:ANOXICt_hrs/dt_hrs+1
            C_ANOXIC(m,1)=9.28211*exp(-(ANOXICt_loop/(60^2))/3.9555)+1.73589*exp(-
(ANOXICt_loop/(60^2))/38.03609);
            if  C_ANOXIC(m,1)<0
                C_ANOXIC(m,1)=0;
            end;
      ANOXICt_loop=ANOXICt_loop+dt;
      end;
         for i=2:(ANOXICt_hrs/dt_hrs-1)
            for j=2:SED/dy+1
                  if j==SED/dy+1
                     C_ANOXIC(i,j)=0;
                  else  C_ANOXIC(i,j)=dt*Ds/(dy^2)*(C_ANOXIC(i-1,j-1)-2*C_ANOXIC(i-1,j)+C_ANOXIC(i-
1,j+1))+C_ANOXIC(i-1,j)-dt*mu*C_ANOXIC(i-1,j)/(k+C_ANOXIC(i-1,j));
                  end;
                     if C_ANOXIC(i,j)<0
                        C_ANOXIC(i,j)=0;
                     elseif C_ANOXIC(i,j)>C_ANOXIC(i,j-1)
                        C_ANOXIC(i,j)=0;
                     end;

            end;
```

```
end;
C_ANOXIC2_plot=C_ANOXIC(2/dt_hrs+1,(1:SED/dy+1));
C_ANOXIC5_plot=C_ANOXIC(5/dt_hrs+1,(1:SED/dy+1));
C_ANOXIC10_plot=C_ANOXIC(10/dt_hrs+1,(1:SED/dy+1));
C_ANOXIC23_plot=C_ANOXIC(23/dt_hrs+1,(1:SED/dy+1));
C_ANOXIC47_plot=C_ANOXIC(47/dt_hrs+1,(1:SED/dy+1));
C_ANOXIC48_plot=C_ANOXIC(48/dt_hrs+1,(1:SED/dy+1));
C_ANOXIC73_plot=C_ANOXIC(73/dt_hrs+1,(1:SED/dy+1));
C_ANOXIC96_plot=C_ANOXIC(96/dt_hrs+1,(1:SED/dy+1));
for r=0:SED
   C_ANOXIC2(1,r+1)=C_ANOXIC2_plot(1,r*1/dy+1);
   C_ANOXIC5(1,r+1)=C_ANOXIC5_plot(1, r*1/dy+1);
   C_ANOXIC10(1,r+1)=C_ANOXIC10_plot(1, r*1/dy+1);
   C_ANOXIC23(1,r+1)=C_ANOXIC23_plot(1,r*1/dy+1);
   C_ANOXIC47(1,r+1)=C_ANOXIC47_plot(1, r*1/dy+1);
   C_ANOXIC48(1,r+1)=C_ANOXIC48_plot(1, r*1/dy+1);
   C_ANOXIC73(1,r+1)=C_ANOXIC73_plot(1, r*1/dy+1);
   C_ANOXIC96(1,r+1)=C_ANOXIC96_plot(1, r*1/dy+1);
end;
for r=1:(SED+1)
SS_ANOXIC2(1,r)=(RawData2(1,r)-C_ANOXIC2(1,r))^2;
   if abs(RawData2(1,r)-C_ANOXIC2(1,r))<0.1
      SS_ANOXIC2(1,r)=0; end;
SS_ANOXIC5(1,r)=(RawData5(1,r)-C_ANOXIC5(1,r))^2;
      if abs(RawData5(1,r)-C_ANOXIC5(1,r))<0.1
      SS_ANOXIC5(1,r)=0; end;
SS_ANOXIC10(1,r)=(RawData10(1,r)-C_ANOXIC10(1,r))^2;
      if abs(RawData10(1,r)-C_ANOXIC10(1,r))<0.1
      SS_ANOXIC10(1,r)=0; end;
SS_ANOXIC23(1,r)=(RawData23(1,r)-C_ANOXIC23(1,r))^2;
      if abs(RawData23(1,r)-C_ANOXIC23(1,r))<0.1
      SS_ANOXIC23(1,r)=0; end;
SS_ANOXIC47(1,r)=(RawData47(1,r)-C_ANOXIC47(1,r))^2;
      if abs(RawData47(1,r)-C_ANOXIC47(1,r))<0.1
      SS_ANOXIC47(1,r)=0; end;
SS_ANOXIC48(1,r)=(RawData48(1,r)-C_ANOXIC48(1,r))^2;
      if abs(RawData48(1,r)-C_ANOXIC48(1,r))<0.1
      SS_ANOXIC48(1,r)=0; end;
SS_ANOXIC73(1,r)=(RawData73(1,r)-C_ANOXIC73(1,r))^2;
      if abs(RawData73(1,r)-C_ANOXIC73(1,r))<0.1
      SS_ANOXIC73(1,r)=0; end;
SS_ANOXIC96(1,r)=(RawData96(1,r)-C_ANOXIC96(1,r))^2;
      if abs(RawData96(1,r)-C_ANOXIC96(1,r))<0.1
      SS_ANOXIC96(1,r)=0; end;
end
SS_ANOXIC_MATRIX=[SS_ANOXIC2
   SS_ANOXIC5
   SS_ANOXIC10
   SS_ANOXIC23
   SS_ANOXIC47
   SS_ANOXIC48
   SS_ANOXIC73
   SS_ANOXIC96];
SS_ANOXIC_depth=sum(SS_ANOXIC_MATRIX);
Weighted_ANOXIC=[0.0685, 0.0888, 0.1742, 0.4927, 1.7233, 6.8977, 25.7069, 107.9784, 400.0000,
1836.7347, 0.0000, 0.0000, 0.0000, 0.0000, 0.0000, 0.0000];
```

```
        for r=1:SED+1
           WSS(1,r)=SS_ANOXIC_depth(1,r)*Weighted_ANOXIC(1,r);
        end;
        WSS_ANOXIC=sum(WSS);
        ANOXIC_PROFILES=[C_ANOXIC2_plot
           C_ANOXIC5_plot
           C_ANOXIC10_plot
           C_ANOXIC23_plot
           C_ANOXIC47_plot
           C_ANOXIC48_plot
           C_ANOXIC73_plot
           C_ANOXIC96_plot];
              if WSS_ANOXIC<WSS_check
                 WSS_check=WSS_ANOXIC
                 WSS_ANOXIC_FINAL=WSS_ANOXIC;
                 mu_FINAL=mu_mgPERliterday;
                 k_FINAL=k;
                 ANOXIC_PROFILES_FINAL=ANOXIC_PROFILES;
                 SS_ANOXIC_MATRIX_FINAL=SS_ANOXIC_MATRIX;
              end;
     end;%end mu loop
end; %end k loop
```

Simulated oxygen curves for zero-order, first-order, and Monod kinetics were plotted for visual comparison against the observed laboratory oxygen profiles, Figures 29–52.

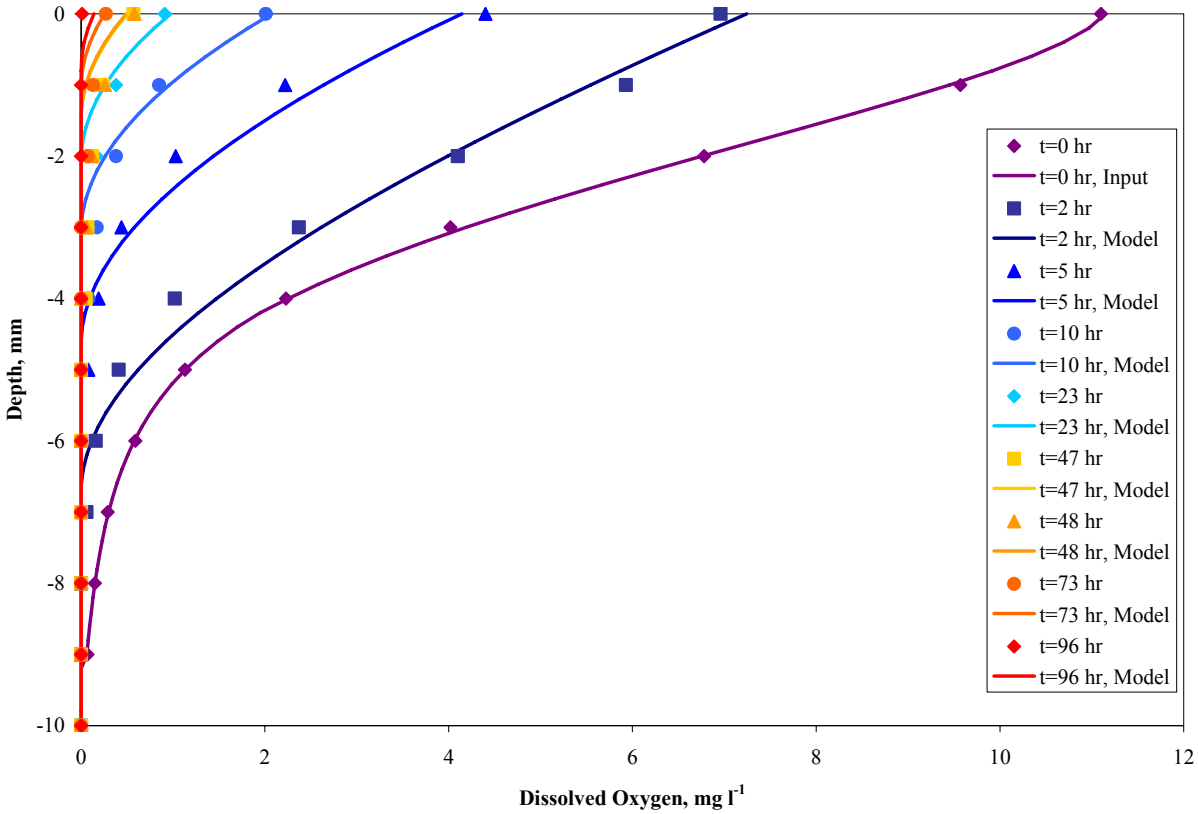

Figure 29. Zero-order model results during oxic-anoxic cycle plotted with observed profiles for 4°C Core A.

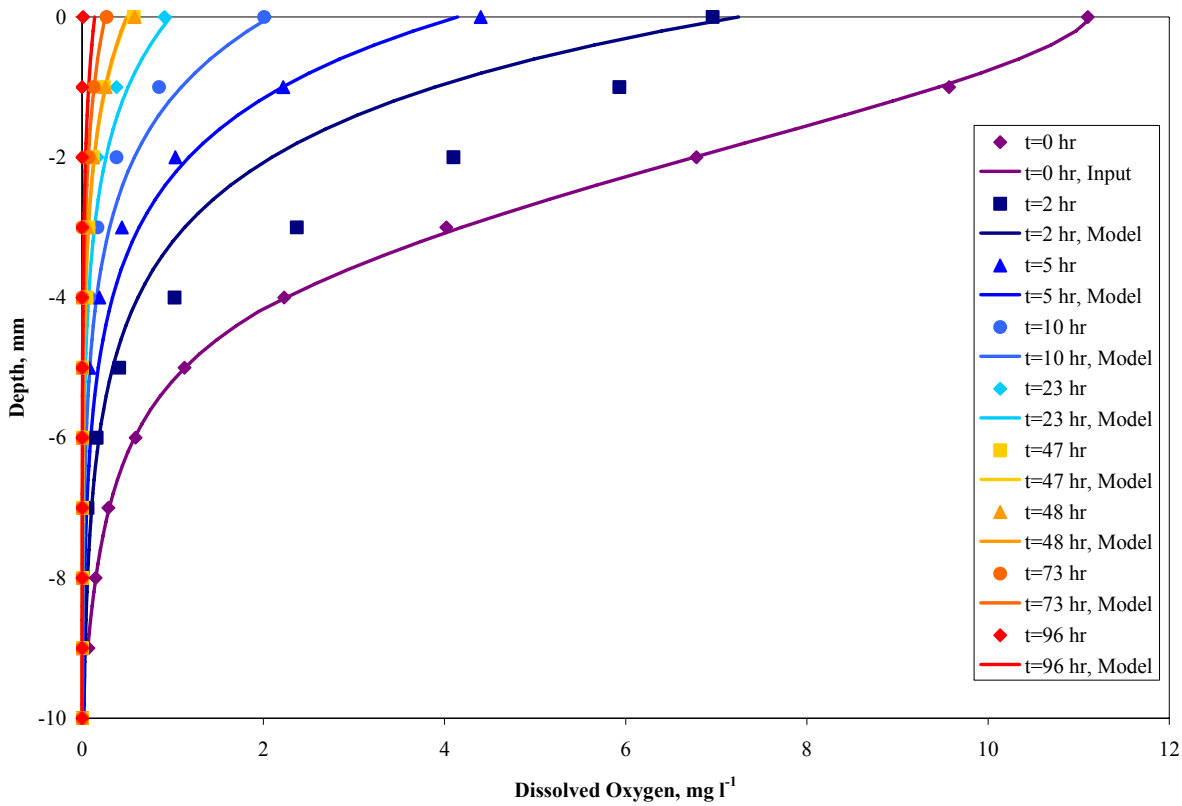

Figure 30. First-order model results during oxic-anoxic cycle plotted with observed profiles for 4°C Core A.

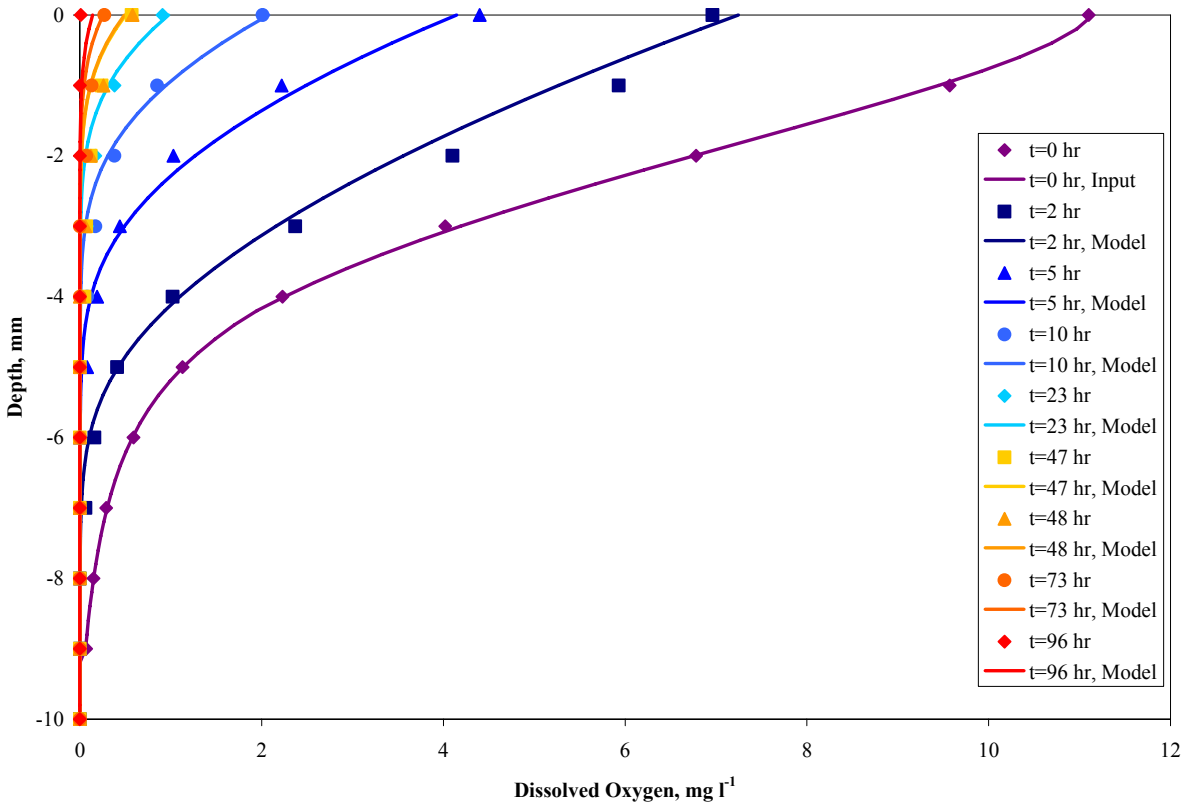

Figure 31. Monod model results during oxic-anoxic cycle plotted with observed profiles for 4°C Core A.

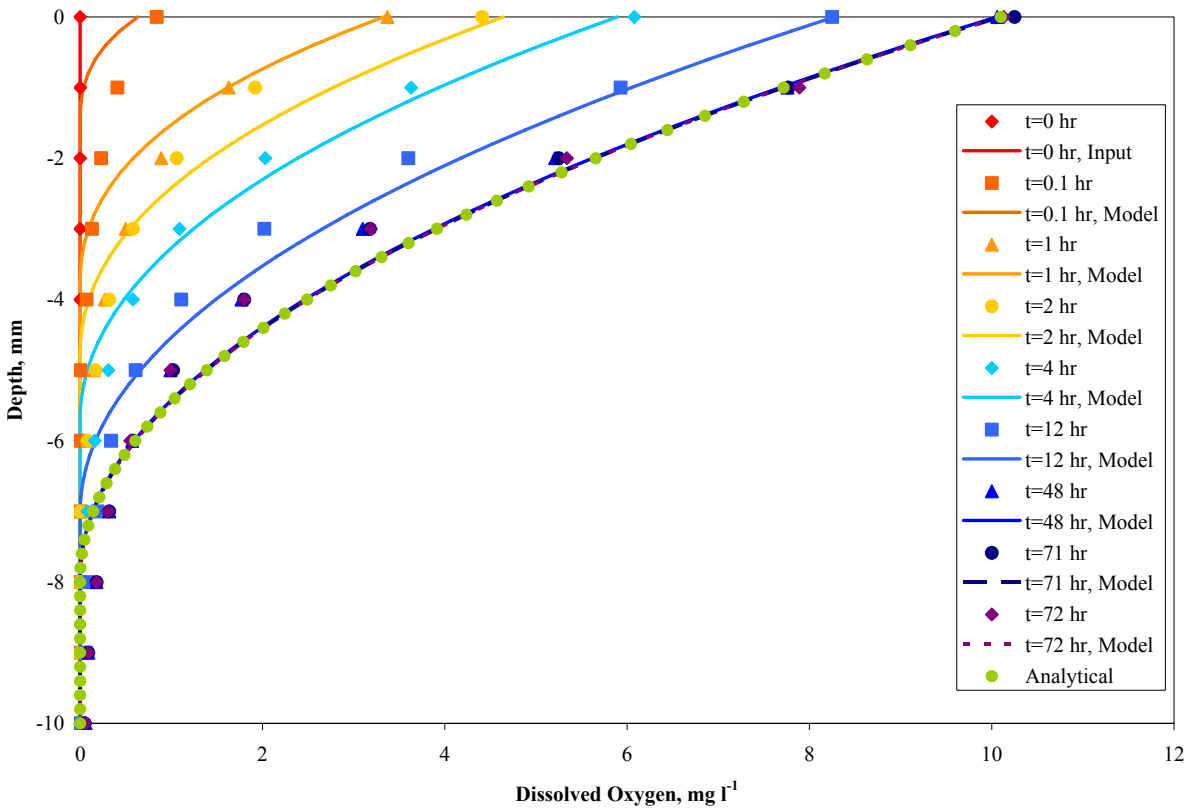

Figure 32. Zero-order model results during anoxic-oxic cycle plotted with observed profiles for 4°C Core A.

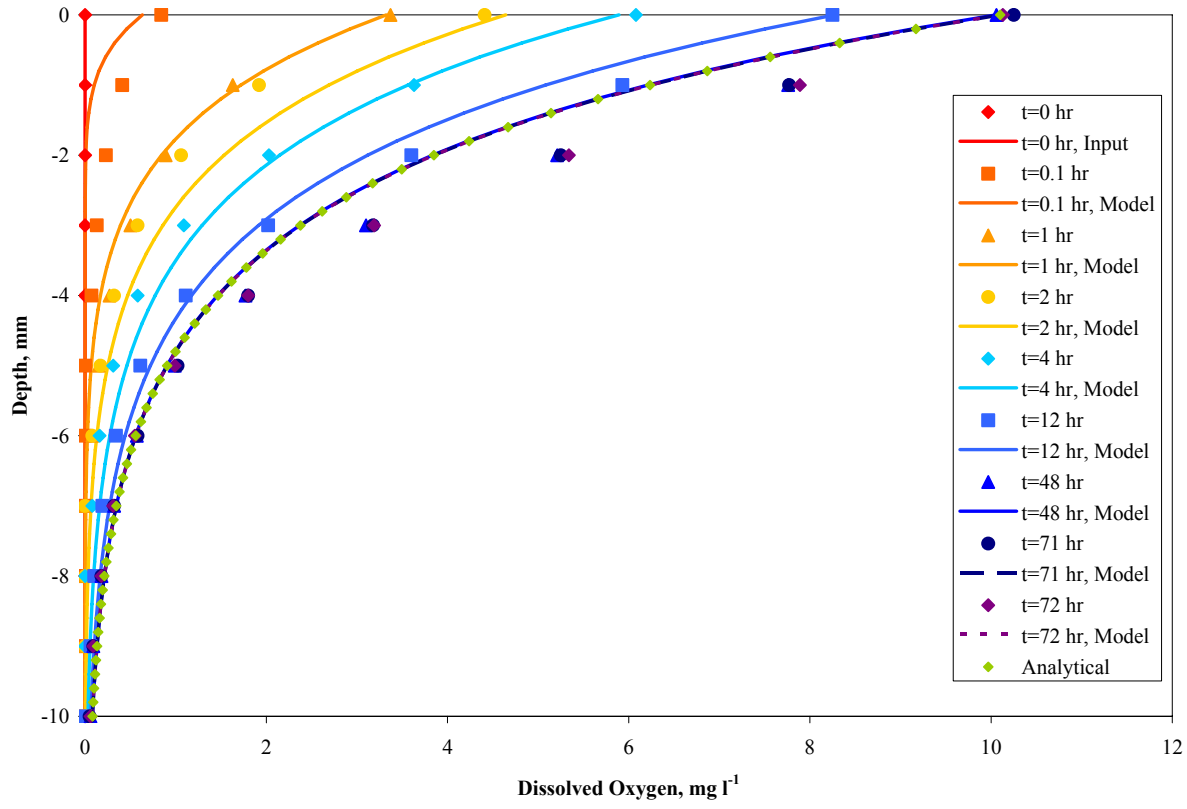

Figure 33. First-order model results during anoxic-oxic cycle plotted with observed profiles for 4°C Core A.

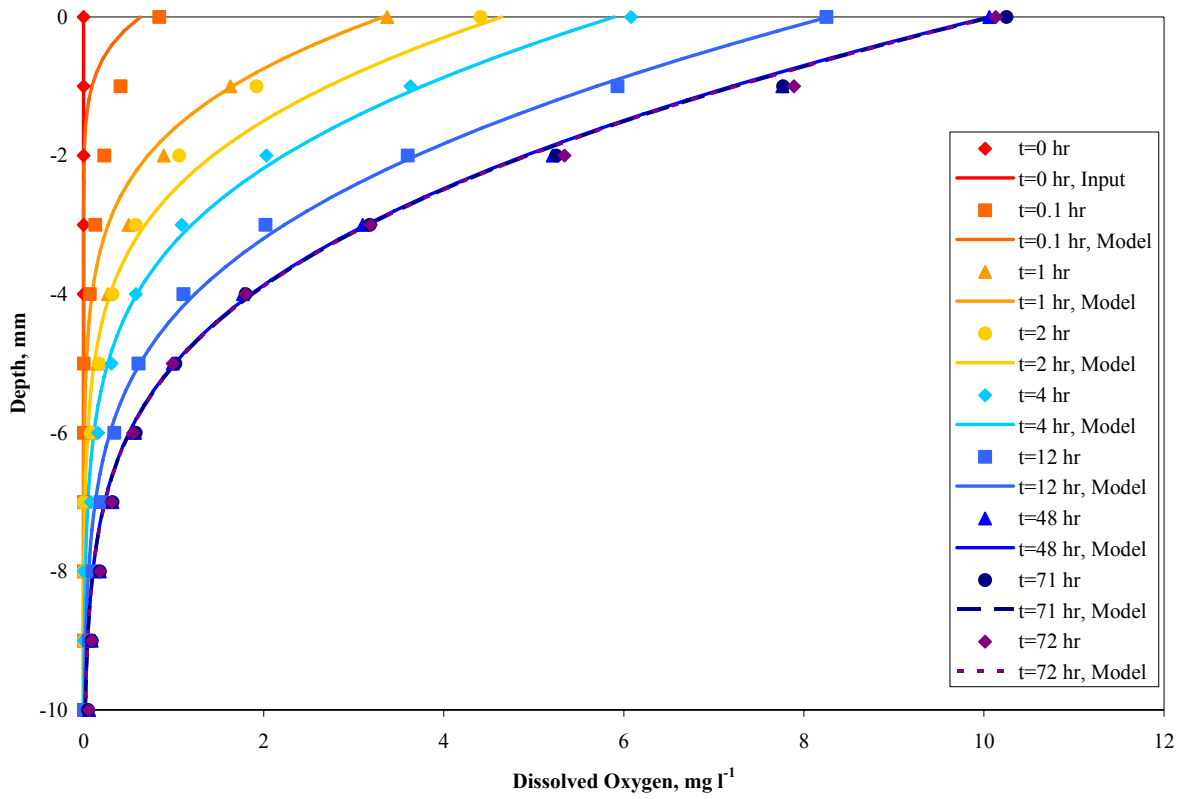

Figure 34. Monod model results during anoxic-oxic cycle plotted with observed profiles for 4°C Core A.

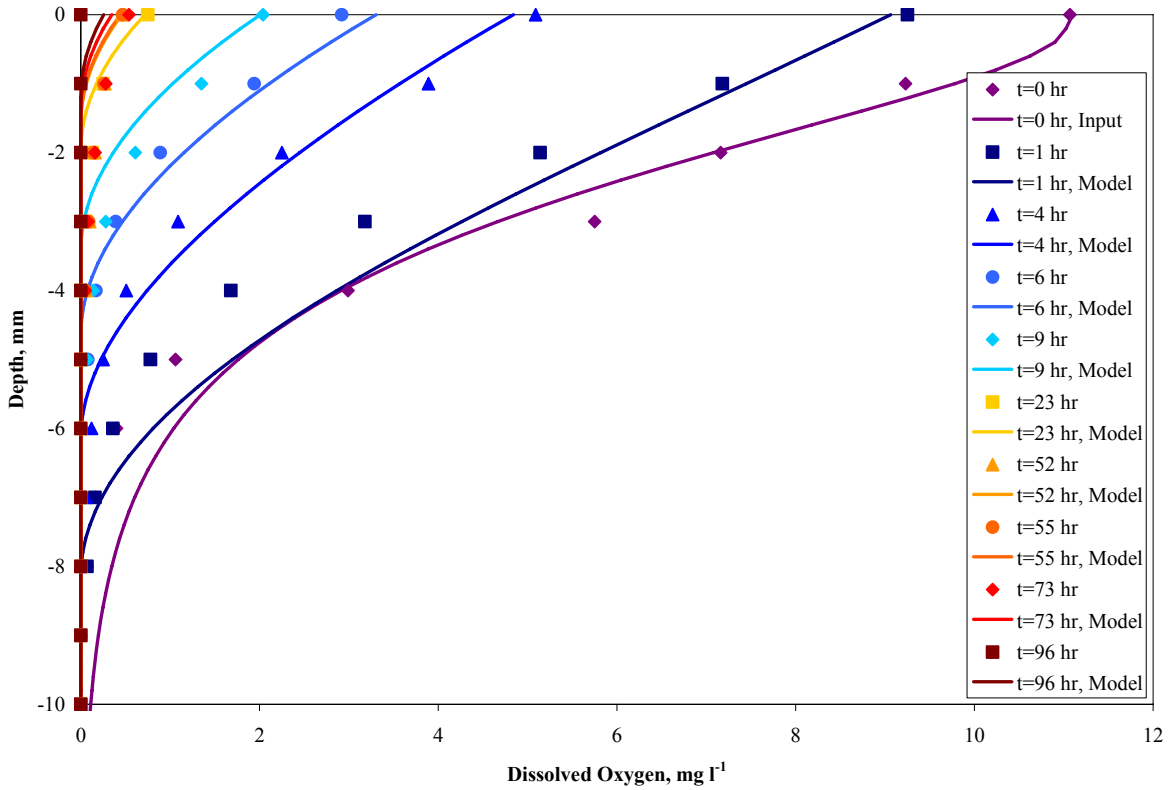

Figure 35. Zero-order model results during oxic-anoxic cycle plotted with observed profiles for 4°C Core B.

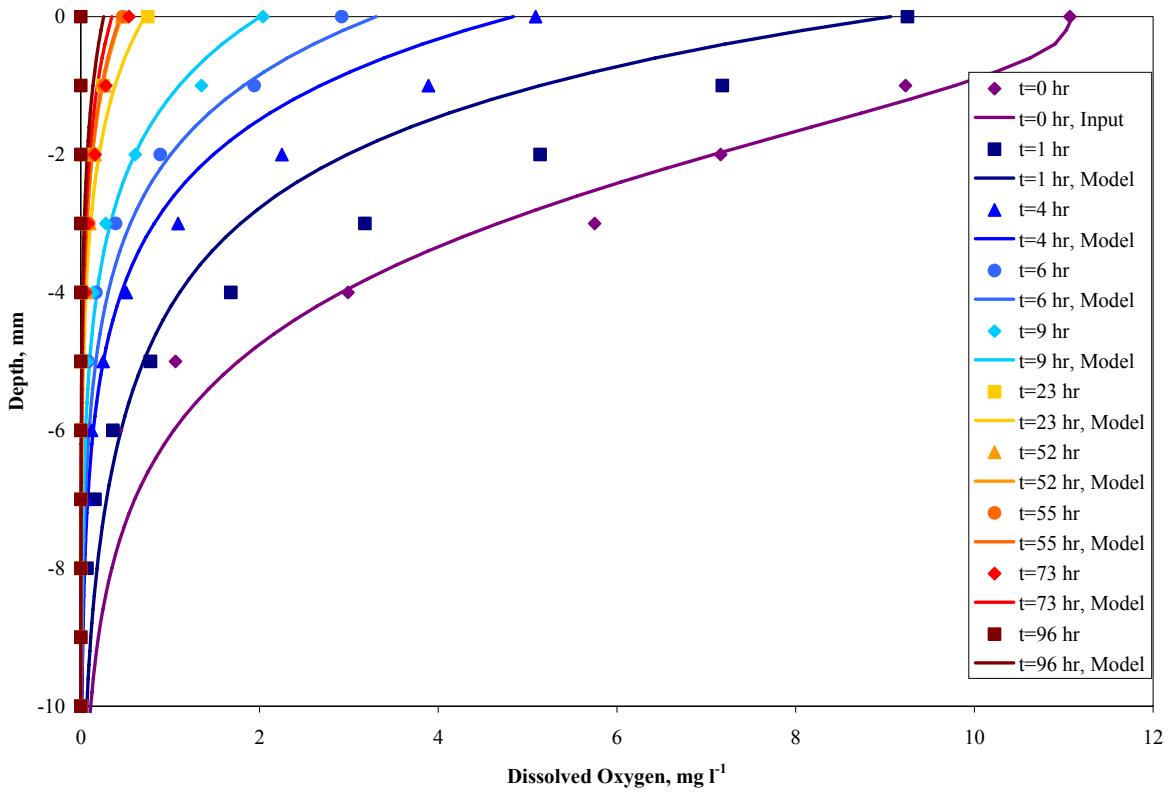

Figure 36. First-order model results during oxic-anoxic cycle plotted with observed profiles for 4°C Core B.

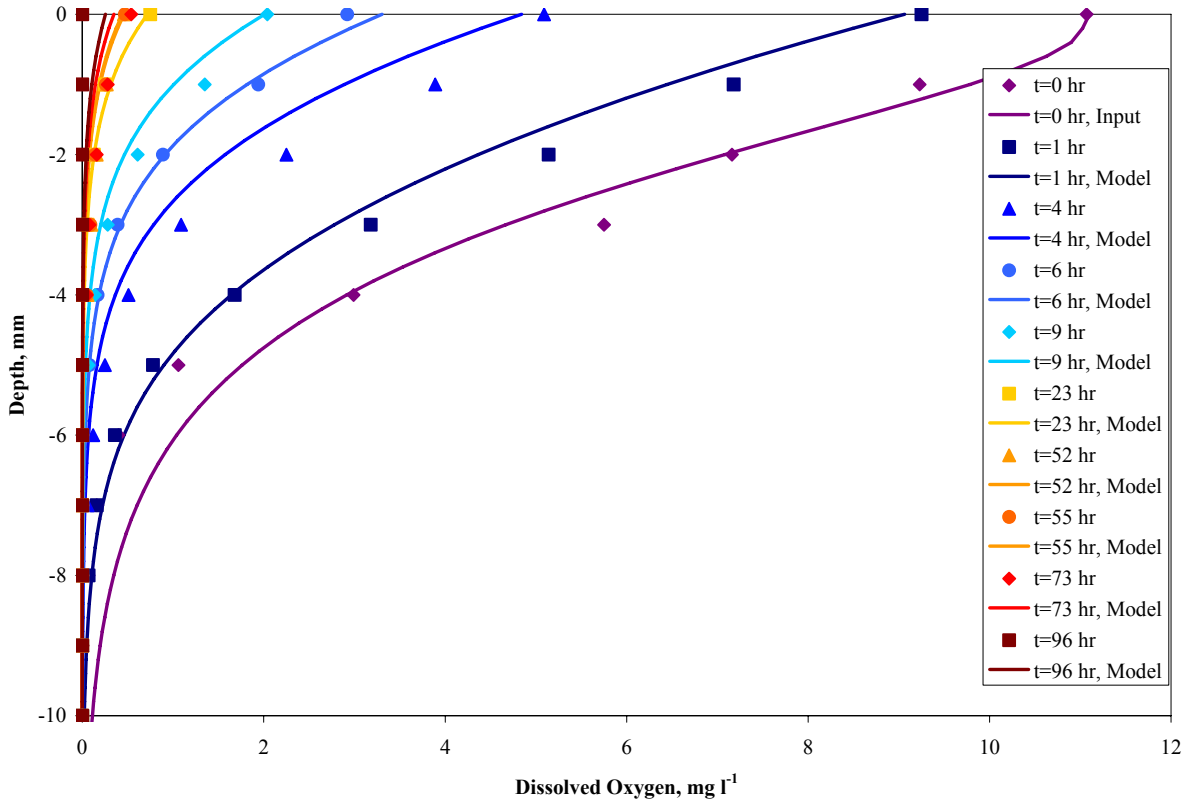

Figure 37. Monod model results during oxic-anoxic cycle plotted with observed profiles for 4°C Core B.

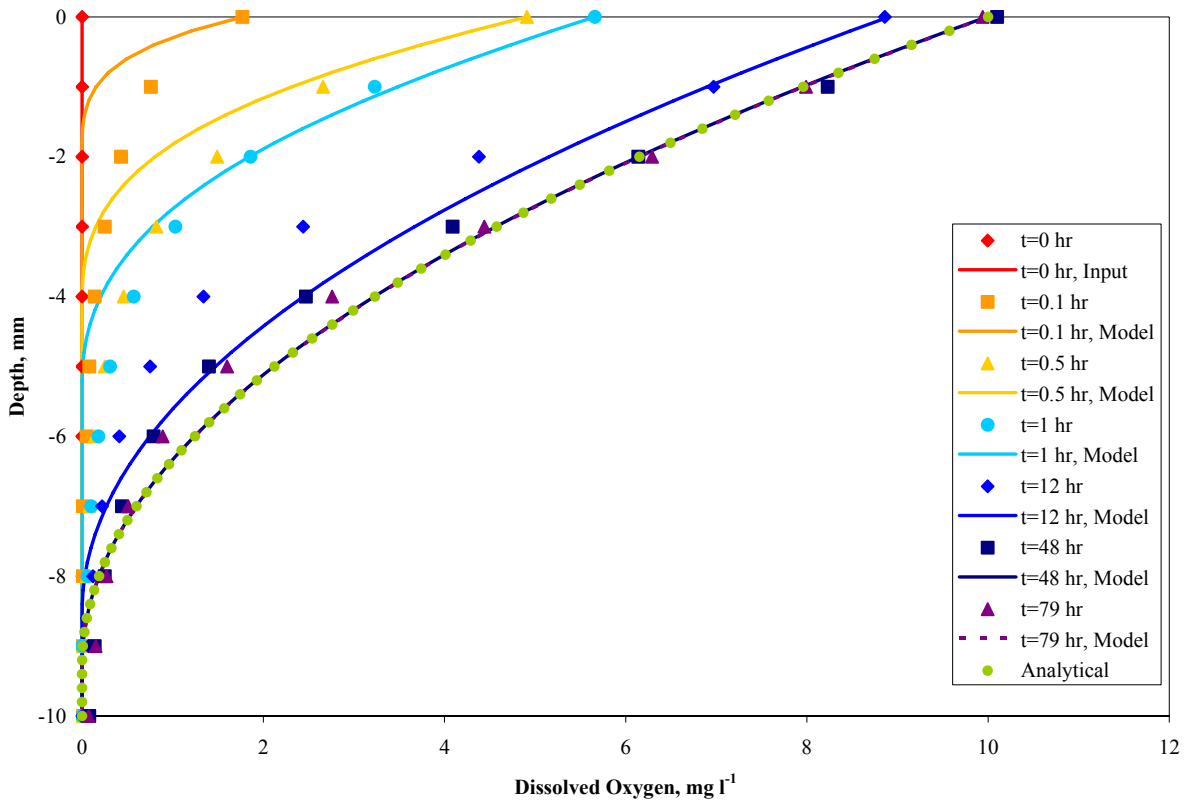

Figure 38. Zero-order model results during anoxic-oxic cycle plotted with observed profiles for 4°C Core B.

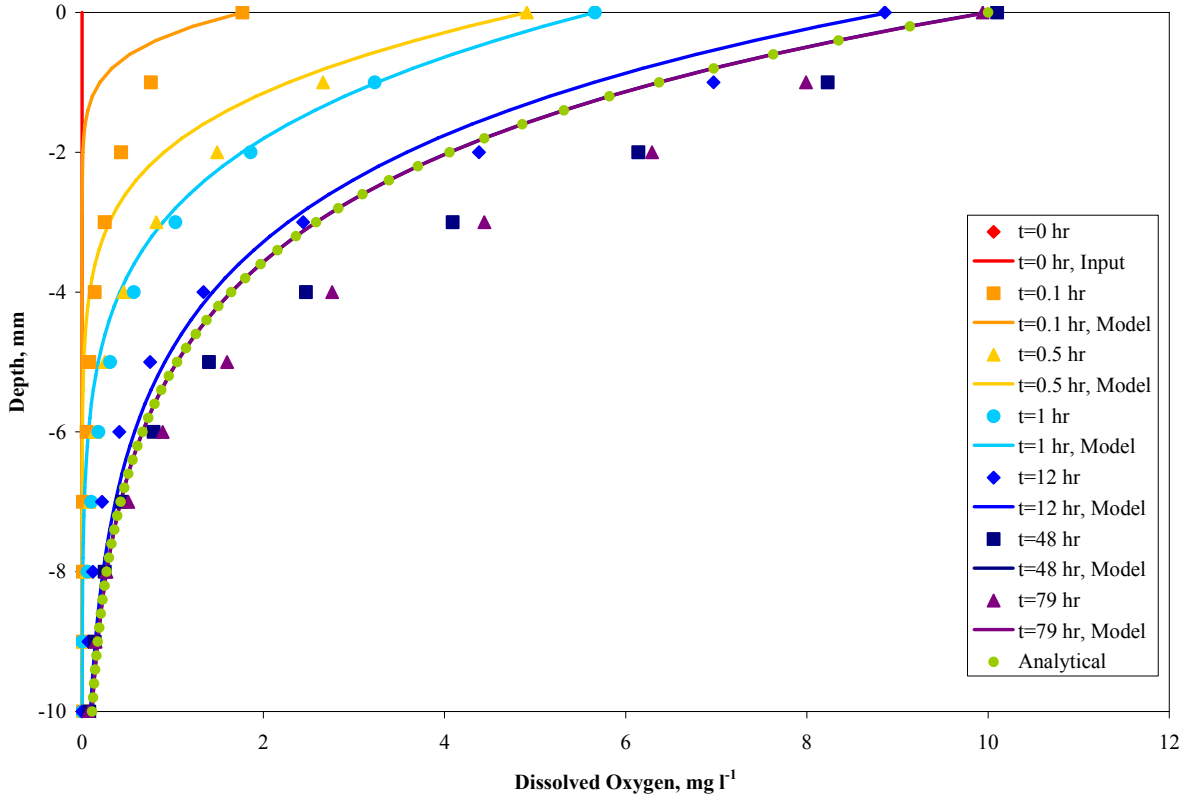

Figure 39. First-order model results during anoxic-oxic cycle plotted with observed profiles for 4°C Core B.

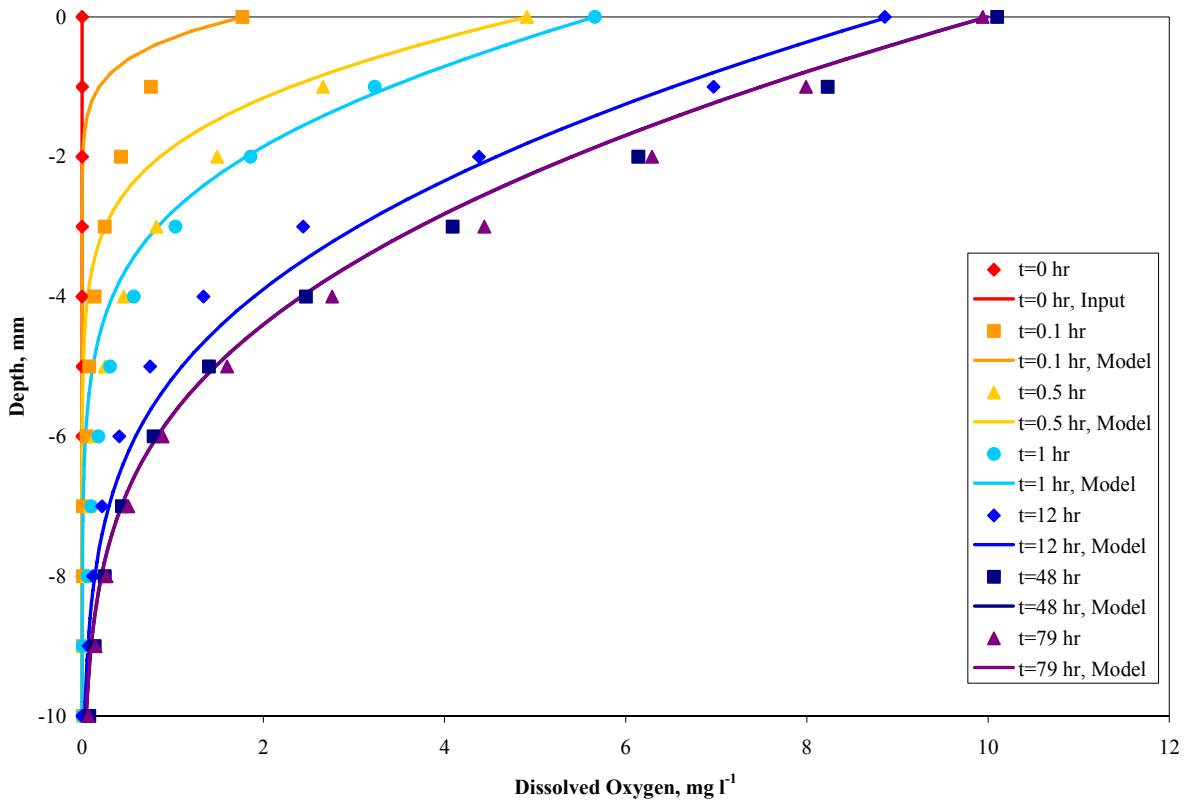

Figure 40. Monod model results during anoxic-oxic cycle plotted with observed profiles for 4°C Core B.

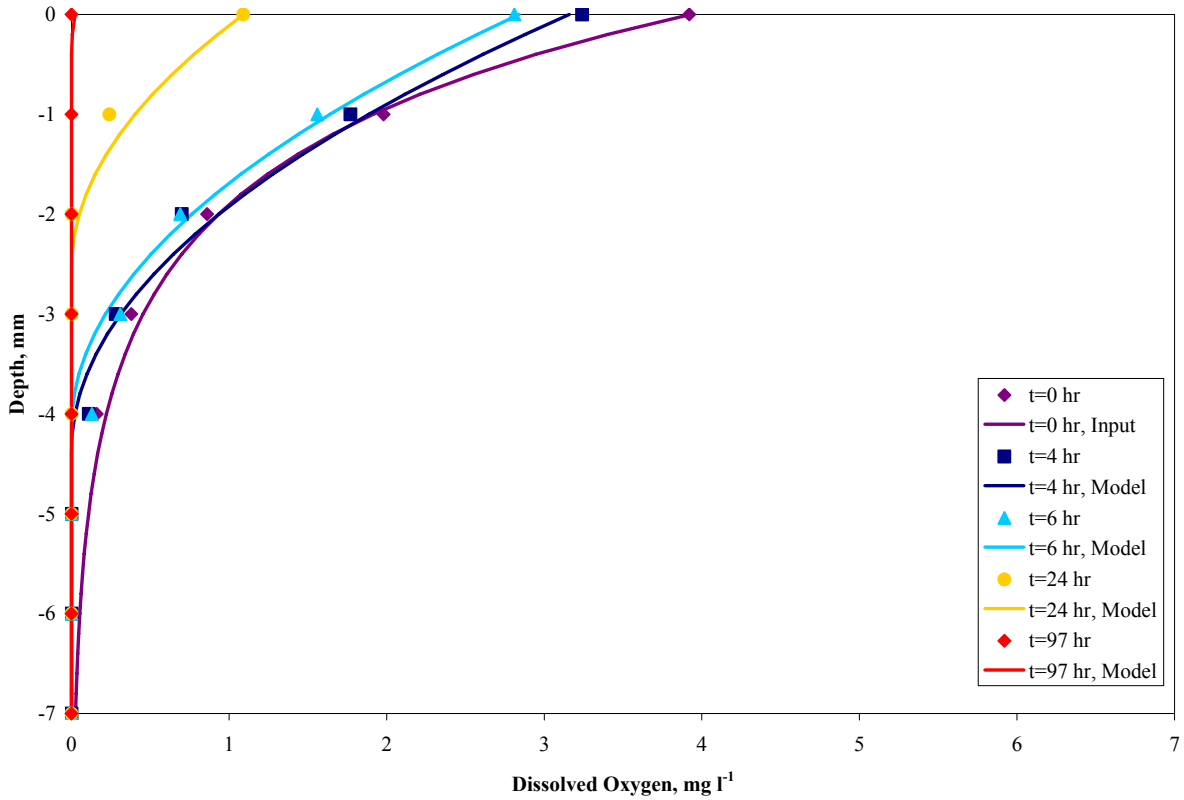

Figure 41. Zero-order model results during oxic-anoxic cycle plotted with observed profiles for 20°C Core C.

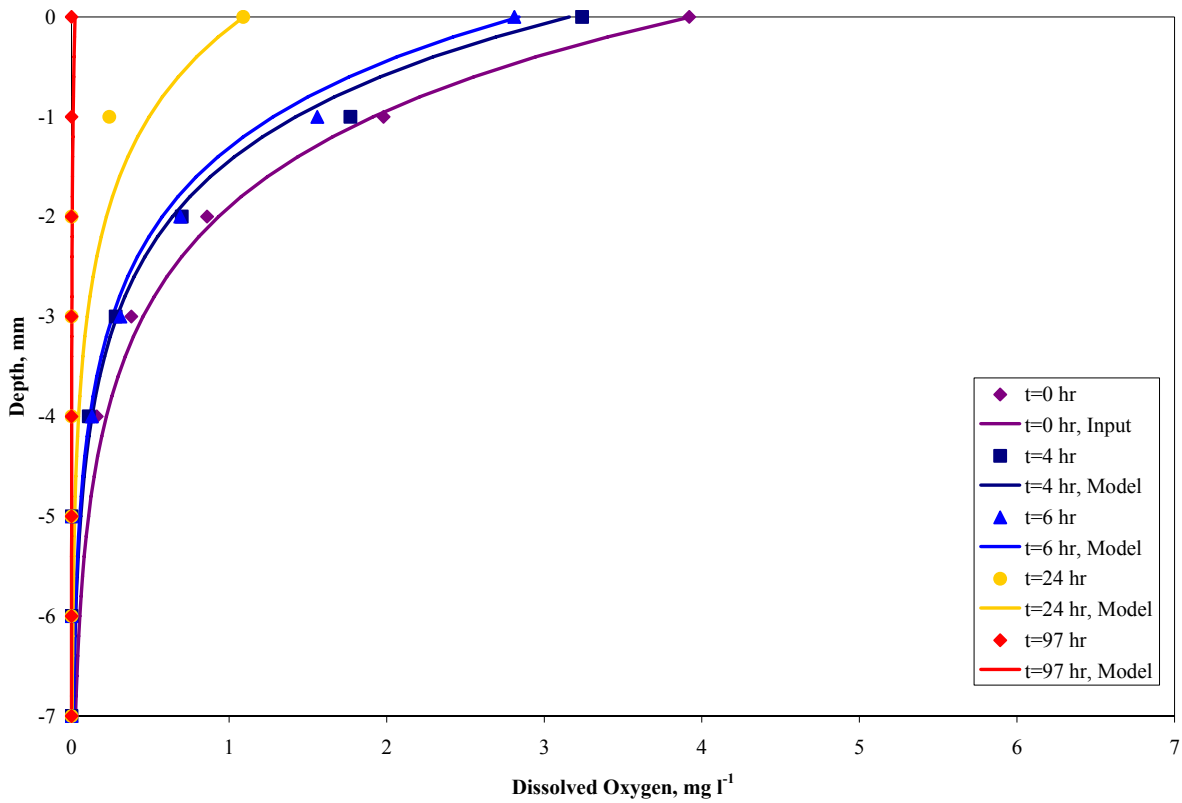

Figure 42. First-order model results during oxic-anoxic cycle plotted with observed profiles for 20°C Core C.

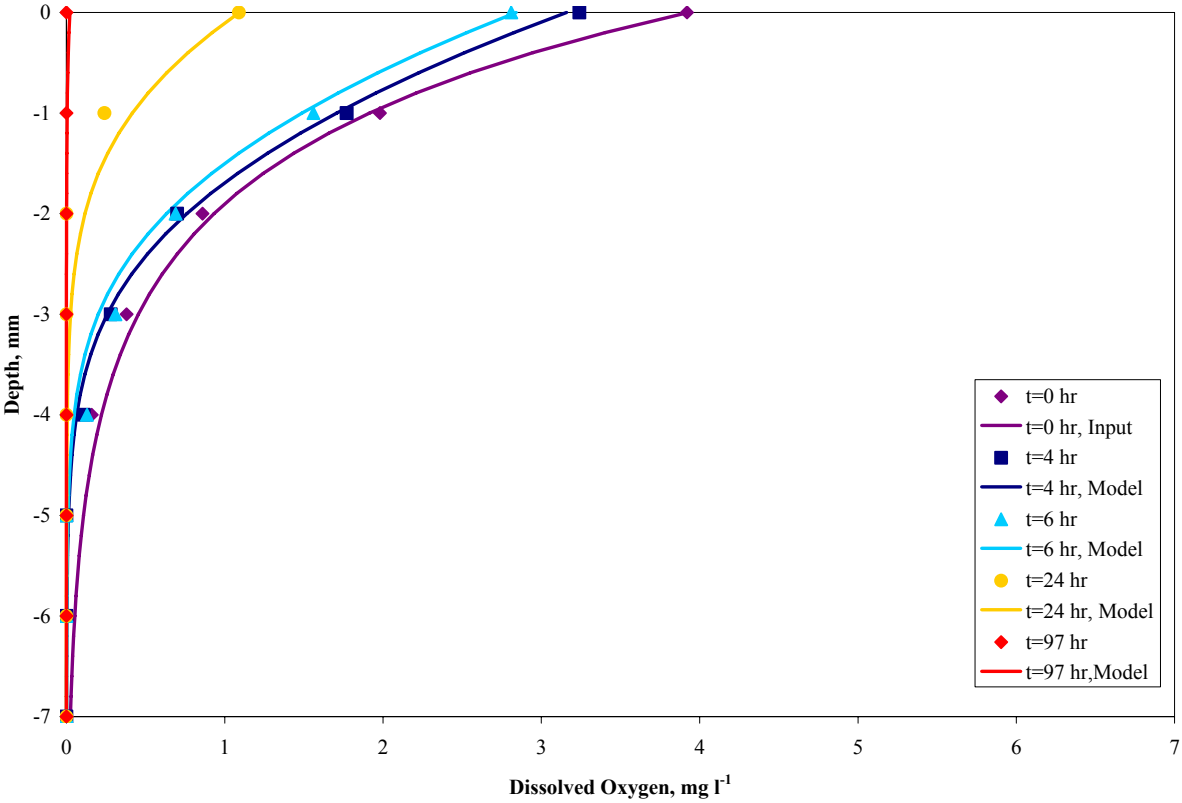

Figure 43. Monod model results during oxic-anoxic cycle plotted with observed profiles for 20°C Core C.

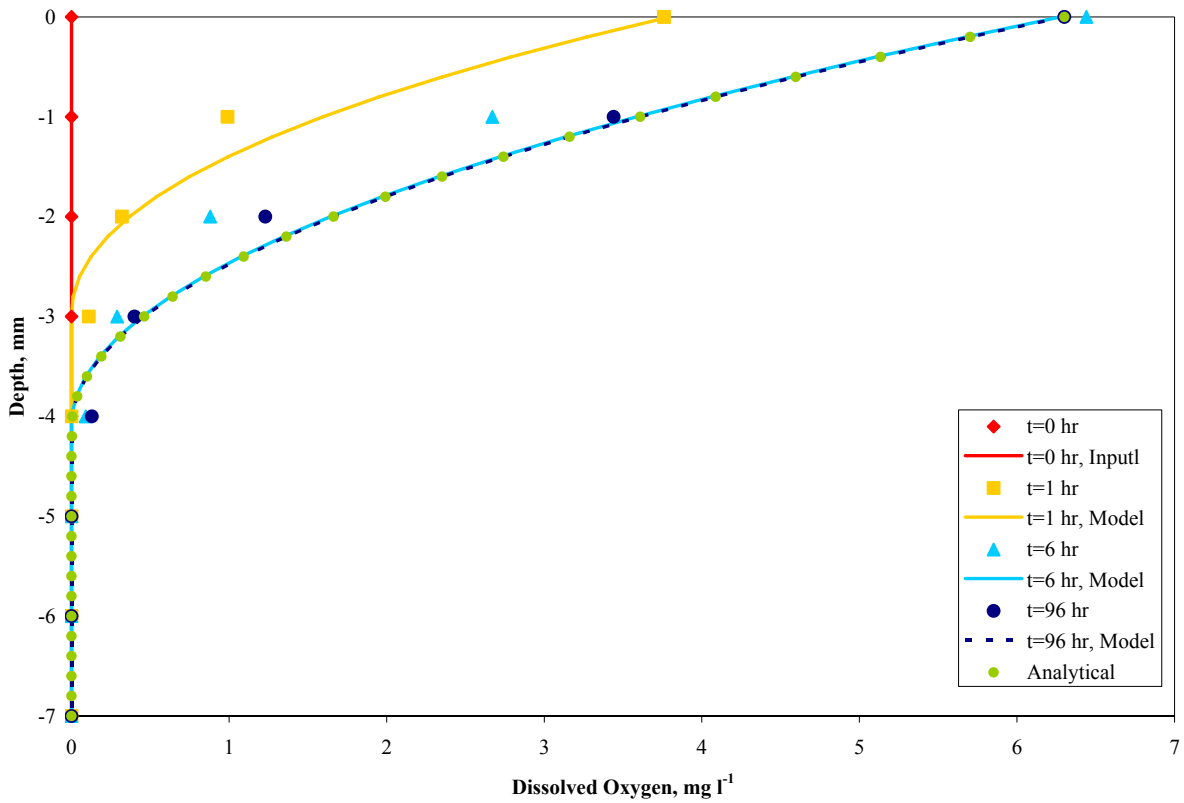

Figure 44. Zero-order model results during anoxic-oxic cycle plotted with observed profiles for 20°C Core C.

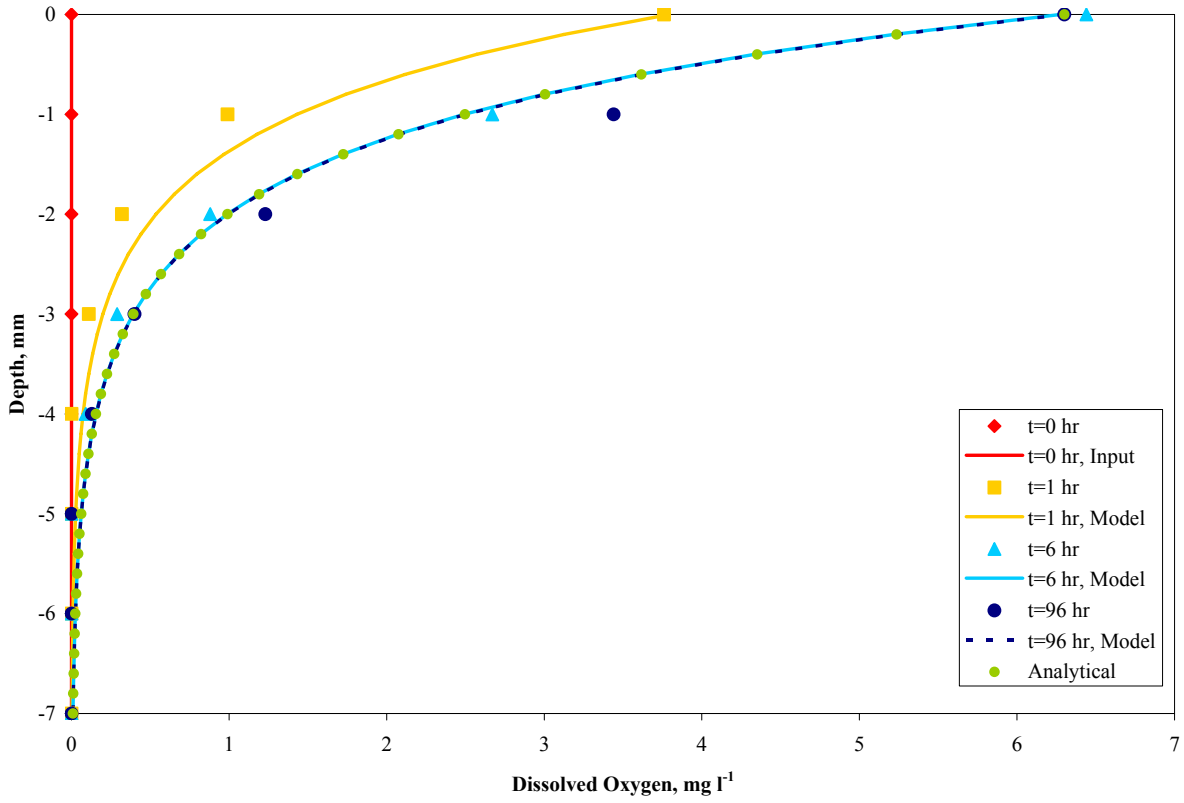

Figure 45. First-order model results during anoxic-oxic cycle plotted with observed profiles for 20°C Core C.

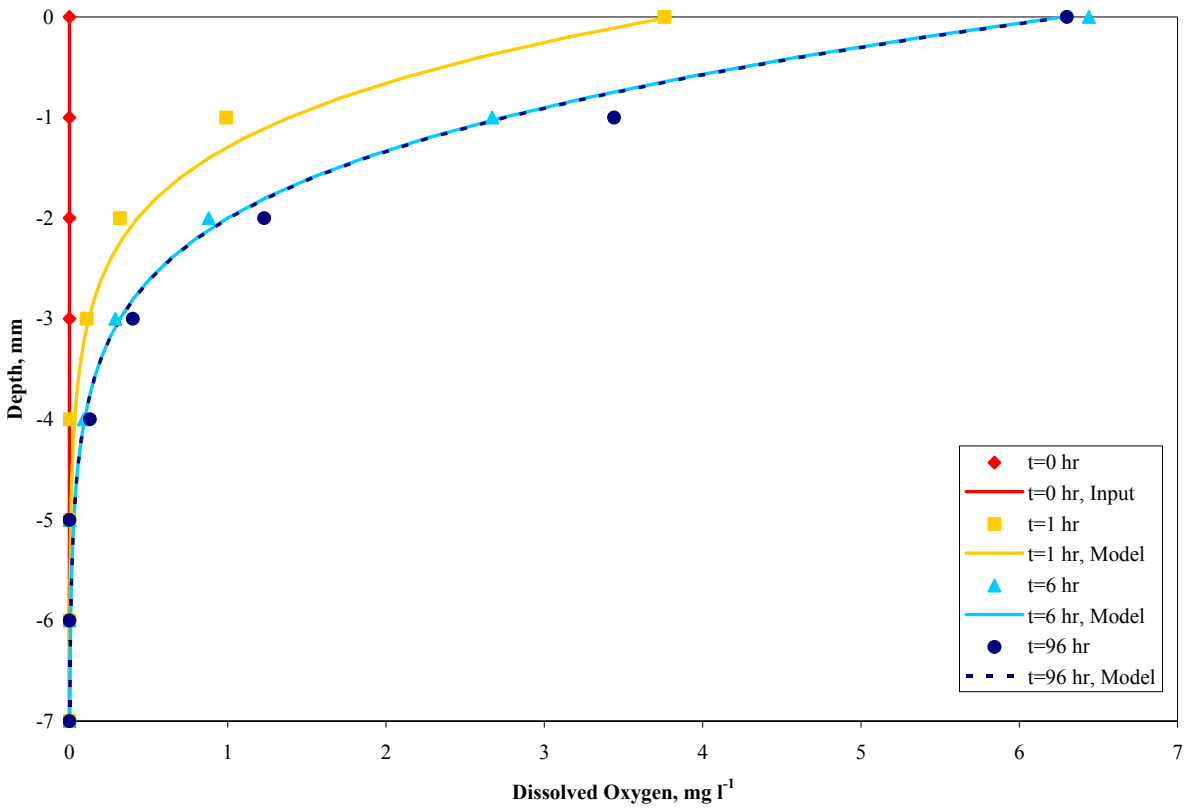

Figure 46. Monod model results during anoxic-oxic cycle plotted with observed profiles for 20°C Core C.

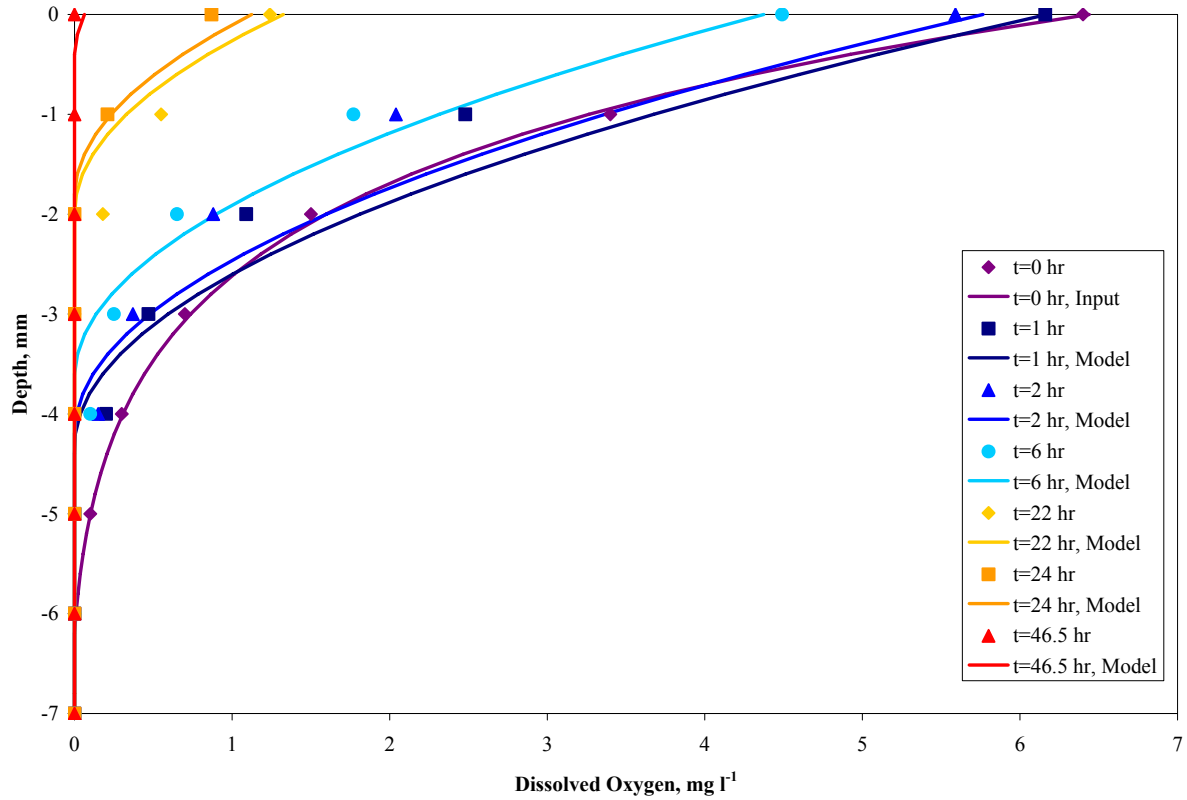

Figure 47. Zero-order model results during oxic-anoxic cycle plotted with observed profiles for 20°C Core D.

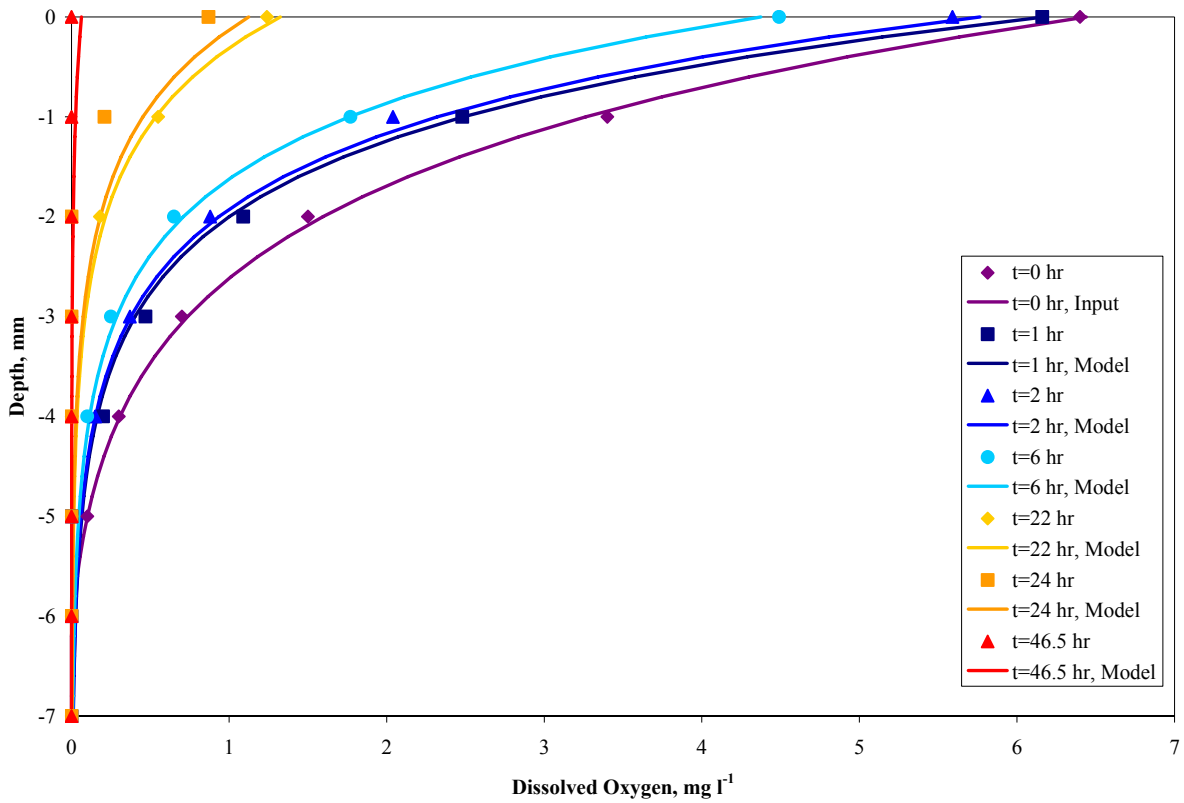

Figure 48. First-order model results during oxic-anoxic cycle plotted with observed profiles for 20°C Core D.

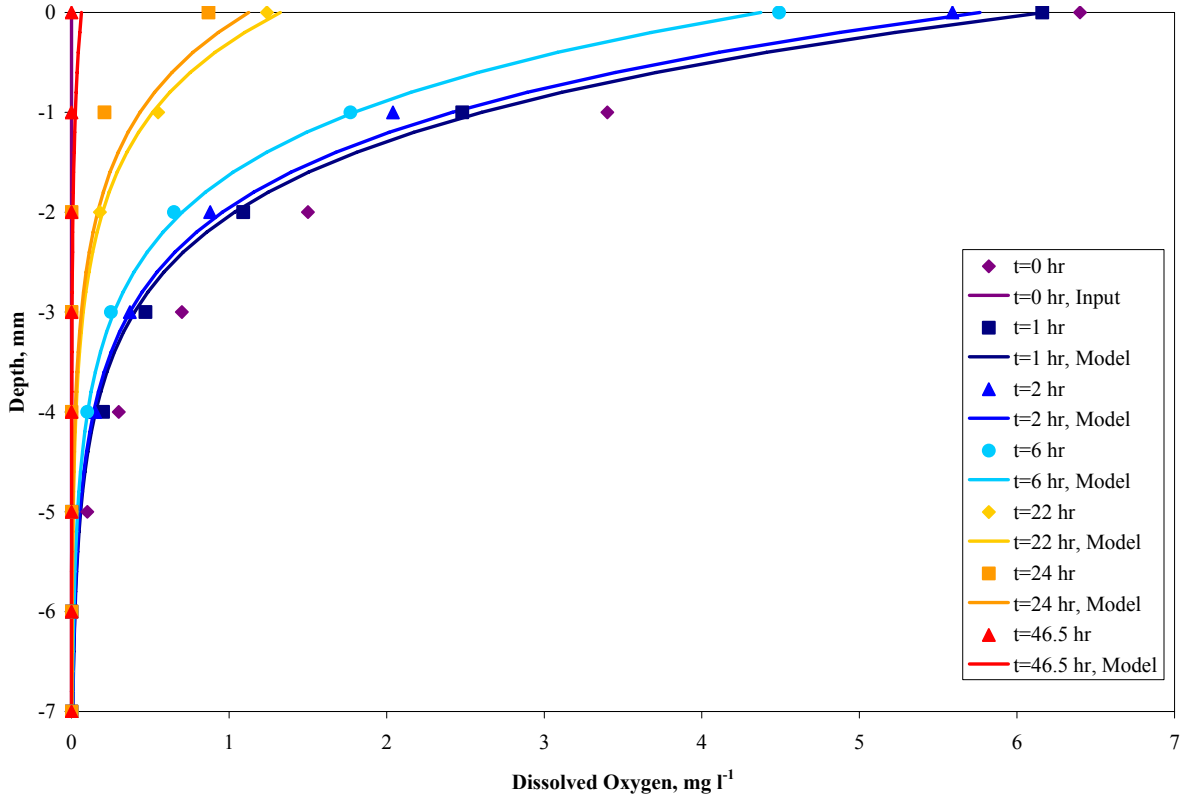

Figure 49. Monod model results during oxic-anoxic cycle plotted with observed profiles for 20°C Core D.

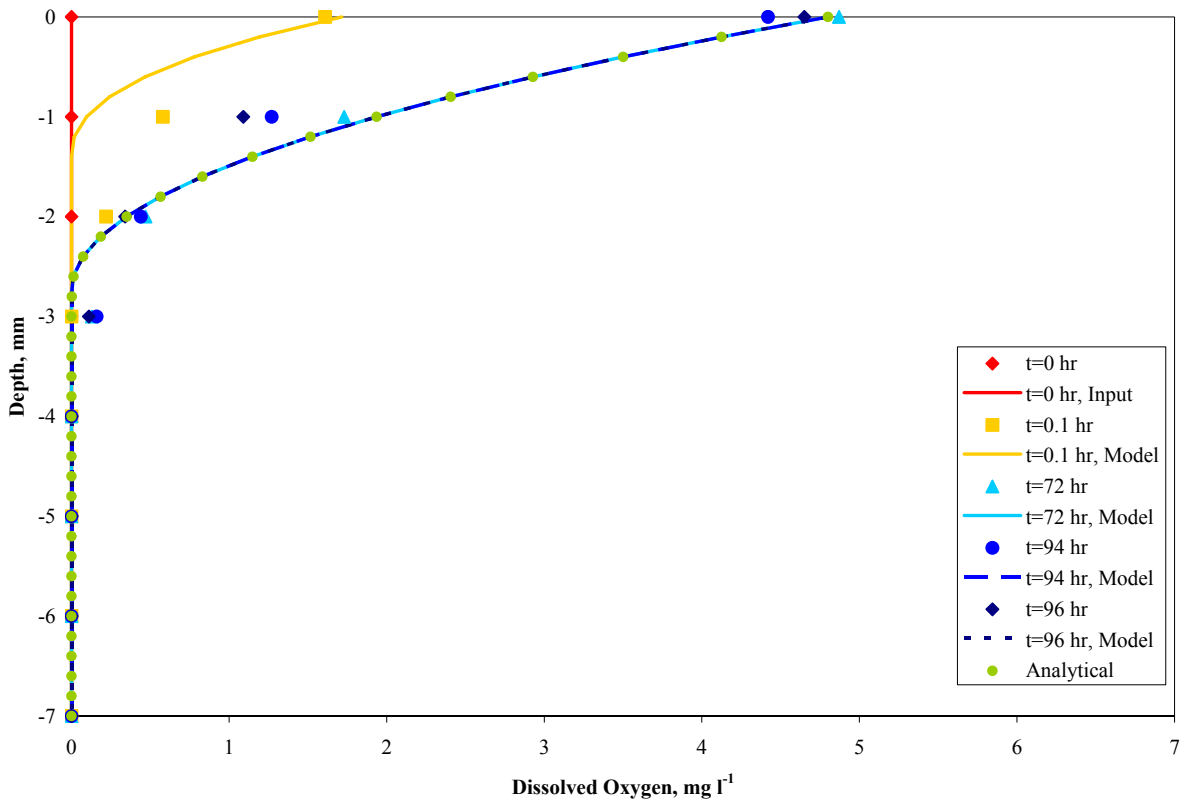

Figure 50. Zero-order model results during anoxic-oxic cycle plotted with observed profiles for 20°C Core D.

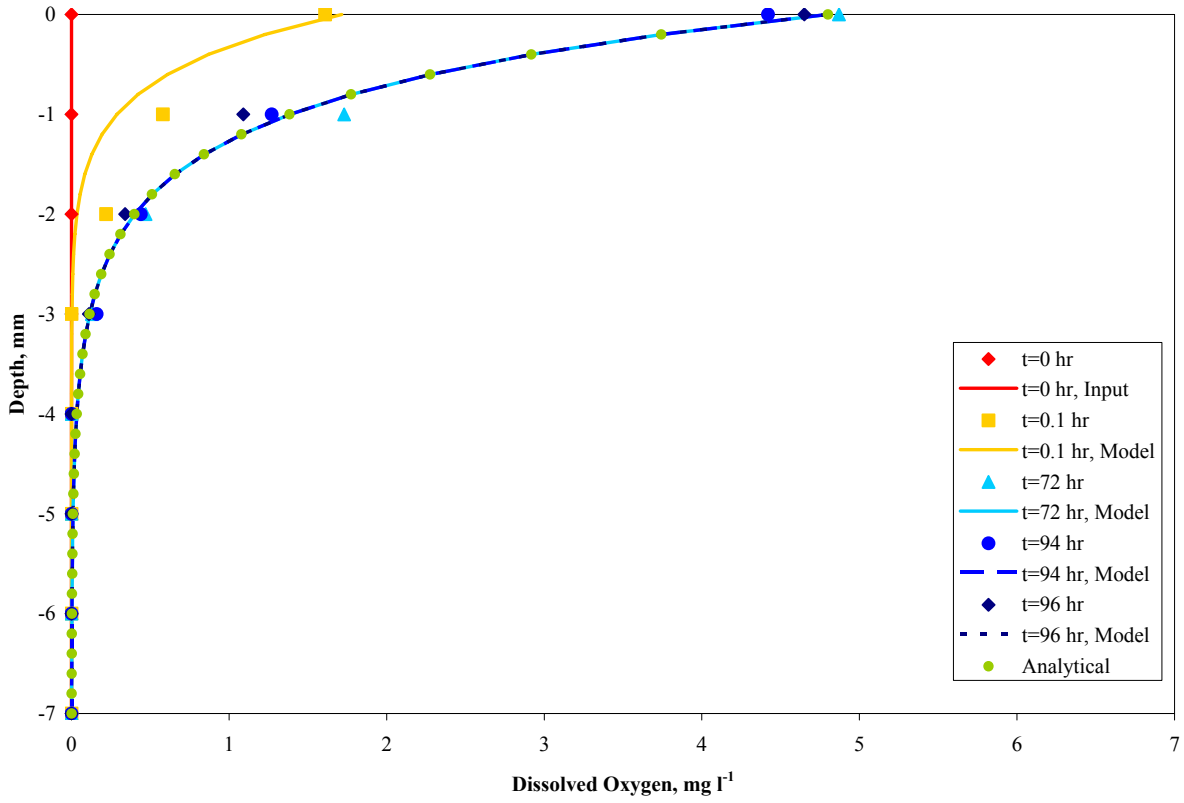

Figure 51. First-order model results during anoxic-oxic cycle plotted with observed profiles for 20°C Core D.

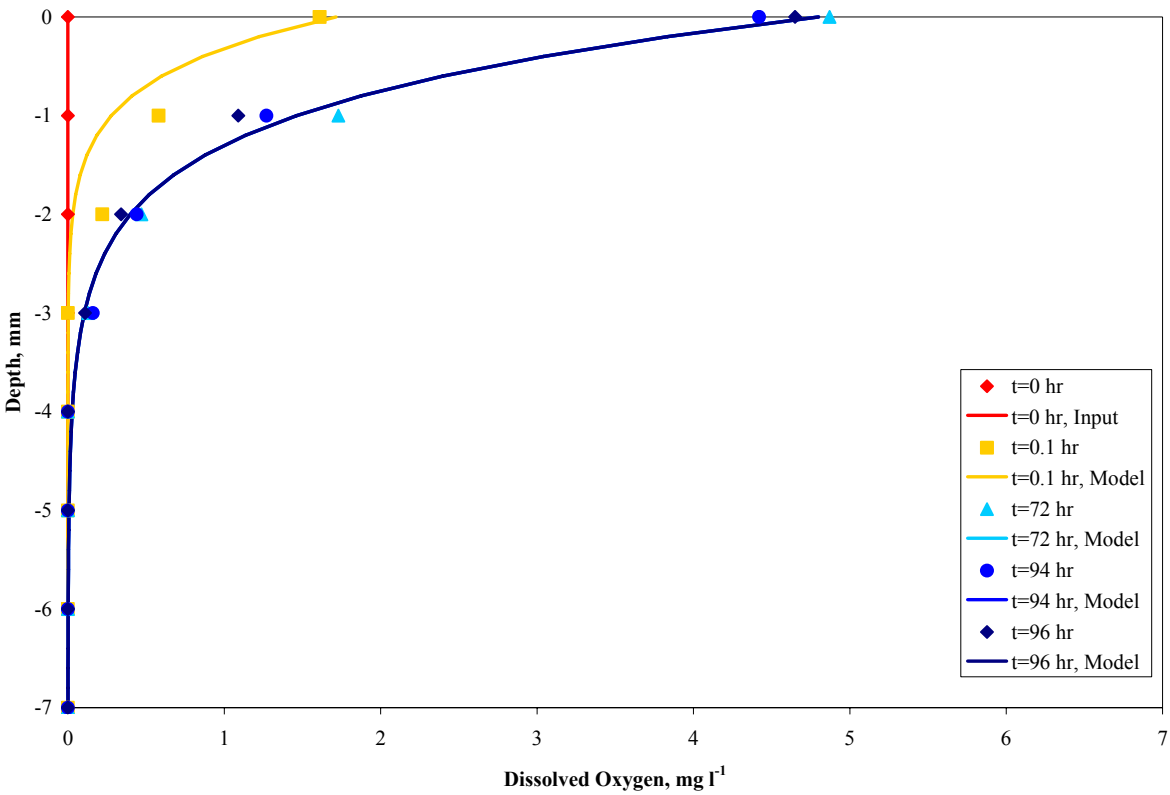

Figure 52. Monod model results during anoxic-oxic cycle plotted with observed profiles for 20°C Core D.